UNIVERSITÀ DEGLI STUDI DI MILANO

CORSO DI DOTTORATO

Fisiologia XXVII ciclo

BIO-09

TESI DI DOTTORATO DI RICERCA

Cellular models for studying and treating abnormal cardiac and neuronal excitability

Dott.ssa Giulia Campostrini

Tutor: Prof. Dario DiFrancesco

Dept. of Biosciences

Università degli Studi di Milano

Coordinatore: Prof. Michele Mazzanti

ANNO ACCADEMICO 2013/2014

SUMMARY

FIGURE INDEX

ABSTRACT

Abnormalities in the electrical activity of cardiac and neuronal cells can cause serious pathologies that affect an increasing number of individuals. In the heart, dysfunctions in the autorhythmic activity of its natural pacemaker, the sinoatrial node (SAN), are becoming progressively more common due to population ageing and are currently treated with implantation of an electronic pacemaker. In the brain, a typical disorder due to neuron hyperexcitability is epilepsy, which is the third most common brain disorder.

The first part of this thesis studied a cell-based method to generate a biological pacemaker, that is a cellular substrate able to drive the beating rate of the host tissue. Potentially, a biological pacemaker presents several advantages compared to electronic devices: it can respond to nervous system regulation and does not need maintenance or substitution. We adopted the strategy of stem cell differentiation to select early pacemaker precursors. As a selection marker, we used CD166, since it is transiently but specifically expressed in the SAN during embryonic development. Accordingly, here we show by immunofluorescence that CD166 is co-expressed with the SAN marker HCN4 in mouse forming heart at day 10.5. CD166-selected cells were previously shown to express SAN genes. In this study, we functionally characterized CD166-selected cells showing that they present morphological and electrophysiological characteristics of SAN cells, expressing functional HCN and calcium channels. They can respond to autonomic nervous system regulation: isoproterenol increases (+57%) and acetylcholine decreases (-23%) their firing rate. Importantly, they are also able to drive the rate of rat neonatal cardiomyocytes in co-culture, thus acting as a real pacemaker *in vitro*. We also set the foundations for translating this selection protocol to human cells, showing that CD166 is expressed during human induced pluripotent stem cell (hiPSC) cardiac differentiation.

This study demonstrated that at early stages CD166 selects mouse pacemaker precursors that function as SAN-like cells *in vitro*. Moreover, it opens promising perspective for translating the method to hiPSCs, with the aim of generating patient-specific biological pacemakers.

The second part of this thesis presents a study aimed at identifying genetic mutations in epileptic patient and assessing whether they may contribute to the phenotype, in order to provide new targets for pharmacological treatments. We

found M54T MiRP1 mutation in an epileptic patient and in her daughter. MiRP1 was shown to act as β-subunit of HCN channels, whose alterations in the brain have been previously linked to the epileptogenic process. Moreover, the same M54T mutation has been recently found in a patient with long-QT and sinus bradycardia, causing a decrease of HCN4, but not of HCN2 current when expressed in neonatal rat cardiomyocytes. Therefore, we decided to evaluate whether M54T mutation was involved in excitability alterations proper of the epileptic disorder, acting on HCN channels. We firstly verify the effect of M54T mutation in CHO cells by co-expressing wild-type (WT) MiRP1, M54T mutant or both (WT/M54T) with either HCN2 or HCN4. Electrophysiological analysis shows that M54T mutation does not affect HCN2 or HCN4 voltage dependence and current densities. We observed a slower activation of HCN2 at -95 and -85 mV and a slower deactivation of HCN4 in the range of -25/-45 mV, however no difference were found at other voltages. Notably, no effect of WT MiRP1 on HCN2 or HCN4 properties was observed. We then replicated the same co-transfection experiments in rat neonatal cortical neurons. Again, we found no difference in HCN2 or HCN4 voltage dependence and current densities, but only a slower HCN2 activation at -85 mV in M54T MiRP1 transfected neurons compared to control and WT. Finally, we assessed whether M54T mutation may alter neuronal excitability acting on other ion channels, by transfecting neurons with only WT or mutated MiRP1. We found that WT MiRP1 induced a two-fold decrease in the threshold of action potential firing and increased their rate, causing an overall increased cell excitability compared to control. This effect was reverted by M54T mutation.

These data oppose a possible contribution of M54T mutation to the epileptogenesis and also rule against the previously acknowledged role of MiRP1 in modulating HCN channels.

PART I:

ISOLATION OF CD166^{+} STEM CELL-DERIVED PACEMAKER PRECURSORS: FUNCTIONAL CHARACTERIZATION AND APPLICATION TO HUMAN SUBSTRATE

FOREWORD

Rationale and relevance of the project

My thesis project was part of a larger project, aimed at generating a biological pacemaker, in order to overcome the already discussed problems associated with electronic pacemakers. This is particularly important in sight of the increasing rate of electronic pacemaker implants[11] likely due to the population ageing.

We chose the strategy of cell therapy to attempt obtaining a biological pacemaker, focusing on cardiac differentiation of pluripotent stem cell, in order to obtain a cellular substrate able to pace other cells once inserted and integrated within the cardiac tissue. This cell-based method was preferred to the gene therapy previously adopted by others[31,44,53,72,96], because it provides the generation of *de novo* pacemaker cells avoiding the genetic manipulation of resident cells. The idea is to select precursors during stem cell differentiation and assess their SAN-like characteristic in culture, verifying importantly the loss of teratogenic potential and the maintenance of the phenotype for long periods.

The main challenge with this strategy is to find a selection method, since pacemaker cells upon ESC differentiation are interspersed among other cardiac cell types[7]. Importantly, in order to be suitable for future clinical applications, the selection method should avoid genomic modification of the selected cells.

Previous data

Evidences on CD166 expression during embryonic development make it a possible surface marker for early cardiomyocytes. Thus, the aim of this project was to evaluate whether CD166 expression could be used as a selection marker to isolate SAN progenitors from ESC-differentiating cardiomyocytes.

Since cardiac expression of CD166 is restricted to a specific developmental stage (E8.5-10.5), the first part of the project focused in determining the best time-

window for selecting SAN precursors from ESCs. After sorting CD166-positive and negative populations at different days (6, 8, 10 and 15) of in vitro differentiation, the expression of the cardiac marker α-actinin was assessed.

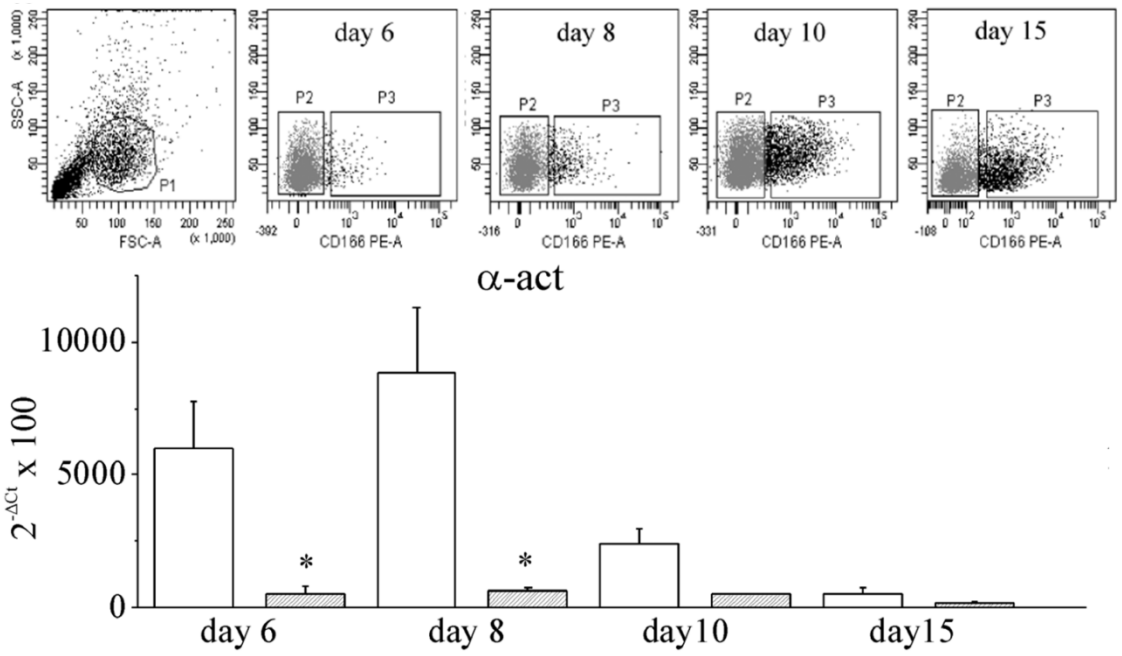

Figure 1: CD166 recognizes cardiac precursors.
Upper panel: representative dot plots of $CD166^-$ and $CD166^+$ populations (P2 and P3 gates, respectively) obtained by flow cytometry analysis of cells dissociated from embryoid bodies (P1 gate) at different time points of differentiation. Below panel: Quantitative reverse-transcriptase polymerase chain reaction analysis of cardiac α-actinin (α-act) in $CD166^+$ (white bars)and $CD166^-$ (gray bars) at the various times.

As shown in **figure 1**, this analysis indicated day 8 as the time point associated with both a sufficient percentage of $CD166^+$ cells and the highest expression in $CD166^+$ cells of α-actinin. At later days, even though the percentage of $CD166^+$ cells increased, the cardiac specificity (α-actinin expression level) decreased. Flow cytometry analysis revealed that at day 8, only a very limited fraction of $CD166^+$ population expressed markers of cardiovascular, mesenchymal or hematopoietic precursors, suggesting that CD166 may be a specific marker for cardiac-fated cells (**Figure 2**). Day 8 was then chosen as the best day to select SAN precursors.

The second part of the project concerned the characterization of $CD166^+$ cells by gene expression analysis. At the day of selection, they expressed higher levels of early cardiac-specific genes (cTnT, Mef2c, Gata4) compared to $CD166^-$ population

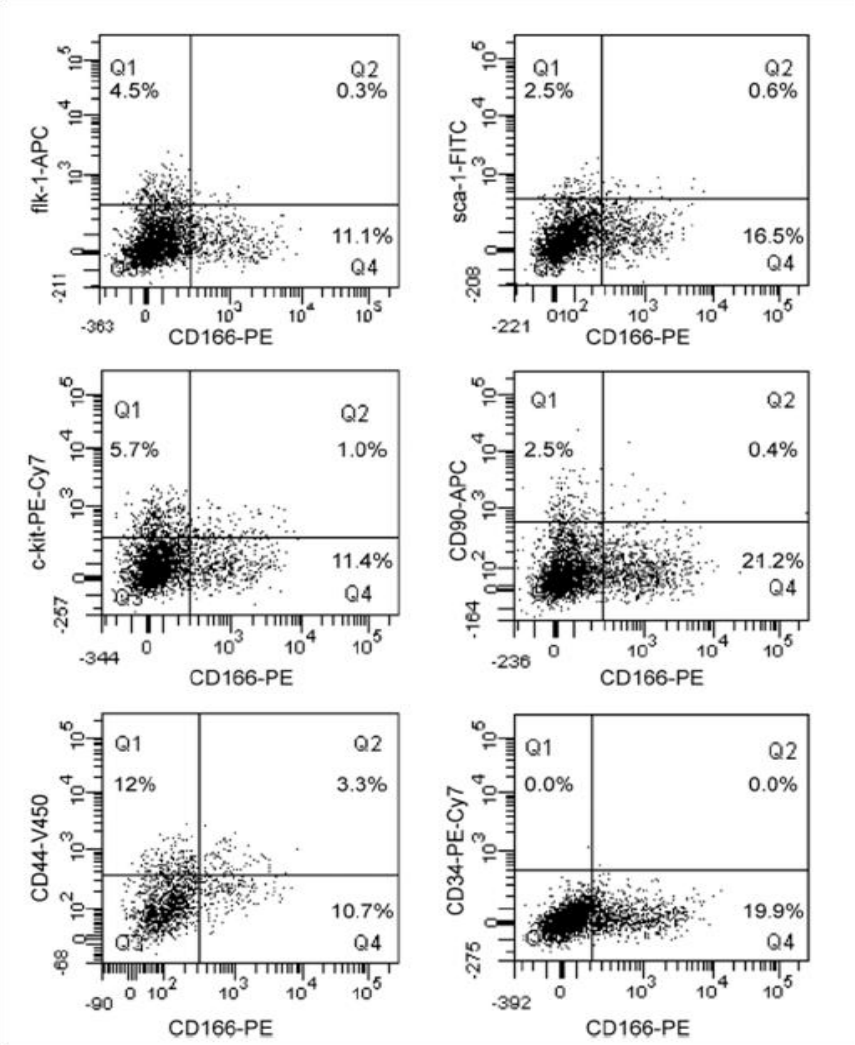

Figure 2: Flow cytometry characterization of the CD166+ population.
Representative dot plots showing the proportion of CD166+ cells coexpressing cardiovascular (flk-1, Sca-1, and c-kit), mesenchymal (CD90 and CD44), and hematopoietic (CD34) markers at day 8 of differentiation. APC indicates allophycocyanine; and FITC, fluorescein isothiocyanate.

and importantly they presented insignificant levels of other germ layer or stem cell markers. To confirm the loss of pluripotency, *in vitro* proliferation assay and teratoma tests in CD1 nude mice have been performed; the proliferation rate revealed that proliferative cells were less than 4% after 48 hours; injection of $1{,}5x10^6$ $CD166^+$ cells did not induce teratoma in any of the animals injected after more than 1 year. This data clearly indicate that CD166-selected cells represent a safe substrate for a possible *in vivo* use[109].

When re-aggregated for 24 hours and plated on culture dish, $CD166^+$, but not $CD166^-$, started to beat spontaneously. This ability was maintained also in long-

term culture (4 weeks). Therefore, subsequent evaluations regarded gene expression analysis in early (8 days) and late (3-4 weeks) cultures (**Figure 3**).

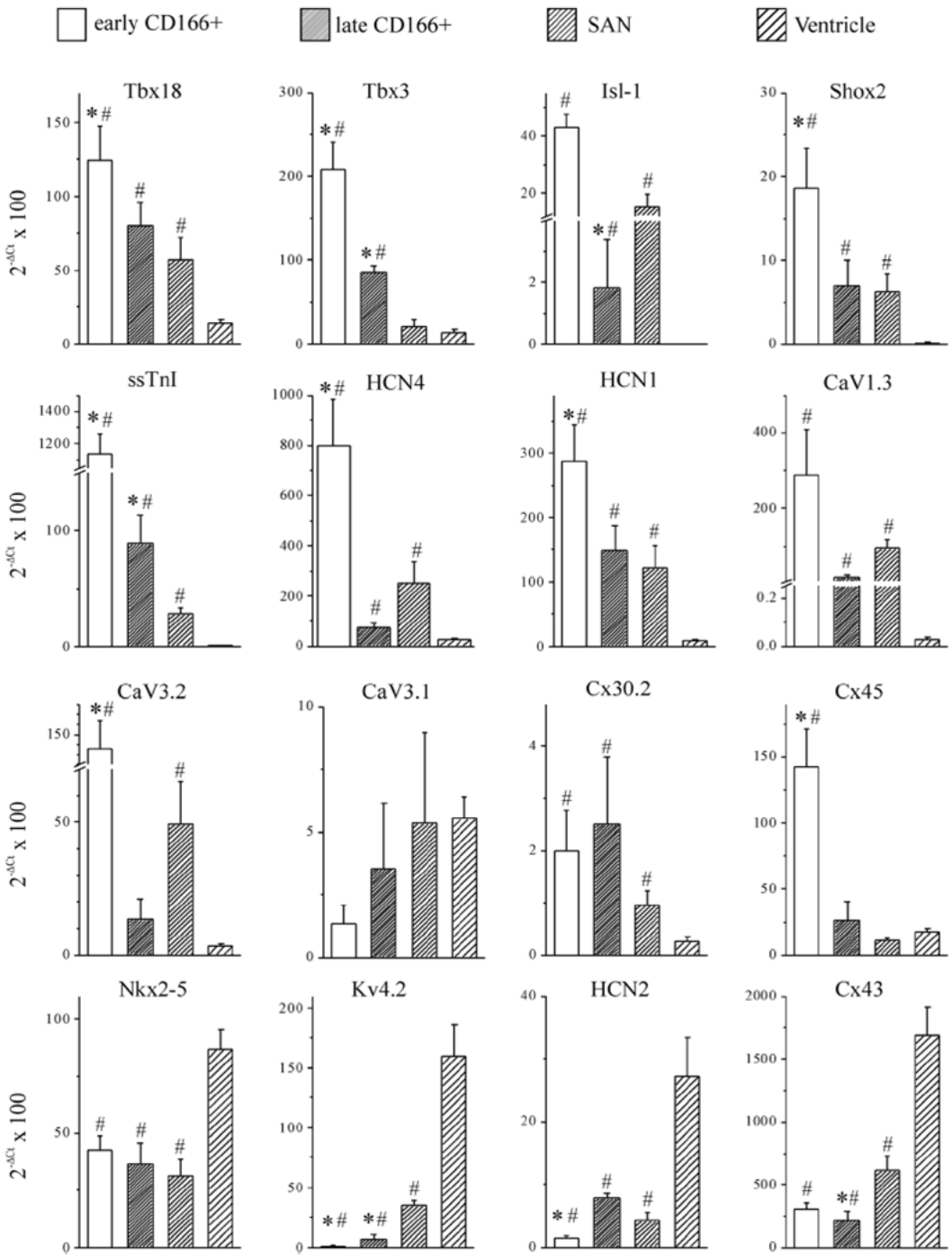

Figure 3: Comparison of gene expression in early and late CD166+ cells, sinoatrial node (SAN), and ventricle.

Quantitative reverse transcriptase polymerase chain reaction analysis of transcription factors (Tbx18, Tbx3, Isl-1, and Shox2), structural proteins, and ion channels (ssTnI, HCN4, HCN1, CaV1.3, CaV3.2, CaV3.1, Cx 30.2, and Cx 45) involved in SAN development and function and of ventricular genes (Nkx2.5, Kv 4.2, HCN2, and Cx43). *P<0.05 vs SAN; #P<0.05 vs ventricle.

$CD166^+$ cells expressed high levels of genes important in SAN development (TBX18, TBX3, Isl1, Shox2)[76] at early days of culture, while afterwards their expression decreased becoming more similar to the expression levels found in the adult SAN. A similar situation was observed for genes involved in the SAN function (ssTnI, HCN4, HCN1, CaV1.3 L-type channel, connexin 30.2). Instead, when the expression of ventricular-specific genes (Nkx2-5, Kv4.2, HCN2, connexin 43) was evaluated, the levels found in $CD166^+$ at early and late days of culture were always significantly lower than those of the ventricle. In conclusion, these data on gene expression previously obtained in our laboratory showed that the phenotype of $CD166^+$ is similar to that of SAN pacemaker cardiomyocytes.

The project: current aims

The third part of the project, which is here presented, aimed to complete the study. In order to support the *in vitro* data presenting CD166 as a good marker for early SAN cells, we analyzed the expression pattern of CD166 *in vivo* during mouse embryonic development. In particular, we investigated whether it is co-expressed with the SAN marker HCN4 in the forming heart.

In parallel, we aimed to deepen the *in vitro* characterization, analyzing the functional aspects of CD166-selected cells, to define whether their gene expression similarities with the SAN correspond to an actual ability to act as biological pacemaker.

First of all, to play the role of the SAN, these cells need to express functional ion channels required to generate action potentials. Thus, we firstly analyzed the functional expression of ion channels fundamental to the generation of the electrical impulse, such as calcium and HCN channels.

Second, pacemaker cells need to be responsive to nervous system regulation; therefore, we evaluated expression of adrenergic and muscarinic receptors and tested cell responsiveness to their respective agonists.

Third, we tested the ability of these cells to connect to and pace other excitable cells *in vitro*, thus acting as a real pacemaker.

Finally, the continuation of the project concentrated in verifying whether the findings in the mouse model can be applicable to a human substrate. Therefore we started to lay the basis for translating the protocol developed for mouse ESC to human induced pluripotent stem cells (iPSCs).

INTRODUCTION

The heart autorhythmicity

The mechanism of heart contraction is similar to the one of other striated muscles, involving actin and myosin fibers that contracts in response to electrical impulse, the action potential. The contractile cells of atria and ventricles receiving the stimulus are part of the so called working myocardium. The initiation of the action potential in the heart differs however from other skeletal muscles, as it is not due to the nervous system, but to the autorhythmic activity of a specialized tissue within the heart itself, called the sinoatrial node (SAN). The SAN together with the atrioventricular node (AVN), the His bundle and the Purkinje fibers constitutes the conduction tissue of the heart, which generates the electrical impulse and propagate it to the working myocardium (**Figure 4**).

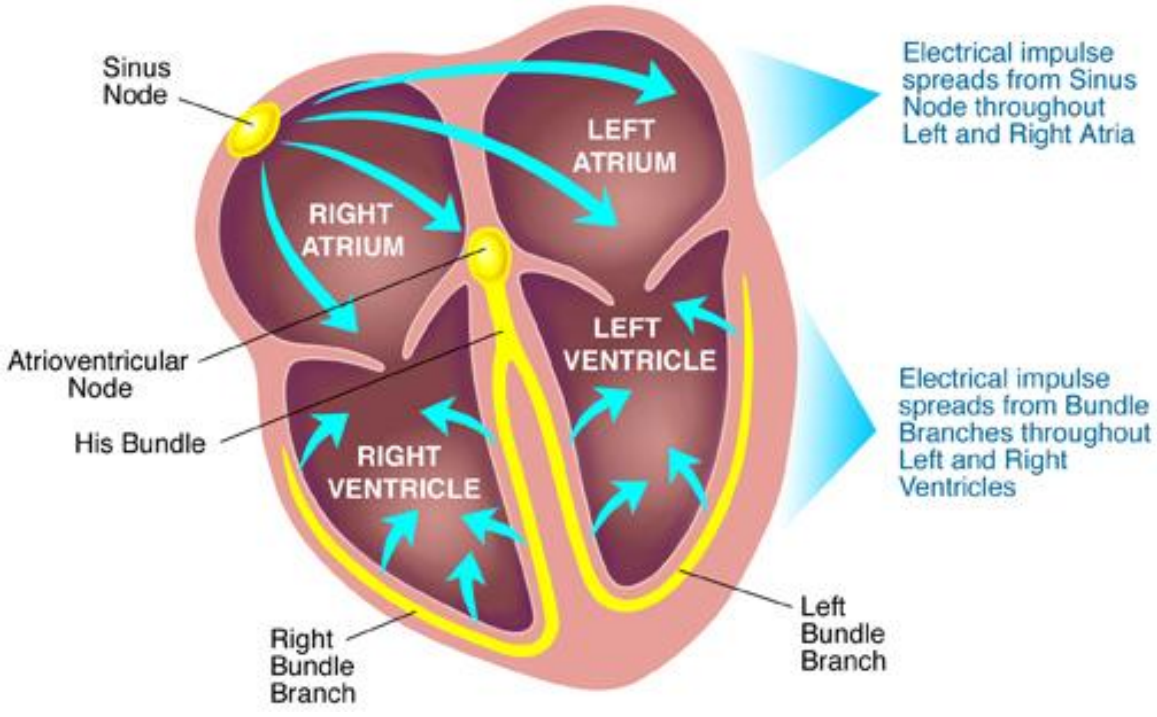

Figure 4: The heart conduction system.
Cartoon of the impulse propagation in the heart. The electrical impulse is generated in the SAN and spreads throughout left and right atria, reaching the AVN. From the AVN, through His bundle branches, the impulse reaches the left and right ventricle at more delayed time.

Each component of the conduction tissue is able to generate spontaneous action potentials, but the SAN generates them at higher rate masking the activity of the other elements through the phenomenon known as overdrive suppression, and thus imposing its rhythm. For this reason, the cells of the SAN represent the natural pacemaker of the heart.

The action potential generated in the cardiac cells is different from that of other excitable cells in shape and length. Notably, the cardiomyocytes can produce two types of action potentials: the working myocardium cardiomyocytes generate the rapid response action potentials (**Figure 5A**), while the SAN and the AVN cells generate the slow response action potentials (**Figure 5B**). The different profiles of action potential depends on different ion channels expressed on the plasma membrane of these cells. The slow response action potentials is characterized by the absence of a proper resting potential due to the activation in phase 4 of a slow diastolic depolarization, called also pacemaker depolarization (**Figure 5B**). This slowly leads to the threshold potential (around -40 mV) for the initiation of the action potential (phase 0), which is due in this case to a inward calcium current mediated by L-type channels, or in mouse by both sodium and calcium currents.

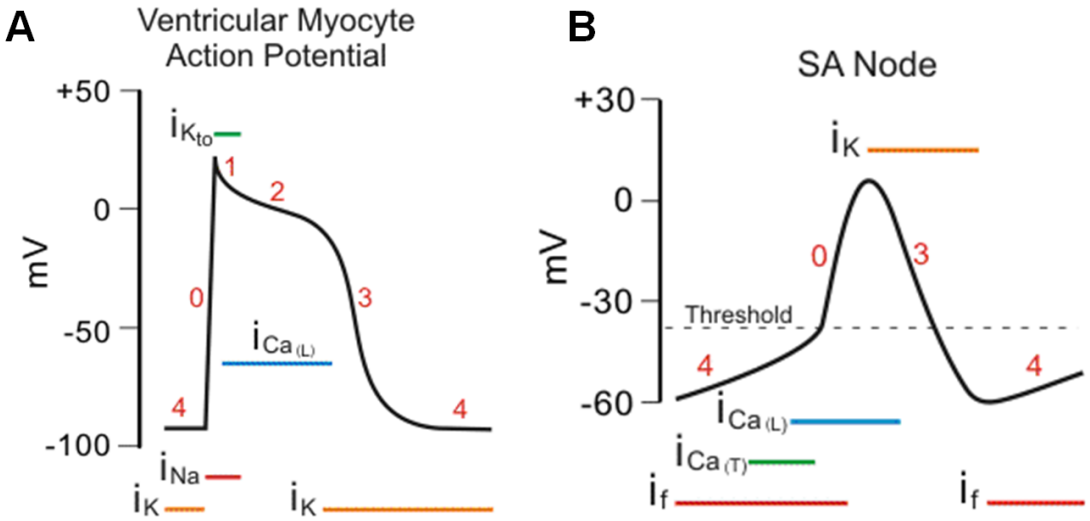

Figure 5: Schematic representation of a ventricular (A) and sinoatrial (B) action potential.
In the figure are indicated the conventional phases of the action potential and the main currents involved.

This early activation of calcium channels causes also their early inactivation; thus, the phase 0 is immediately followed by the ripolarization phase. The pacemaker depolarization is mainly attributable to a mixed sodium potassium current called "funny" current (I_f) or pacemaker current, mediated by the hyperpolarization activated cyclic nucleotide-gated (HCN) channels. The slow depolarization is favored also by the absence of the inward rectifying I_{K1} in these cells.

Voltage-dependent calcium channels[57]

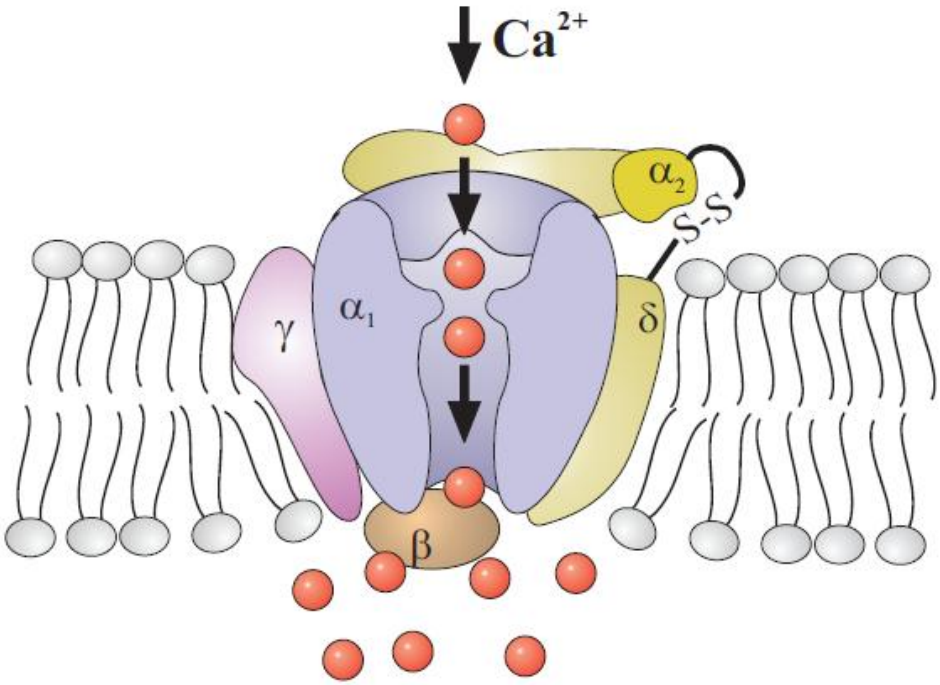

Figure 6: L-type calcium channel structure.
The cartoon shows the putative assemble of the various subunits of L-type calcium channels. The pore and ion selectivity is due to α_1 subunit. (*from Lancinova et al. 2005*)

Voltage-dependent calcium channels (VDCC) are activated upon membrane depolarization, mediate an inward calcium current and are classified into two main categories based on electrophysiological properties: high-voltage-activated (HVA) or L-type (long-lasting type) calcium channels and low-voltage-activated (LVA) or T-type (transient type) calcium channels. The L-type channels present high single channel conductance and slower kinetics of current decay, on the contrary T-type channels have tiny conductance and fast decay. L-type channels are responsible for

the depolarization phase (phase 0) of the action potential in the conduction system and together with the T-type channels contribute to the slow diastolic depolarization. The L-type calcium channels are the most studied, because T-type mediated currents are mostly masked by L-type currents: they can be studied only using pharmacological techniques.

L-type channel structure consists in a α_1-subunit, which is different for the diverse isoforms, that can assemble with various β-subunits and $\alpha_2\delta$-subunits in a tissue-specific way (**Figure 6**). Functionally L- and T-type calcium currents can be assessed thanks to the availability of more or less specific blockers. L-type calcium channels are blocked by nifedipine; T-type calcium channels are instead blocked by μM concentration of Ni^{2+}, even though the affinity depend greatly depend on the α_1-subunit isoform.

HCN channels and I_f current

The HCN channels are pore-loop cation channels structured as four subunits assembled to form a central pore (**Figure 7**).

HCN channel mediate the I_f current, a time- and voltage-dependent mixed sodium/potassium current, which was identified for the first time in pacemaker cells[16] and called "funny" because, differently from the other known currents, was activated upon membrane hyperpolarization. The biophysical properties of HCN channel show a higher permeability to K^+ compared to Na^+, which leads the I_f current to have the inversion potential at -15 mV; this is consistent with the inward current, constituted principally by a Na^+ flux, during the slow diastolic depolarization phase.

In mammals the HCN channel family comprises four isoforms (HCN1-4) coded by different genes, that can form homo- or hetero-tetramers[10]. The monomer is composed by six transmembrane alpha-helical segments and a N-terminal and C-terminal regions, both located in the cytoplasm. The transmembrane segments include the positive charged voltage sensor (S4) and the loop between S5 and S6

segments responsible for the formation of the ion selective pore. The selectivity is guaranteed by the GYG motif, typical of highly selective potassium channels, and by the downstream presence of two positively charged residues and a histidine, providing the sodium permeability. The C-terminal domain presents a cyclic nucleotide-binding domain (CNBD), which permits the modulation of channel activity by the nervous system[122] (**Figure 7**).

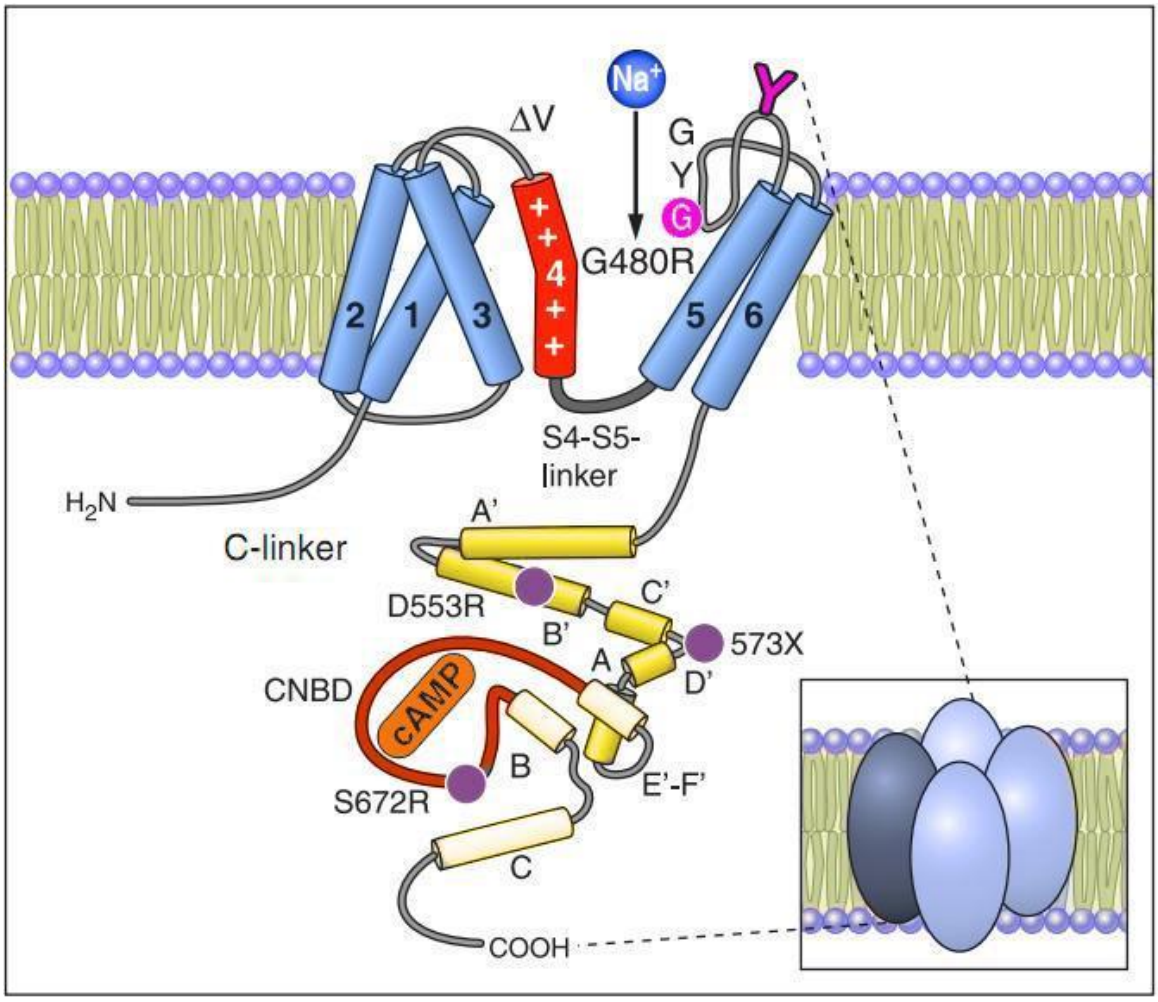

Figure 7: HCN channel general structural organization.
HCN channel are tetramers and each monomer is composed by six transmembrane segments. In red is shown S4 voltage sensor. The region comprised between S5 and S6 is the pore region, containing the selectivity filter motif GYG. The C-terminal domain comprises the cyclic nucleotide-binding domain (CNBD) organized in 3 αα-helices (A-C) and a β-roll between A- and B-helices. (*adapted from Biel et al. 2009*)

This domain and the transmembrane core are highly conserved among the different HCN isoforms, while they present structural differences mainly the N-terminus and in the length of the C- terminus. These differences produce different

functional properties, in the kinetics of activation and in the sensibility to cyclic nucleotides: HCN1 has the most rapid activation[107], most positive voltage of half activation ($V_{1/2}$), compared to HCN2 and HCN4[4], and almost no response to cyclic adenosine monophosphate (cAMP)[122]; HCN4 present instead the slowest activation[110] and, together with HCN2, is the most sensitive to cAMP[82]. HCN3 is the less studied but it has been shown that the human channel is insensible to cAMP, while the mouse channel is slightly inhibited[74].

The four isoforms of HCN channels are mainly expressed in the heart and in the nervous system with different patterns, depending also on species and age. In the heart, the expression of HCN channels strongly depends on cardiac region and are found mostly in the conduction system rather than in the working myocardium. In all the studied species, HCN4 is the most expressed in the conduction system and in particular in the SAN, where it plays a fundamental role in generating and sustaining the heart beat[113,120]. In the SAN also HCN1 is expressed[67]; with HCN4 it can form omo- or heterotetramers, resulting in channels with different biophysical and regulatory properties. In addition, HCN1 is expressed in the AVN and in the Purkinje fibers[67]. HCN3 is poorly express in the conduction system[10]. HCN2 is instead the isoform highly expressed in the ventricular cells and moderately expressed also in the atria. Nonetheless, HCN channel expression levels in these cells are normally low compared to those of the conduction system[10].

Regulation of cardiac activity by the nervous system

Although the cardiac electrical activity is not initiated by the nervous system, it can influence the beating rate, modulating the cytoplasmic level of cAMP. This regulation is performed by the neurotransmitters noradrenaline and acetylcholine released by the sympathetic and the parasympathetic branches of the autonomic systems, respectively. Once secreted, noradrenaline bind to β-adrenergic and acetylcholine to muscarinic receptors on the plasma membrane (**Figure 8**). These receptors are coupled to trimeric G proteins. β-adrenergic and muscarinic receptor activations produce opposite effects though, because they are associated with different types of G protein, the stimulating $G_{\alpha s}$ and the inhibiting $G_{\alpha i}$, respectively.

Indeed, adrenaline stimulation causes an increase of intracellular cAMP, while acetylcholine induces a decrease. Higher levels of intracellular cAMP increase the opening probability of HCN channels that causes a shift in the activation curve towards more positive potentials. This implies that at the same membrane potential the amplitude of I_f current is larger, leading to a steeper slow diastolic depolarization phase that results in higher firing rate of action potentials[26].

On the contrary, lower levels of intracellular cAMP due to muscarinic stimulation decrease the opening probability of HCN channels, which slows down the diastolic depolarization phase and thus decreases the beating rate[27].

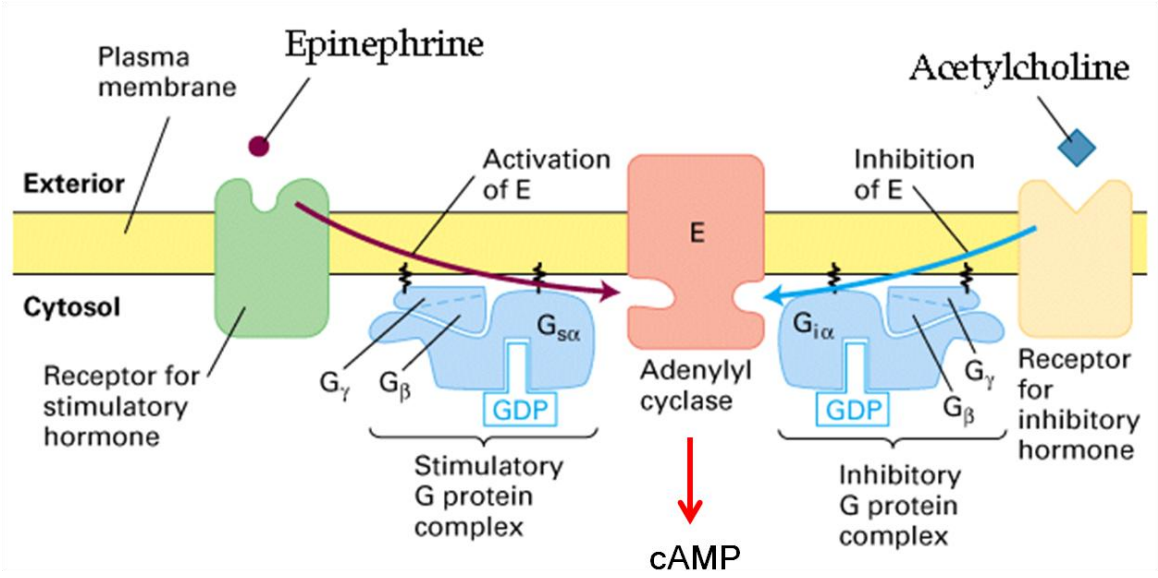

Figure 8: Schematic representation of the activation of β-adrenergic and muscarinic receptors. Epinephrine bind to the β-adrenergic receptor inducing the activation of the stimulatory G protein complex which in turn acts on adenylyl cyclace, causing an increase in cAMP synthesis. Acetylcholine binds to the muscarinic receptor inducing the activation of the inhibitory G protein complex, which in turn inhibits adenylyl cyclace, causing a dccrease in cAMP synthesis.

The embryionic development of the heart

The heart is the first organ that becomes functional in the embryo. Its formation is extremely complex and this is consistent with the high incidence of congenital heart abnormalities in the population[97].

During gastrulation, in the developing embryo three germ layers are formed: ventrally the endoderm, dorsally the ectoderm and the mesoderm in between. The

mesoderm is then further subdivided into somatic and splanchnic layers by the formation of the intra-embryonic *coelum*.

The heart originates from few cells of the splanchnic mesoderm that compose the so called lateral mesoderm, that is the anterior part of the primitive streak. These precursors are committed to the cardiac phenotype during and immediately after gastrulation, and are induced to migrate giving rise two bilateral heart-forming fields. The transcription of particular genes guides the specification of the splanchnic mesoderm into cardiogenic mesoderm. This fate is imposed by stimuli arising from neighbouring cells: a positive regulation from the endoderm, including Hedgehog, FGF, transforming growth factor and BMP signalling; and a suppression from the neural plate and the somatic mesoderm, mostly due to Wnt signalling[97] (**Figure 9A**). For cardiac specification in vertebrates the T-box transcription factor Eomes is required[6], which activates Mesp1 that down-regulates pluripotency genes and up-regulates cardiac transcription factors such as Gata4, Nkx2-5 and Mef2c.

Afterwards, the cells of the heart-forming field migrate to the midline originating the cardiac crescent. During the subsequent folding of the embryo, the cardiac crescent becomes a bowl-shaped heart. The cells forming this primitive heart are the first precursors to differentiate and are therefore named the "first heart field" (FHF). Notably, most of the cardiac mesoderm cells remain in an undifferentiated state for a longer period of time, maintaining high proliferation rate, and are then progressively added to the primitive heart tube to allow its elongation. Since these precursors present a delayed differentiation, they are called the "second heart field" (SHF)[97]. In a subsequent phase, the bowl-shaped heart detaches form the dorsal *coelum* wall and form a close heart tube. In this phase the cells are already committed to originate different heart region: the *sinus venosus* originating the SAN, the atria, the ventricles, the cardiac bulb and the outflow tract. Lineage tracing experiments revealed that the FHF is responsible for the development of

the primitive ventricle originating the left ventricle, while the other regions of the heart require the contribution of SHF cells[78].

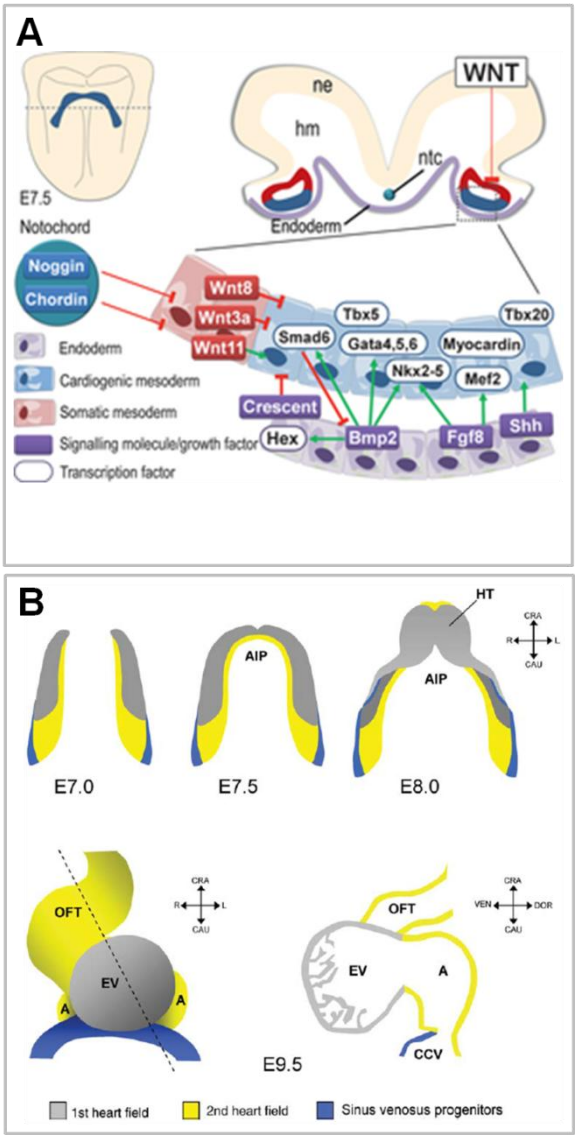

Figure 9: Cell fates during heart embryonic development.
(A) Schematic representation of the stimulatory and inhibitory signals arising from the endoderm and the notochord (ectoderm) to induce the cardiogenic mesoderm. (*from Rana et al. 2013*)
(B) Schematic representation showing the fate map of the cardiac mesoderm. The FHF (grey) originates the left ventricle, the SHF originate the atria, while sinus venosus progenitors belong to a population placed in the caudal-lateral part of the cardiogenic mesoderm. A, atrium; AIP, anterior intestinal portal; CCV, common cardinal vein; EV, embryonic ventricle; HT, heart tube; OFT, outflow tract;VEN, ventral; DOR, dorsal; CRA, cranial; CAU, caudal: L, left; R, right. (*from Mommersteeg et al 2010*)

The addition of SHF cells is parallel to an asymmetric growing of the cardiac tube determining the left-right differences necessary to the chamber formation. The

outer curvature of the heart tube begins to express a specific set of genes that cause a localized differentiation and proliferation of cells, eventually leading to the expansion of the atria and the ventricles. This process reminds the inflation of a balloon and thus it is called the ballooning model of chamber formation[97]. First, the right ventricle is formed, thanks to the so called primary ring[79] located at the position where the ventricular septum will develop. Further folding of the heart completes the chamber septation.

In the forming heart, the cells of the prospective SAN, AVN and His bundle represent a small subset which retains the embryonic phenotype. Indeed, they share many characteristics with the primitive embryonic myocardium such as a high glycogen content, a less developed sarcomeric organization and fewer mitochondria. In particular, the SAN cells originate from the caudal-lateral region of the splanchnic mesoderm, which is distinct from FHF and SHF[75] (**Figure 9B**). By day 8.5 of mouse embryonic development, these precursors present a specific gene signature: they express T-box 18 (TBX18), Islet 1 (ISL1) and SHOX2, but do not express Nkx2-5, which is instead crucial for cardiac looping and thus chamber formation[76]. Shox2 represses Nkx2-5 expression in a specific region where the sinus venosus can develop, allowing the expression of the SAN-specific genes TBX3 and HCN4; the former represses the expression of working myocardium genes, while the latter codes for the pacemaker channel mediating I_f.

Pathological alterations of the heart rhythm[71,123]

Normally, the beating rate can increase or decrease depending on the body activity or condition. The heart rate depends also on the developmental stage, since in the newborn and in the fetus it results higher compared to adults. This variability in heart rate is mainly due to the autonomous nervous system stimulation or to hormonal response.

Under some pathological conditions, for example if the SAN firing rate decreases under a certain threshold, other regions of the conduction system can prevail on the basis of the overdrive suppression, generating ectopical foci or latent pacemakers. In particular, in case of a block of the SAN activity, the AVN

supplants its role. However its rate is significantly slower and although it can prevent heart block, it cannot sustain increased oxygen demand and this may cause serious problems such as ischemia. On the other hand, the emergence of ectopical foci can lead to premature atrial or ventricular contraction that may cause paroxysmal ventricular tachycardia, atrial or ventricular fibrillation, pathologies that increase the risk of heart failure.

The heart rhythm disorders can occur also for dysfunctions in the conduction of the signal, despite the proper generation by the SAN. This is often due to inflammation, fibrosis or ischemia or to the treatment with some drugs. The pathological condition that can arise in this case is called heart block or atrio-ventricular block, which can present diverse levels of severity, the worst being the complete block of the conduction from atria to ventricles.

The pathologies arising from heart rhythm disorders are initially contrasted with pharmacological treatment. However, when these treatments are not sufficient, the implantation of an electronic pacemaker is needed. The electronic pacemaker is a device composed by an impulse generator, a connector and two electrodes that are placed on the right atrium and right ventricle (**Figure 10**). This device is implanted for example in the case of pathologies resulting in lack of blood flow to the brain, such as Stokes-Adams syndrome, or for complex cardiac dysfunctions, such as the Sick Sinus Syndrome, or in cases of severe atrio-ventricular block.

In the last years, an increase in the electronic pacemaker implantation has been reported and notably this is mainly due to isolated sinus node dysfunctions[11]. This increase can be attributed to the population ageing and thus it is probable that this phenomenon will further grow in the next years.

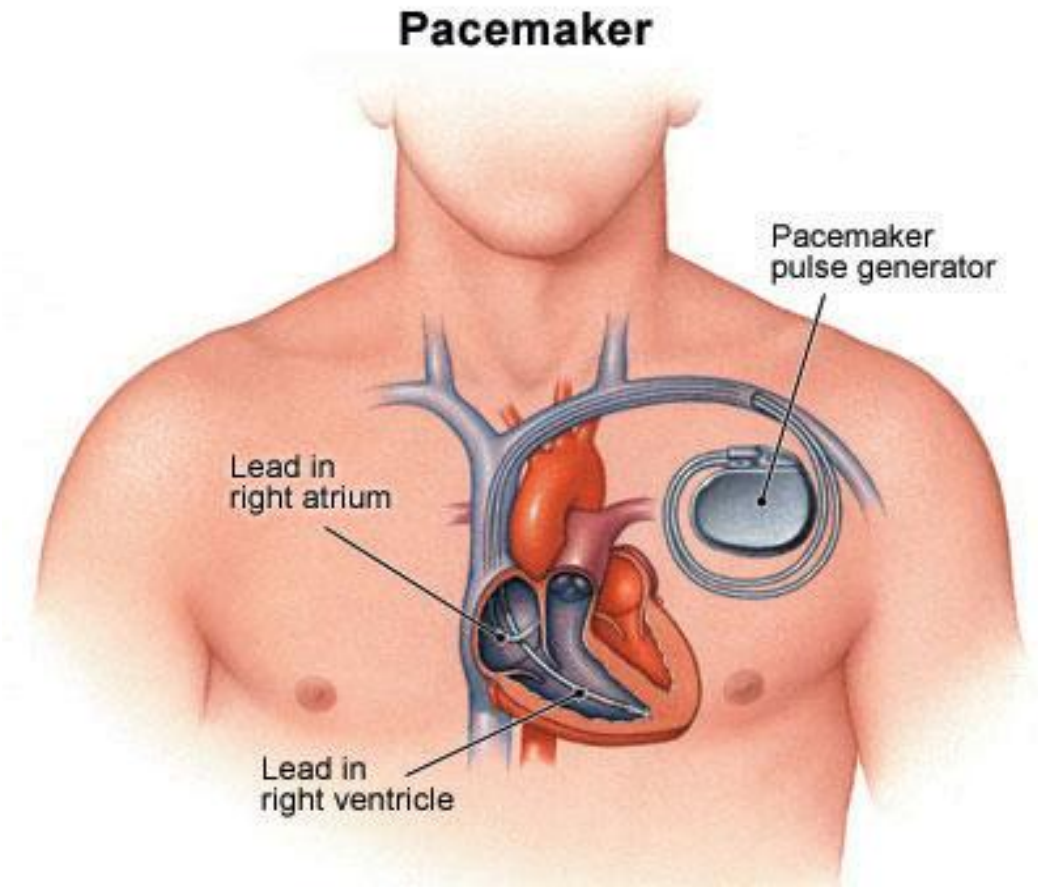

Figure 10: The electronic pacemaker.
The drawing shows a general overview of the electronic pacemaker device, composed by a pulse generator connected with two electrodes to the right atrium and right ventricle.

The artificial pacemaker: from electronic to biological

Although life-saving, the electronic pacemakers present several limitations. Beside showing an inhibiting interactions with other common electronic devices of daily life, electronic pacemakers need above all a periodic maintenance. The battery must be usually replaced after 7-10 years[46] and this occurs in the 25% of all implantation procedures[77]. The replacement is an invasive surgery with costs and some risks of complications such as infections. To overcome this problem, efforts in developing alternatives to the currently used lithium batteries are ongoing. Many attempts focused on building self-powered devices based on energy harvesting systems[39,46]. However, the amount of the harvest energy resulted not enough to power a pacemaker. Recently, a study from Hwang and colleagues[46]

used a material with high piezoelectric coefficient to electrically stimulate heart beating in a living rat, increasing output current efficiency. In another recent study, Haeberlin and colleagues[39] developed a sunlight-powered pacemaker with subcutaneous implantation, that provide enough energy and has a predicted lifetime of 20-30 years. Even though the technique is interesting and very new, important limitations to this study must be considered, such as the test limited to only one pig, the issues concerning skin color for subcutaneous light penetration and the need of a large capacitor for energy storage to pace during darkness.

Despite the improvements of newly available technologies, the electronic pacemaker remains a device which cannot perfectly integrate within the body of the patient and importantly it is not sensible to nervous system and hormonal regulation. This leads to a reduced response in case of physical or emotional stress that may results in inconveniences or even in dangerous conditions.

For this reason, the scientific community is focusing on the development of a "biological pacemaker", that is a cellular substrate able to generate and transmit the electrical impulse and to integrate in the cardiac tissue, thus responding to the nervous and hormonal regulation. The idea is to use cells that share the pacemaker characteristics of SAN cardiomyocytes. The strategies used to reach this goal until now are of two types: the "gene therapy", aiming to genetically modify cardiac cells in order to generate or to increase the spontaneous autorhythmic activity; and the "cell therapy", aiming instead to build a new tissue that can be implanted and function as a pacemaker.

The initial examples of the first strategy come from the works of Edelberg *et al.*[31] and Miake *et al.*[72] from the early 2000s. The first group overexpressed the β-adrenergic receptor by injection of a plasmid in a mouse right atrium. This produced an increase in beating rate, however it was transient and involved a over-activation of adrenergic system that at a certain point cause desensitization of the receptors[31]. The latter group attempted instead to convert ventricular myocytes into pacemaker cells inhibiting the I_{K1} current by means of viral expression of a dominant mutant[72]. This approach presented the important limitation of generating

ectopical foci in the ventricle leading to arrhythmias. In addition, no regulation of the nervous system was observable.

Subsequent studies focused on the expression of HCN channels in ventricular myocytes. HCN channels present the advantage to be active only during the slow diastolic depolarization phase and to be modulated by the nervous system. Qu *et al.*[96] succeeded in expressing the HCN2 gene *in vivo* in the left atrium of a dog, obtaining an autorhythmic area able to be modulated by nervous system. Because gene transfer was mediate by an adenovirus, the effect of the infection was transient though, and this method presents the risks of infection or neoplasia connected to the use of a viral vector.

The most recent study based on gene therapy was performed by the group of H.C. Cho, who delivered the TBX18 first into rodent ventricular cardiomyocytes[53] and later in pig models of heart block treated with electronic pacemakers[44]. They demonstrated that the expression of TBX18 can convert quiescent cardiomyocytes into pacemaker cells both *in vitro* and *in vivo*. In addition, after 14-days follow-up the TBX18-injected pigs showed enhanced response to nervous system and chronotropic support to physical activity compared to animals implanted with only the electronic pacemaker. In these studies an adenoviral vector was used, which allows shorter term virus expression, however a decline of heart rate was observed after 11 days in both TBX18-transduced and GFP-transduced control animals, suggesting that the adenoviral itself may have an effect. Notably, some adenoviral vector may cause inflammation that can induce impulse initiation[104].

The same research group who infected HCN2 in dog atrium, attempted also to use the strategy of cell therapy, by expressing HCN2 in adult mesenchymal stem cells and using these cells to induce action potentials in endogenous myocytes, as a passive pacemaker. Nevertheless, this approach used a viral vector and adult mesenchymal stem cells which are little controllable and can differentiate in other cell types[93].

More recently, Cho *et al.*[21] overcome the problem of using not fully differentiate cells by overexpressing HCN1 into fibroblasts and by fusing them with the

endogenous cardiomyocytes. It remains to be elucidated whether this system can have a long-term effectiveness, especially *in vivo*.

A promising strategy to obtain pacemaker cells is the in vitro differentiation of embryonic stem cells (ESCs) or of induced pluripotent stem cells (iPSCs) (**Figure 11**).

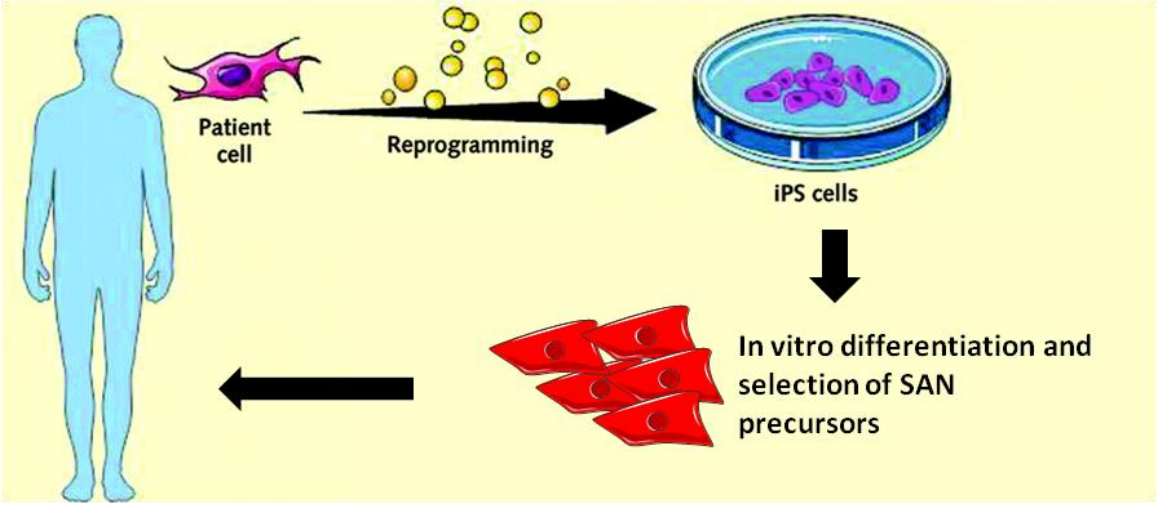

Figure 11: Scheme of the cell therapy approach for generating a biological pacemaker using pluripotent stem cells.
The figure summarize the principal phases of the stem cell-based idea. Human iPSCs obtained reprogramming patient cells are differentiated in culture. During differentiation, SAN precursors are selected and used to generate a de novo cell substrate that can be implanted back in the patient to restore the proper heart rhythm.

These cells can be induced to differentiate *in vitro* into cardiac cells, which spontaneously beat in culture.

The actual capability of ESC-derived cardiomyocytes to pace other cells was demonstrated by Kehat *et al.* and subsequently by Xue *et al.*. The first group showed that cardiomyocytes obtained by hESC spontaneous in vitro differentiation expressed gap junction, integrated *in vitro* with rat cardiomyocytes and were able to sustain heart rhythm *in vivo* of 50% of atrioventricular blocked pigs[54]. Also Xue et al. demonstrated that hESC-derived cardiomyocytes can functionally integrate with co-cultured quiescent cardiomyocytes and in vivo in guinea pig left ventricle[129].

Despite the powerful proof-of-concept of these works, the method is limited by the fact that pacemaker cells represent only a small fraction of the obtained cell types interspersed among the others[7]. The main challenge with this approach is then to isolate a homogenenous cell population that shows a pacemaker phenotype and that has lost the characteristics of pluripotency leading to teratoma formation.
An initial attempt of pacemaker cell selection upon ESC differentiation was performed by Morikawa *et al.*[81] using HCN4 as selection marker. They used an engineered cell line with HCN4-driven expression of the green fluorescent protein (GFP). Unfortunately, in the GFP-positive cell population, the 65% did not present autorhythmic activity and some of them expressed neuronal markers.

Pluripotent stem cells: an *in vitro* model

Stem cells are undifferentiated cells able to differentiate in many cell types. They are able to indefinitely self-renew maintaining their undifferentiated state and at the same time to differentiate into somatic cells, through asymmetrical division. The stem cells are divided into different types, based on their origin and their differentiation potential. The zygote cells until the 4/8-cell stage are the only totipotent cells, that are the cells able to give rise to all embryonic and extraembryonic tissues. ESCs are cells derived from the inner cell mass (ICM) of the blastocyst and are pluripotent, as they can give rise to all the cell types of the body but not to the extra-embryonic tissues. The adult stem cells present instead a reduced differentiation potential, as they are multipotent, thus able to differentiate only into the cell types of some precise tissues or organs (**Figure 12**). These stem cells are present the adult organism with the main function of regenerating the damaged tissues. The iPSC are cells artificially reprogrammed to the pluripotent state from cells already differentiated. They present characteristics similar to ESCs.

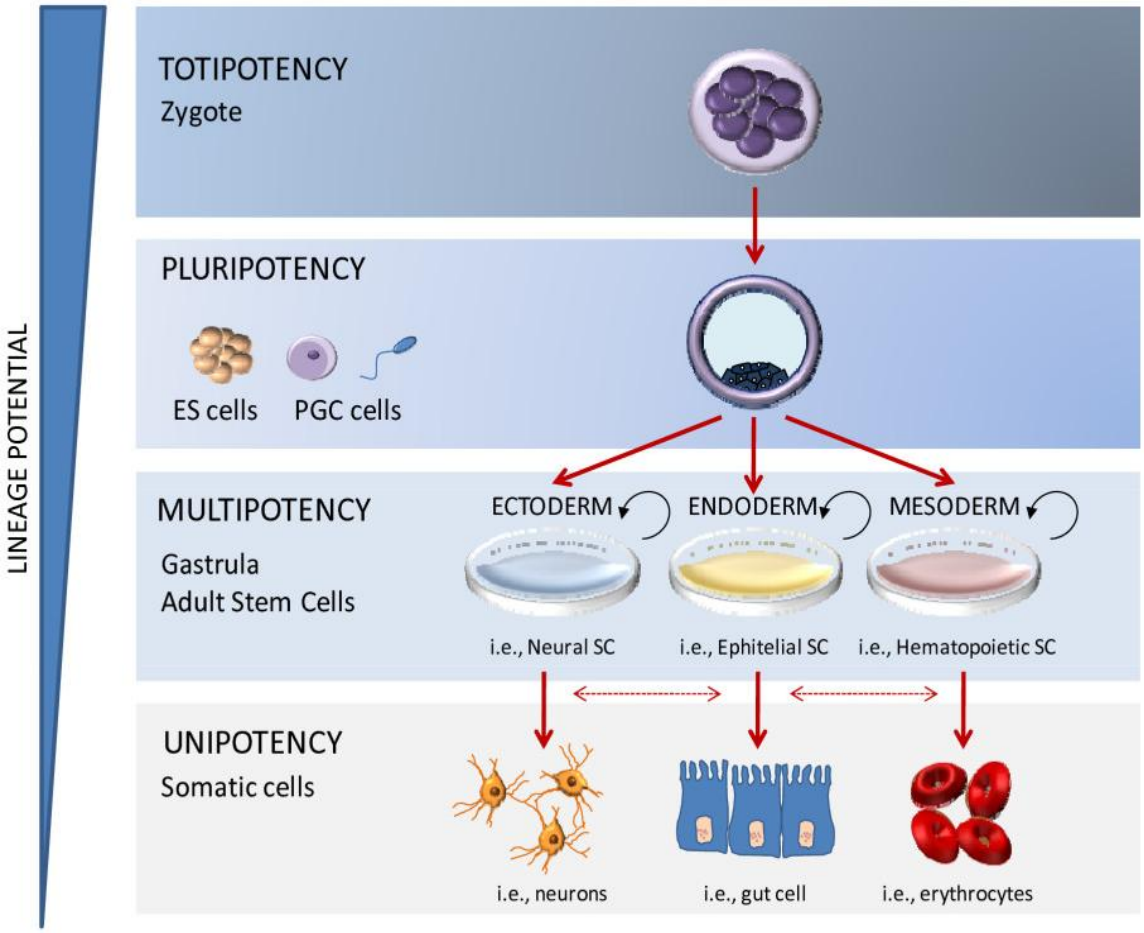

Figure 12: Scheme of cell differentiation potentials during development.
The bar on the left indicate the decreasing differentiation potential. The totipotent zygote has the highest differentiation potential, the ES cells are pluripotent and can differentiate in all the three germ layers: ectoderm, endoderm and mesoderm. The precursors cells of these layers comprise also adult stem cells and are multupotent. The finally differentiated somatic cells can originate only a precise cell type, because they are unipotent. (*from Berdasco and Esteller 2011*)

ESCs

ESCs can be cultured *in vitro* at the undifferentiated state, present a normal karyotype and grown indefinitely without undergoing senescence[128]. Mouse ESCs are the most used in research laboratories. They can grow as couple-shaped colonies on feeder-layer of mouse embryonic fibroblast that supplies the stimuli for proliferation and survival maintaining ESCs undifferentiated. They can also grow in suspension in a feeder-free condition, provided that the leukemia inhibitor factor (LIF) is added to the culture medium[68]. This factor induces the inhibition of MAP kinase (MAPK) pathway and the expression of some transcription factors, such as Oct4, Nanog and Sox2 which maintain the pluripotent state[19]. The properly

cultured ESCs can be recognize by the expression of some surface antigens, such as SSEA-1 (stage-specific embryonic antigen 1) for mouse cells, and by the high activity of alkaline phosphatase or telomerase. Notably, *in vivo* they produce teratoma.

An important application of mouse ESCs is the *in vitro* differentiation. Diverse cell types can be obtained, such as cardiac, neuronal, skeletal muscle, blood, adipose tissue cells[128]. The ESC differentiation tool is particularly relevant in order to obtain cell types that cannot be kept in culture after isolation from the adult animal models, such as cardiomyocytes or neurons. Another important advantage of ESC differentiation is the possibility to study *in vitro* the effects of mutations of particular genes and test a proper treatment at different stages of development.

The differentiation can be induced toward a specific cell type based on the composition and the factors present in the culture medium. It is firstly operated by removing the undifferentiated state keepers (LIF or feeder layer cells) and by the formation of cell aggregates called embryoid bodies (EBs) that recapitulate the embryonic development. The EBs can be obtained through the "hanging drop" method by which a defined number of cells is clumped within small drops hanging from the bottom of an inverted dish. The EBs are subsequently cultured in suspension for a determined period (4-7 days) while they receive gradually decreasing amount of stimulant factors from the outer to the inner part. This diversification address the cells to the different embryonic germ layer fates. The EBs are then plated and let to adhere in order to obtain the final differentiation in a specific cell type. The ESC-derived cells show the properties of the corresponding *in vivo* cell type. In fact, ESC-derived cardiomyocytes express the ion channels that allow them to produce spontaneous action potentials and to contract in culture. They are a mixture of atrial-like, ventricular-like and pacemaker-like cells, as defined by electrophysiological characterizations[7,42]. In particular ESCs are the only cell type able to originate pacemaker cells.

iPSCs

The iPSCs can be obtained using three different technology of somatic cell nuclei reprogramming: the nuclear transfer, the fusion of somatic cells with stem cells and the reprogramming induced by specific transcription factors. These methods are able to force a completely differentiated cell again to a pluripotent state changing its genetic expression profile[130].

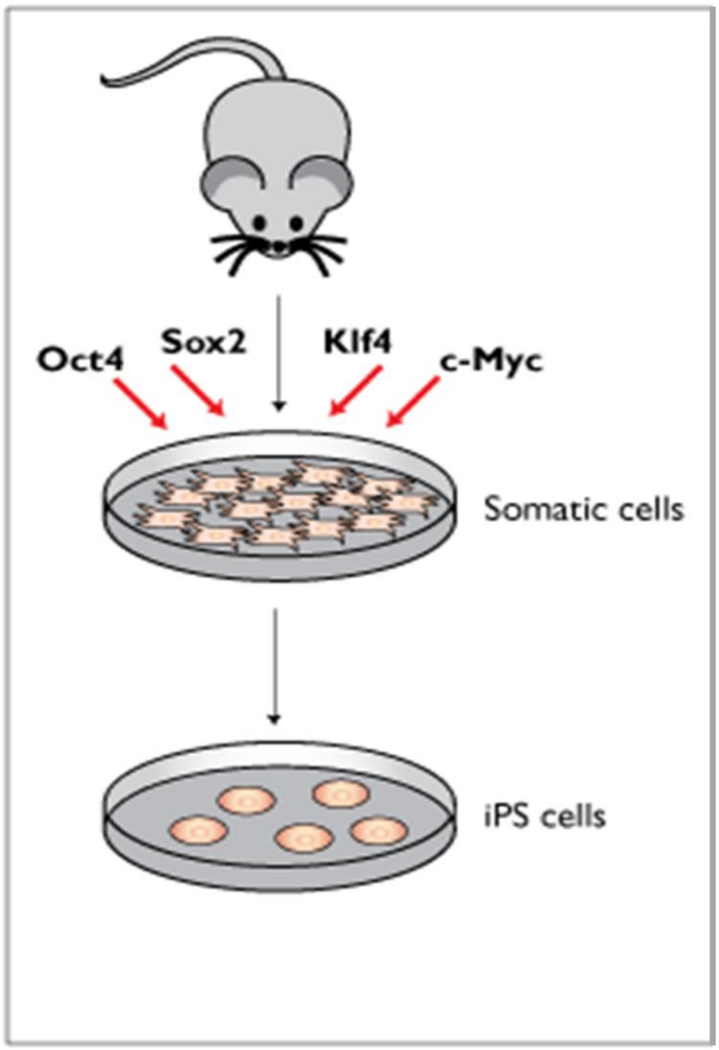

Figure 13: Schematic representation of reprogramming of somatic cells into iPSCs.
The Yamanaka method consists in the infection of somatic cells with Oct4, Sox2, Klf4 and c-Myc. The expression of these genes induces the reprogramming and the appearance of iPSC colonies.

In 2006 Shinya Yamanaka hypothesized the existence of trascriptional factors in ESC that could reprogram the genome of a somatic cell again into a pluripotent stem cell. Among 24 different selected factors, he demonstrated that only 4 factor are sufficient and necessary to reprogram a somatic cell into a pluripotent stem

cell: Oct4, Sox2, Klf4 and c-Myc[118] (**Figure 13**). Human iPSCs were thus generated, reprogramming human skin fibroblasts using Yamanaka factors (Oct4, Sox2, Klf4 and c-Myc)[117] and also using a similar cocktail factors (Oct4, Sox2, Nanog and Lin28)[134]. The cell lines obtained from these protocols have the same morphologic characteristic, the same expression markers and the same plasticity of mESC *in vitro*, so they are defined induced pluripotent stem cells.

To introduce the transcriptional factor within the somatic cells the Yamanaka protocol involves the use of retroviral or lentiviral vectors bringing the information of the four transcriptional factors. This strategy induces the permanent integration in the genome of the exogenous genes; their initial expression necessary for a correct reprogramming is down-regulated autonomously by the iPSC, while the endogenous genes are activated.

Different reprogramming procedures are being investigated involving miRNA[5], episomal vector[133], recombinant protein[55] or Sendai virus[35,87,111].

Also iPSCs, as ESCs, can differentiate *in vitro* into the cell types of the three germ layers[23,83]. Concerning human cells, iPSCs are pluripotent cells lacking the ethical problems associated with human ESCs, because are obtained reprogramming cells coming from biopsies, usually of the skin. hiPSCs present also the advantage of having the same genome of the patient, and so do the cells differentiating from hiPSCs. The generation of patient-specific cells is important for clinical applications; for example in the regenerative medicine this can avoid the phenomena of rejection.

Activated Leucocyte Cell-Adhesion Molecule (ALCAM) or CD166

ALCAM, also called CD166 (cluster of differentiation 166) or in some cases CD6 ligand (CD6L), is a transmembrane protein belonging to the superfamily of immunoglobulins, involved in homotypic and heterotypic (with the T-lymphocyte stimulatory molecule CD6) adhesions[13]. The main function of CD166 is to mediate cell-to-cell contacts in epithelia, mesenchymal, neuronal and connective tissues.

Indeed, it plays a role in many different processes, such as cell migration, hematopoiesis, immune response[41], orientation and extension of axons[20], and it is also deregulated in many forms of tumor, leading to migration and metastasis[124].

In addition, it has been shown to be expressed during embryonic development. It results transiently expressed in the human blastocysts, where it appears to be involved in the early interaction of the embryo with the maternal endometrium[34]. CD166 expression is instead silenced in several adult tissues, being confined in the above cited tissues.

An interesting study showed that CD166 is specifically expressed at day 7.5 of mouse embryonic development in the cardiac crescent, while at day 8.5 high levels are found in the cardiac tube and in the *sinus venosus*. Notably, at day 12.5 CD166 expression is not associated to cardiac cells anymore, but its expression broadens to other organs[43]. Subsequent studies demonstrated that the CD166 is expressed in the mouse yolk sac, both in endothelial and cardiac precursors. The latter are however recognizable by the lack of Flk-1 expression, while the Flk-1/CD166 positive cells give rise only to endothelial cells[84]. Other developmental studies in Xenopus Laevis, showed that CD166 is involved in the morphogenesis and maintenance of the FHF giving rise to the cardiac tube[38].

Recently, Rust and collaborators obtained a population enriched in cardiomyocytes by selecting CD166-positive cells at day 12 of human ESC differentiation. This population expressed the L-type calcium, sodium and pacemaker ion channels and contractile proteins such as α-actinin, tropomyosin, alpha-myosin heavy chain (MHC) and atrial myosin light chain 2 (Mlc2a), typical markers of cardiomyocytes. These cells are shown to beat in culture for 3 weeks if they were seeded at high densities promoting cell aggregation in suspension[105].

Interestingly, CD166 is also expressed in the human fetal heart, specifically in cardiomyocytes and not in smooth muscle cells neither in endothelial cells[61]. In agreement with this, also iPSC-derived cardiomyocytes and not smooth muscle or endothelial cells were shown to be positive to CD166 signal in immunofluorescence analysis[61]. The same study used CD166 ad a selection marker for cardiomyocytes from multipotent cardiovascular progenitors at day 20

of iPSC differentiation, although expression of CD166 was present also during all the differentiation period.

These evidences suggest that CD166 could be a suitable marker to select cardiomyocytes upon pluripotent stem cell differentiation in a specific time-window.

MATHERIALS AND METHODS

Embrionic Stem Cell culture and differentiation

Mouse ESCs (D3 line, ATCC) were grown in suspension in ES-medium containing ES-DMEM (ATCC), 15% Knock-Out Serum Replacement (Life Technologies), 0.1 mM Non Essential Amino Acids (Life Technologies), 0.1 mmM β-mercaptoethanol (Sigma-Aldrich), 2 mM L-glutamine (Life Technologies), 103 U/ml Leukemia Inhibitory Factor (LIF, Chemicon), 1X PenStrep (100U/ml Penicillina and 0,1mg/ml Streptomicina, Sigma-Aldrich) and were differentiated with the "hanging drop" method. ESCs were divided with Tryple Express (Life Technologies) obtaining an homogeneous suspension, counted and resuspended at specific density ($2{,}5x10^4$ cells/mL) in a differentiating medium containing DMEM (Life Technologies), 4mM L-Glutammine (Sigma-Aldrich), 0,1mM β-Mercaptoethanol (Sigma-Aldrich), 0,1mM Non Essential Aminoacids (NEA, Life Technologies), 20% Fetal Bovine Serum (FBS, Life Technologies), 1mM Na-Piruvate (Sigma-Aldrich), 1X PenStrep (Sigma-Aldrich). ESCs were then cultured as hanging drops containing ~ 500 cells/20 µl for 2 days at 37°C with 5% of CO_2 and then they were grown in bacterial dishes for 5 days. 7 day-old Embryoid Bodies (EBs) were plated on tissue culture dishes coated with gelatin 0.1% (Type B, Sigma) in differentiating medium containing: DMEM (Life Technologies), 4mM L-glutamine (Life Technologies), 0.1 mM NEA (Life Technologies), 0.1 mM β-mercaptoethanol (Sigma), 20% FBS (Life Technologies), 1X PenStrep and let to grow for one day before enzymatic dissociation and sorting.

The pHCN4-EGFP clone of mouse ESCs was obtained cloning 841 bp sequence located 2.30 Kb upstream of the 5' ATG of the mouse HCN4 gene, and corresponding to its promoter (pHCN4), and inserting it into the expression vector pEGFP-N1 (Clontech) after removal of the constitutive CMV promoter. The resulting pHCN4-EGFP plasmid carries the enhanced green fluorescent protein (EGFP) under the transcriptional control of the pHCN4. 2x106 mouse ES D3 cells

were nucleofected (Mouse ES nucleofector kit VPH-1001, A24 program, Amaxa) with 10 μg of pHCN4-EGFP plasmid and plated in 100 mm dishes in ES-medium. To induce plasmid integration, cells were kept under stringent selection (600 μg/ml of geneticin) for at least two weeks, changing the medium every two days. After this period, the geneticin concentration was lowered to 300 μg/ml.

Generation of human iPS from somatic cells

Dermal biopsies from healthy individuals were maintained in DMEM at 4°C. The tissue was cut in small pieces and incubated in DMEM plus 10% FBS, 2 mM L-glutamine, 100 U/ml penicillin and 100 μg/ml streptomycin at 37°C with 5% CO_2. Culture medium was changed every 3-5 days until visible outgrowths of cells are obtained (usually 1 to 3 weeks). Adherent cells coming out of the tissue were enzymatically dissociated and re-plated to allow for fibroblasts expansion. Subsequently, cells were reprogrammed using CytoTune®-iPS 2.0 Sendai Reprogramming Kit (Life Technologies). Colonies that microscopically present a human iPS-like morphology were manually picked with a micropipette, initially expanded on a feeder layer of murine embryonic fibroblast (MEF), and adapted later to grow on feeder-free, Matrigel™-coated plates in iPSC complete medium, composed by: Knockout DMEM, 20% Knockout serum, 1% B27 supplement, 1% N2 supplement, 2mM GlutaMAX (Life Technologies), 1mM 2-mercaptoethanol, 0.1 mM NEA solution (Sigma Aldrich), 1X PensStrep and 20 ng/ml bFGF (Life Technologies). Selected colonies were then analyzed for the expression of the pluripotency transcription factors (OCT4, SOX2, NANOG) by quantitative real-time PCR.

Differentiation of human iPS

For "spontaneous differentiation protocol" of iPSCs, colonies growing on the feeder layer were adapted to grow on Matrigel™ using mTeSR™1 (Stem Cell Technologies) as maintenance medium to avoid feeder cell contamination during

the differentiation protocol. Cardiac differentiation were induced by aggregation of human iPSCs (hiPSCs) into EBs by detaching and re-plating them on ultra-low attachment plates in EBs medium, composed by: DMEM/F12, 20% FBS, 0.1 mM NEA solution, 0.1 mM GlutaMAX, 50 μM 2-mercaptoethanol, 1X PenStrep (Life Technologies). On day 6, EBs were transferred to 0.1% gelatine-coated plates and monitored for the next 6-7 days for the appearance of spontaneously beating areas. At the appearance of spontaneously contracting areas, serum (FBS) concentration in EBs medium will be lowered to 2%. The beating clumps will be manually dissected with a microscalpel and transferred to gelatin-coated plates. They were kept in culture for several days before detaching them for the different analysis.
For "induced differentiation protocol", the commercial kit from Life Technology was used, consisting in a mono-layer differentiation using definite factor-containing culture media (medium A for days 0-2, medium B for days 2-4, medium C for days 4-14 of differentiation) that actively induce mesoderm and then cardiac differentiation activating intracellularly specific signalling pathways, leading to a general increase in the yield of cardiomyocytes.

Flow cytometry and cell sorting

For flow cytometry analysis and sorting EBs from mouse ESCs or human iPSCs were collected and washed twice in PBS, subsequently treated with Tryple Express (Life Technologies) for 10 min at 37°C under gentle agitation, and then mechanically dissociated. The cell suspension was centrifuged at 310 x g for 15 min and resuspended in PBS plus 1 mM $CaCl_2$, 10% FBS and 5 mM EDTA. Cells were incubated with the fluorophore-conjugated antibody PE Rat anti-mouse CD166 (eBioscience) for 30 min on ice, under gentle agitation in the dark. After incubation, cells were washed twice in PBS and resuspended in PBS with the addition of 1 mM $CaCl_2$, 5 mM EDTA, subsequently filtered through a 70 μm sterile mesh and analyzed by a FACSAria™ flow cytometer and sorter (BD Biosciences). The appropriate isotype control and unstained cells were used to set

the FACS conditions. For following analyses, ES-derived cells were re-aggregated by gravity for 24h in low-adhesion culture dishes in differentiating medium and then plated at either low density for electrophysiological analysis or at high density to allow the formation of a compact layer for immunoistochemistry analysis inside silicon inserts (Giemme), which were removed after about 3 hours.

Mouse embryo tissue sections staining

Mouse embryos at developmental stage E10.5 and E12.5 were isolated from CD1 female mice, then collected in cold PBS and after that fixed in 4% paraformaldehyde for 1 or 2 hours respectively. The embryos were washed twice in PBS, dehydrating them by washing in PBS containing increasing concentration of sucrose (10, 20 and 30%), included in O.C.T compound and frozen in liquid nitrogen-cooled isopentane. Serial 8-µm-thick sections were cut with a Leica cryostat (Leica Microsystems GmbH, Wetzlar, Germany) and the cryosections were incubated in PBS with 1% BSA and 0.1%TritonX-100 for 1 hour at room temperature subsequently blocked with 10% donkey serum in PBS for 30 minutes at RT. The samples were incubated with the primary antibody (anti-CD166; 1:50 or anti-HCN4 1:50) overnight at 4°C followed by secondary staining with secondary antibody 1:250 Alexa488 donkey anti-goat for 1 hour at RT. Slides were then washed three times in PBS, incubated with Hoescht (1mg/ml for 5min at RT), washed, mounted using Fluorescence Mounting Medium (Dako) and analyzed at fluorescence microscopes (Leica).

Immunofluorescence and Video-Confocal Analysis

Samples were fixed on ice in paraformaldehyde (4%) for 30 minutes, rinsed for 20 min with PBS containing 0.1 mM glycine, then permeabilized with 1.5% Triton X-100 in PBS for 30 min and subsequently incubated in a solution containing 0.3% Triton X-100, 1% (w/v) Bovine Serum Albumin (BSA), 10% Normal Donkey Serum in PBS for 1 hour. Samples were incubated overnight at 4°C with primary

antibodies in PBS, 0.3% Triton X-100, 1% Bovine Serum Albumin (BSA), and 2% Serum. The antibodies used were: mouse anti-caveolin-3 (1:500, BD Biosciences); mouse anti-αactinin (1:700, Sigma); rabbit anti-HCN1, -HCN2 and -HCN4 (1:100, Alomone Labs); rabbit anti-β (1:50, Santa Cruz) and anti-β adrenergic receptors (1:50, Santa Cruz); mouse anti-muscarinic M2 receptors (1:200, Santa Cruz). The day after samples were washed in PBS and incubated for 1 hour with PBS, 0.3% Triton X-100, 1% BSA, 2% Normal Donkey Serum and the appropriate fluorophore-conjugated secondary antibodies (donkey anti rabbit Alexa594, donkey anti-mouse Alexa488, goat anti-rabbit Alexa 405 1:500, 1:1000 Molecular Probes). After a final washout in PBS, coverslips were mounted with Vectashield mounting medium with DAPI (Vector) and confocal images were then acquired using a video confocal microscopy ViCo (Nikon).

Neonatal cardiomyocytes isolation and (co-)cultures

Neonatal rat cardiomyocytes were isolated from rat pups of 2 days. The hearts were isolated and then maintained into a PBS solution. Atrium were eliminated and the ventricles were kept in a dish with PBS; then the ventricles were cut into pieces and transferred into a 15 mL Falcon, discarding the supernatant. 0,3 mL of enzymatic solution (in mM: 116,4 Nacl, 5,4 KCl, 1 NaH2PO4 H2O, 0,8 MgSO4 H2O, 5.5 Glucose, 20 Hepes, 0,4 mg/ml Pancreatine and 136 U/ml of Collagenase Type 4) were added for each heart and stirred at 37°C for 20 minutes. At the end of the digestion, the supernatant was transferred in a 15 mL tube adding 1 mL of filtrate FBS to inactivate the enzymes. After a centrifuge of 5 minutes at 300 x g the supernatant were discarded and the pellet were gently resuspended into a tube with 1 mL of FBS, keeping the tube on ice. With the remaining pieces the digestion with enzymes were repeated for almost 4 times. At the end of the digestions the tube was centrifuged at 300 x g and pellet resuspended slowly in 1 mL of medium and plated into a 100 mm dish, waiting 40 minutes to allow the adhesion of fibroblast. At the end, the supernatant was plated into a different dish

and maintained in culture with a medium containing DMEM/M199 (Life Technologies™), adding 10% of HS (Horse Serum) (Life Technologies™), 5% of FBS (Fetal Bovine Serum) (Life Technologies™), 1% of L-Glutamine (Sigma-Aldrich®) and 1% of Pen/Strep (penicillin 100U/mL, streptomycin 0,1mg/mL) (Sigma-Aldrich®). Cardiomyocytes were maintained in incubator at 37°C with 5% of CO_2. For co-culture experiments, either $2.5x10^5$ re-aggregated CD166+ or CD166- were plated in square silicon supports (0.03 cm^2, Ibidi). After 4 hours the support was removed and the culture medium was changed the next day. After 3-4 days, $8x10^5$ rat neonatal ventricular myocytes were plated, in a delimited area using a cloning cylinder. The inserts were removed after about 3 hours. Co-cultures were kept in differentiating medium for at least 3-4 days before electrophysiological analysis.

Electrophysiology

For electrophysiology, cells were placed onto the stage of an inverted microscope and were superfused with a physiological solution called Tyrode containing (mM): 140 NaCl, 5.4 KCl, 1.8 $CaCl_2$, 1 $MgCl_2$, 5.5 D-glucose, 5 Hepes-NaOH; pH 7.4. Patch-clamp pipettes had resistances of 5-8 MΩ when filled with the intracellular solution containing (mM): 130 K-aspartate, 10 NaCl, 5 EGTA-KOH, 2 $CaCl_2$, 2 $MgCl_2$, 2 ATP (Na-salt), 5 phosphocreatine, 0.1 GTP (Na-salt), 10 Hepes-KOH; pH 7.2. Spontaneous action potentials were recorded by the patch-clamp technique in current clamp mode using the whole-cell configuration. For each experiment, temperature was kept at 36±1°C. Isoproterenol (Iso), acetylcholine (ACh), nifedipine or Ni^{2+} (Sigma) were added to the Tyrode solutions at the proper concentration from concentrated stock solutions. For voltage-clamp recordings only single cells were used in order to record ion currents and were also added 1 mM $BaCl_2$ and 2 mM $MnCl_2$ to the Tyrode solution to improve dissection of I_f current. To record I_f, from a holding potential of -35 mV a

hyperpolarizing test steps long enough to reach steady-state current activation to the range -45/ -125 mV were applied followed by a steps at -125 mV, which ensures the opening of all channels. The activation curves were obtained from normalized tail currents measured at -125 mV and fitted to the Boltzmann equation:

$$y = 1/\{ 1 + \exp [(V-V½) /s]\}$$

where V is voltage, y fractional activation, $V_{1/2}$ the half-activation voltage, and s the inverse-slope factor.

RESULTS

CD166 is co-expressed with HCN4 during embryonic development of the heart

The data previously obtained in this study presented CD166 expression specifically restricted to SAN-like precursors during ESC *in vitro* differentiation, since $CD166^+$ cells share the characteristic of gene expression of the SAN cells. To support these results, we investigated whether CD166 expression may recognize pacemaker precursors also *in vivo*, during mouse embryonic development.

Here we show CD166 expression pattern in mouse forming heart at embryonic day 10.5 and 12.5. At these days the prospective atria and ventricles are recognizable, as well as the atrio-ventricular canal and the sinus horn, as shown in **figure 14** (**A-D**). The precursors of the SAN and of the conduction system can be identified by the expression of HCN4 pacemaker channel, as already demonstrated in the literature[36]. Therefore, we compared the expression pattern of CD166 and HCN4, to understand whether they co-localize, meaning that are expressed by the same cells. At day 10.5, CD166 and HCN4 signals are almost totally overlapped (**Figure 14, B-C**). Thus, at this stage CD166 seems to be expressed in the cells that will originate the SAN. At day 12.5 instead, although still co-localizing with HCN4 in the prospective SAN region, CD166 expression results pronounced in the ventricles, which are HCN4-negative (**Figure 14, E-F**) and also in some extracardiac tissues and organs, such as the laryngo-tracheal groove, the mid gut, the esophagus, the carotid artery and the descending thoracic aorta (**Figure 15**). These data confirm that CD166 can be used as a transient selection marker for pacemaker cells at early stages of development.

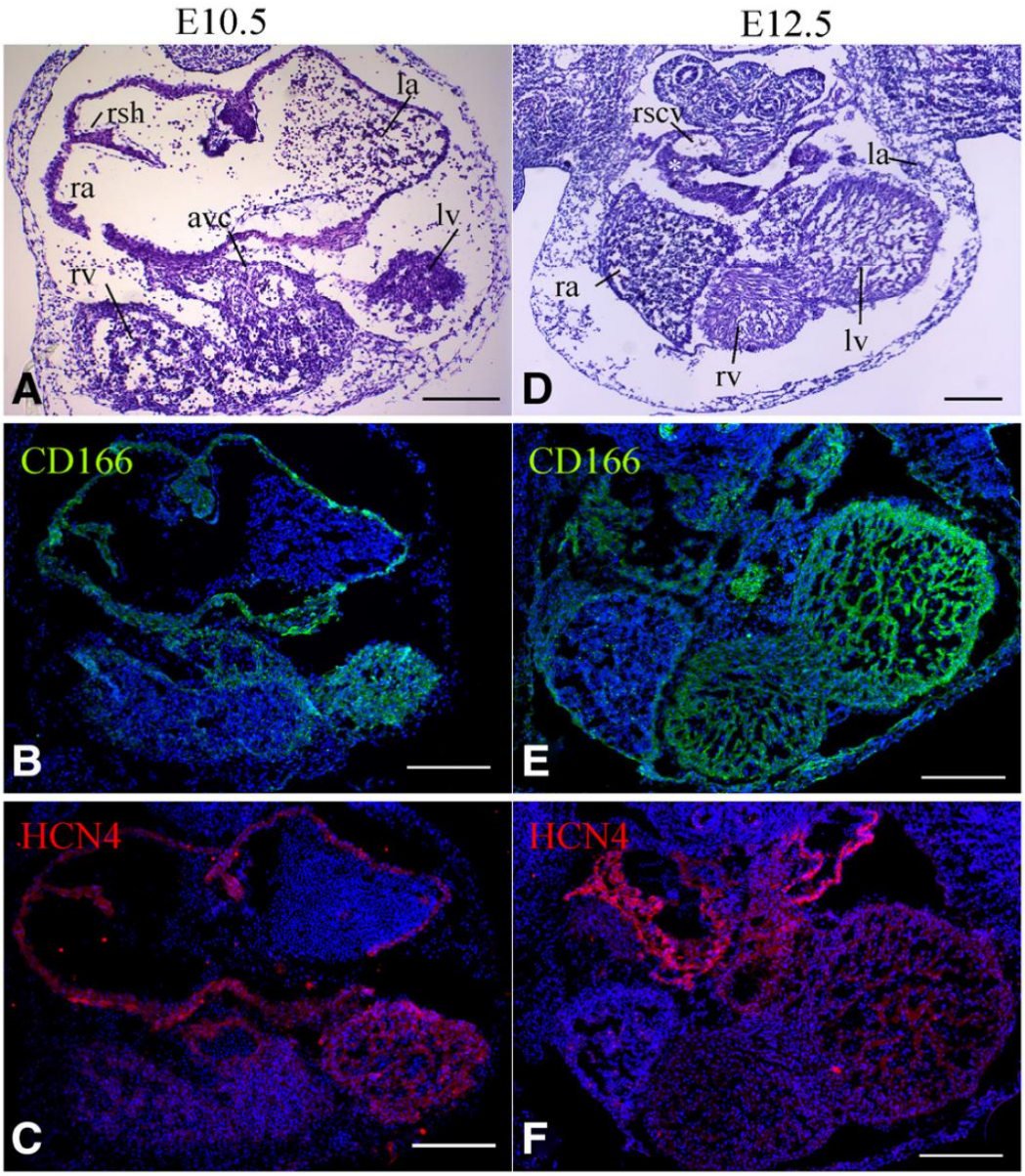

Figure 14: CD166 expression in the developing cardiac conduction system.
Hematoxilin and eosin staining of embryonic day 10.5 (**A**) and embryonic day 12.5 (**D**) hearts. Confocal images of adjacent slices of embryonic day 10.5 (**B, C**) and embryonic day 12.5 hearts (**E, F**) showing the expression of CD166 (green) and HCN4 (red) proteins. Nuclei stained by 4',6-diamidino-2-phenylindole (DAPI) (blue). Calibration bar, 200 μm. Avc, atrioventricular canal; la, left atrium; lv, left ventricle; ra, right atrium; rscv, right superior caval vein; rsh, right sinus horn; and rv, right ventricle.

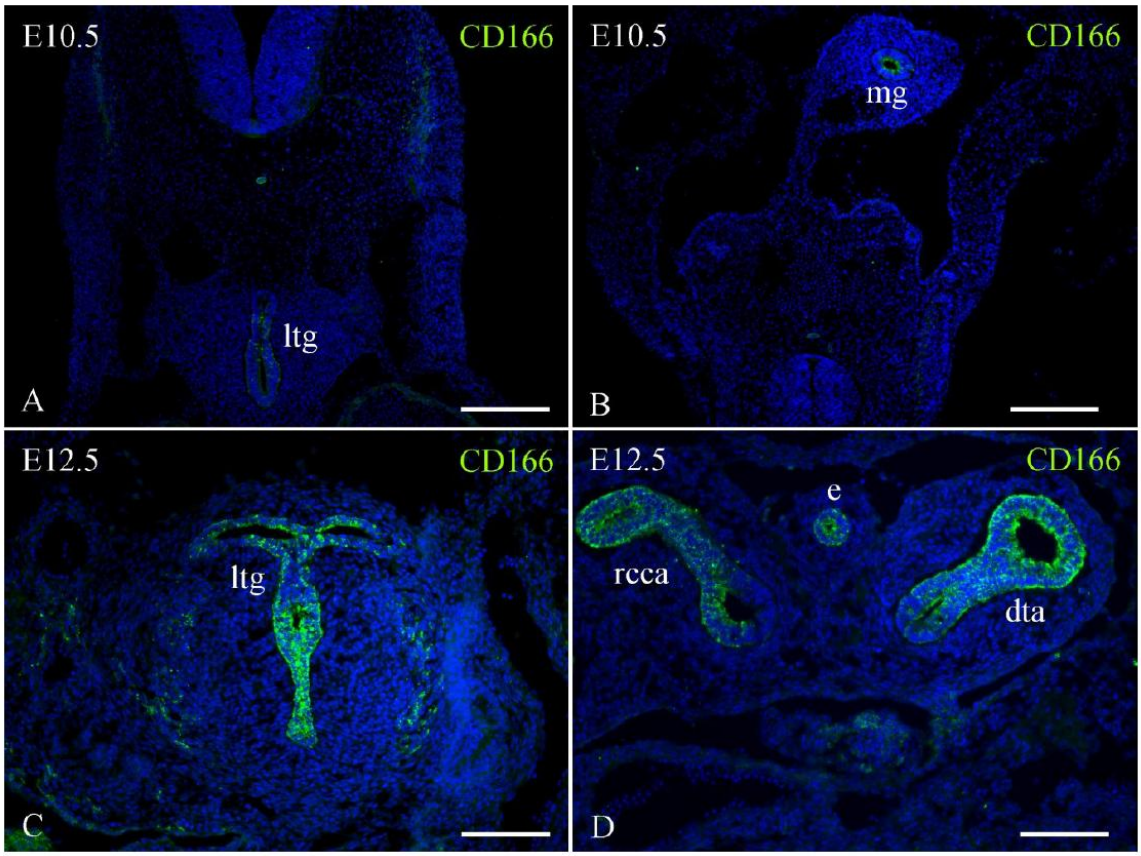

Figure 15: CD166 expression in extracardiac tissues
Confocal images obtained from slices of E10.5 (**A,B**) and E12.5 (**C;D**) embryos showing the expression of CD166 (green) in extracardiac tissues/organs. Ltg, laryngo-tracheal groove; mg, mid gut; e, esophagus; rcca, right common carotid artery; dta, descending thoracic aorta

HCN channels and calcium channels are present and contribute to action potential generation in CD166-selected cells

HCN channels play a pivotal role in slow diastolic depolarization phase, consequently are important for the pacemaker profile of action potentials and thus for the auto-rhythmic activity. HCN1 and HCN4 are the isoforms mostly expressed in the SAN and the expression of HCN2 is sufficient to induce spontaneous activity when injected in the left atrium[96]. Therefore, to functionally characterize $CD166^{+}$ cells, we evaluated the expression of HCN channel at protein level at different stages of culture.

After 1 week of culture HCN1 and HCN4 are both expressed in CD166+ cells together with the cardiac marker α-actinin (**Figure 16, A-B-C, D-E-F**). Instead the

HCN2 signal, which has been shown to be the isoform expressed mainly in the ventricles[113], was not observed in CD166$^+$ (**Figure 16, G-H**); neonatal rat ventricular cardiomyocytes were used as a positive control (**Figure 16I**).

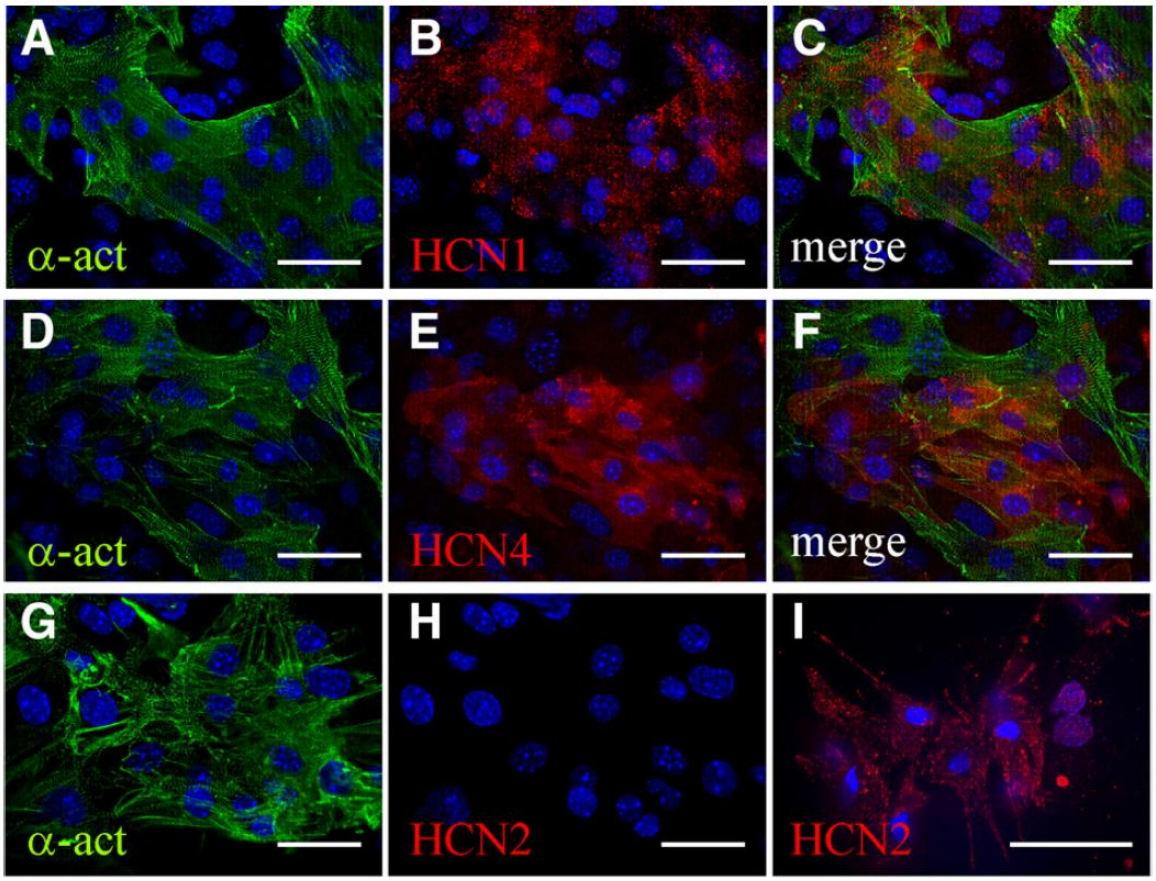

Figure 16: HCN channel expression in CD166-selected cells after 1 week of culture.
Confocal images of CD166-selected cells after 1 week of culture, labeled with the cardiac protein α-actinin (α-act, green) and the various HCN isoforms (red). Neonatal ventricular myocytes were used as positive control for HCN2 staining (**I**, red). Nuclei were stained with DAPI (blue). Calibration bars, 50 μm.

After 3 weeks of culture CD166$^+$ cells assume characteristics that make them more similar to adult SAN cells, in agreement with the gene expression analysis performed before. Firstly, the morphology of CD166$^+$ cells results very similar to that of SAN cells in culture (**Figure 17, A-B**). From immunofluorescence staining we can notice that they still express HCN4 protein and, as the mature SAN cardiomyocytes, the expression of this channel co-localize with the expression of caveolin-3 (cav3) (**Figure 17, C-D-E**), which determines the formation of functional

membrane microdomains[7]. In addition, the expression pattern of HCN4 expression in 25-day-old CD166-derived aggregates resembles that observed in adult SAN slices (**Figure 17, F-G**).

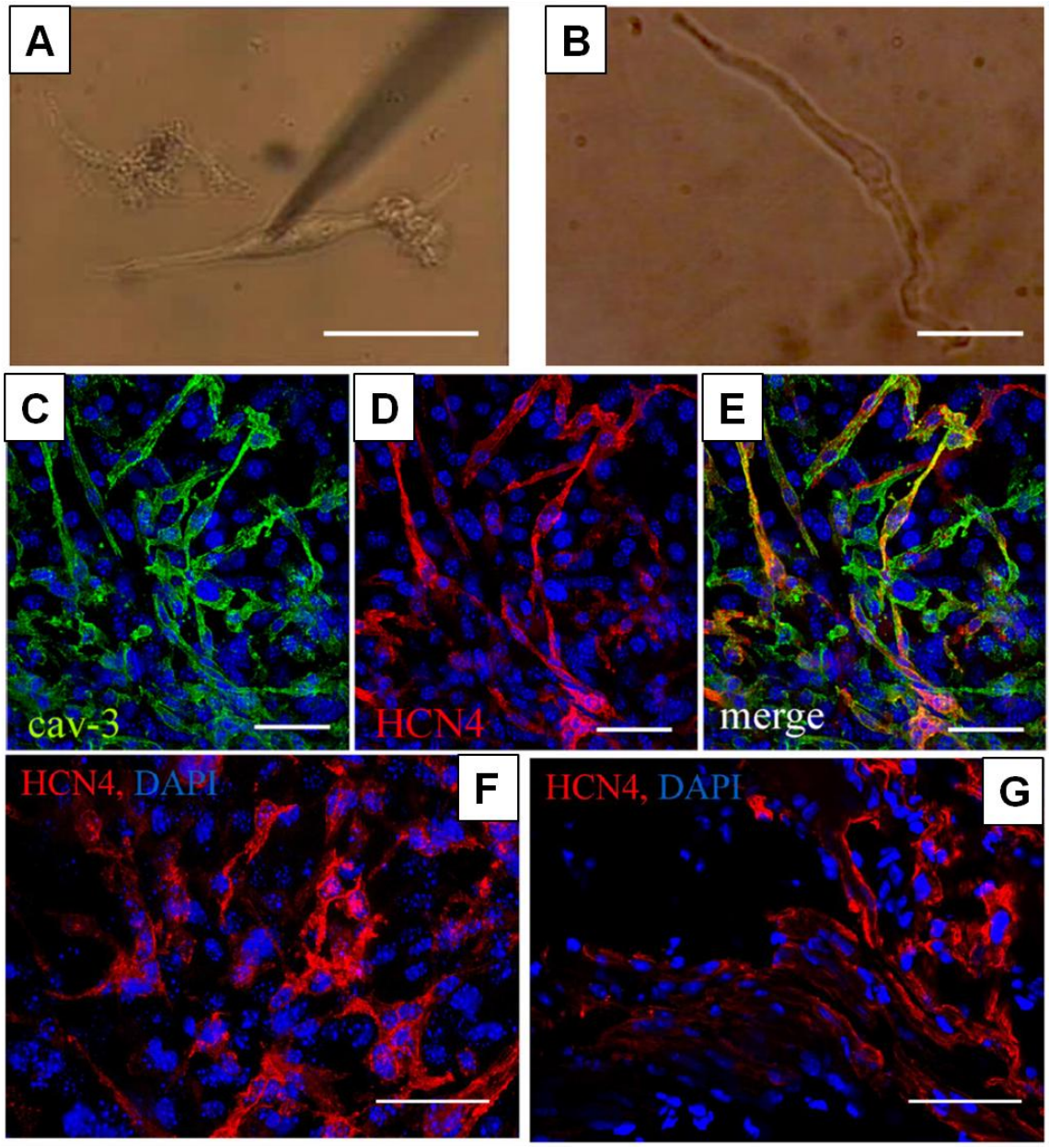

Figure 17: HCN4 channel expression in CD166-selected cells compared to SAN cells.
Phase contrast images of a single CD166-derived cell 25 days after cell sorting (**A**) and of an acutely dissociated mouse sinoatrial node cell (**B**). **C-E**: Confocal images of CD166-selected cells after 3 weeks in culture, labeled with either the cardiac protein caveolin-3 (cav-3, green) and HCN4 (red). Nuclei were stained with DAPI (blue). Calibration bars, 50 µm. Confocal images of a 25 day-old CD166-selected cell aggregate (**F**) and of a mouse SAN slice (**G**) labeled with an antibody anti-HCN4 (red). Nuclei were stained with DAPI. Calibration bars 50 µm.

These data show that HCN channel isoforms characteristic of the SAN are expressed in CD166-selected cells. However, this is not sufficient to affirm that these channels are also functional. For this reason, we also analyzed the I_f current by electrophysiological measurements, at the same stages of culture considered before (1 week and 3 weeks). We were able to record the I_f in cells of both stages of maturation, demonstrating that the expressed HCN channels are also active (**Figure 18A**). Furthermore, we compared the properties of the I_f current recorded from $CD166^+$ cells with that recorded from adult SAN cells. From the current traces recorded we generated the activation curves and compared the voltages of half activation (**Figure 18B**). In 1-week-old CD166-derived cells the $V_{1/2}$ was -77.4±2.4 mV, while in 3-week-old cells it was -73.4±1.2 mV. These values were similar to that of native mouse SAN cells, which presents a $V_{1/2}$ of -73.6±1.4 mV.

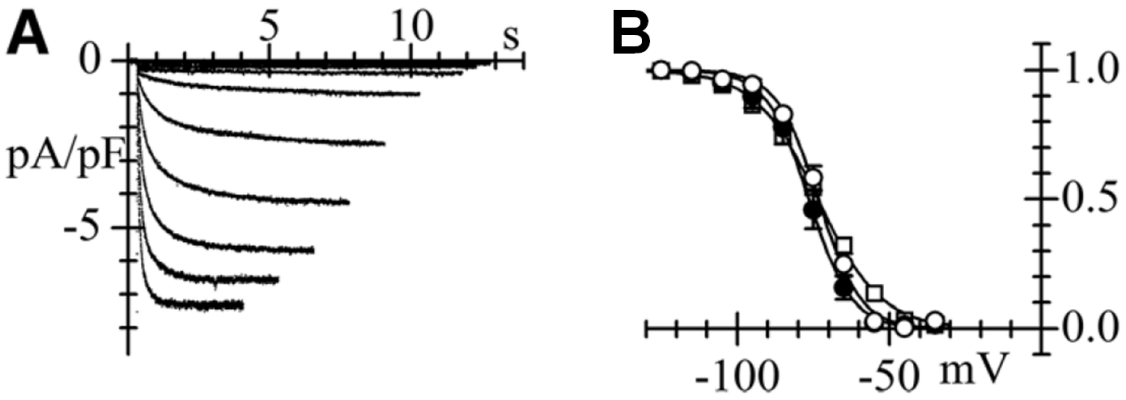

Figure 18: Functional comparison of I_f current between CD166-selected cells and SAN myocytes. **(A)** Representative I_f traces recorded from single CD166-selected cell after 1 week in culture; **(B)** Mean activation curves obtained from CD166-selected cells after 1 (filled circles) and 3 weeks (open circles) in cultures and from mouse SAN myocytes (open squares); lines represent the best fitting by the Boltzmann equation.

Other channels important for the generation of pacemaker action potentials are the calcium channels. Specifically, in mouse SAN L-type calcium channels are responsible together with Na^+ channels for the fast depolarization phase while T-type calcium channels contribute to the final part of the slow diastolic depolarization phase. Thus, we evaluated their contribution to the spontaneous

activity of CD166-selected cells cells. During action potential recordings, we superfused alternatively the L-type calcium channel blocker nifedipine (0.1 μM) or the T-type calcium channel blocker Ni^{2+} (50 μM). The partial block of these calcium currents is expected to produce an overall decrease in the firing rate. The effect of both blockers on the spontaneous activity of CD166-derived cells is shown in **figure 19A**. The treatment with nifedipine and Ni^{2+} caused on average a rate decrease of 16.9±6.4% and of 17.7±2.6%, respectively. Interestingly, these reductions were comparable to those obtained with the perfusion of same blockers on mouse SAN cells (**Figure 19B**), where the nifedipine caused a decrease in the rate of 16.5±2.2% and Ni^{2+} caused a decrease of 21.6±7.5%. These data show that calcium channels are functionally active in CD166-selected cells and their contribution is comparable to that of the same channels in SAN cardiomyocytes.

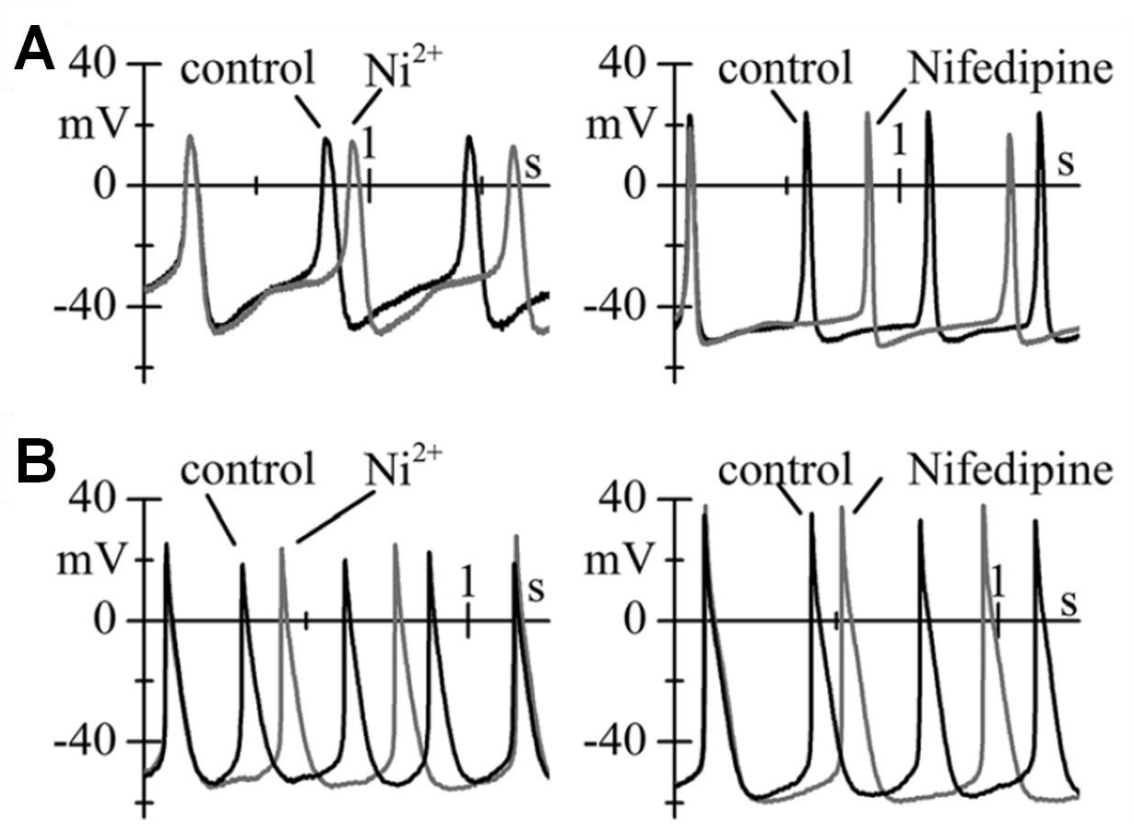

Figure 19: Functional comparison of action potentials between CD166-selected cells and SAN myocytes.
Representative action potentials recorded from CD166-selected cells (**A**) and SAN cells (**B**) in control (Tyrode) and during superfusion of either 50 μMNi2+ or 100 nM nifedipine.

The spontaneous activity of CD166-selected cells is maintained in culture for long periods (3-4 weeks), as observed in the previous part of this study. Here, after recording action potentials at different stages of culture, we found that on average $CD166^+$ firing rate increases during time in culture (**Figure 20**), starting from approximately 1.5 Hz at 2-4 days in culture and reaching 6 Hz at 20-22 days. This increase in the rate is similar to that occurring during mouse embryonic development[136] and is thus consistent with a maturation of the CD166-derived cardiomyocytes.

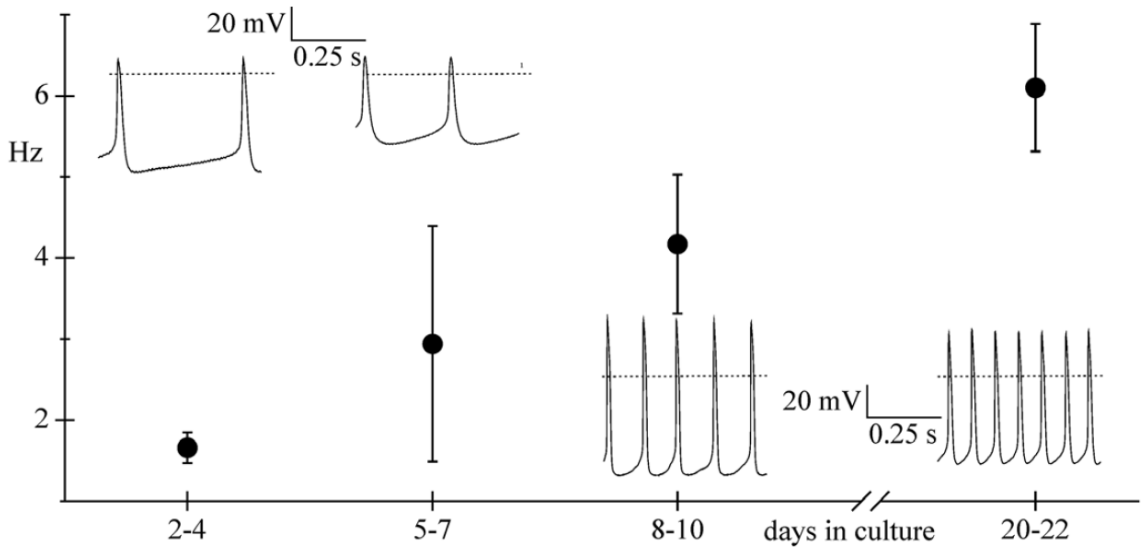

Figure 20: Autorhythmic activity of CD166+-derived cells.
Mean rate calculated from spontaneously beating CD166-selected cells at different time points in culture; insets show representative action potential traces.

CD166-selected cells are able to respond to nervous system stimuli

An important feature of the SAN is the ability to respond to autonomic nervous system stimulation, so that the heart rate can be modulated depending on the situation or condition that the body is experiencing. This modulation is achieved thanks to the activation of the signal transduction pathway initiated by the adrenergic and muscarinic receptors expressed on the plasma membrane of SAN cardiomyocytes. To investigate whether these receptors are also present on CD166-selected cells, we double-stained them with anti-β_1-adrenergic, anti-β_2-adrenergic, or

anti-M2-muscarinic receptors together with the cardiac markers cav3 or α-actinin. The confocal images shown in **Figure 21A** demonstrate that these receptors are indeed expressed. Then we further investigated the response ability by analyzing the rate response to perfusion of the β-adrenergic agonist, isoprotenerol (1 μM), or of the muscarinic agonist, acetylcholine (0.1 μM). We recorded the spontaneous action potentials and found that upon isoprotenerol treatment the firing rate increased on average by 56.9±8.0% (n=5) while upon acetylcholine treatment it decreased by 22.9±5.4% (n=3), compared to the rate of the same cells in the control solution (**Figure 21B**).

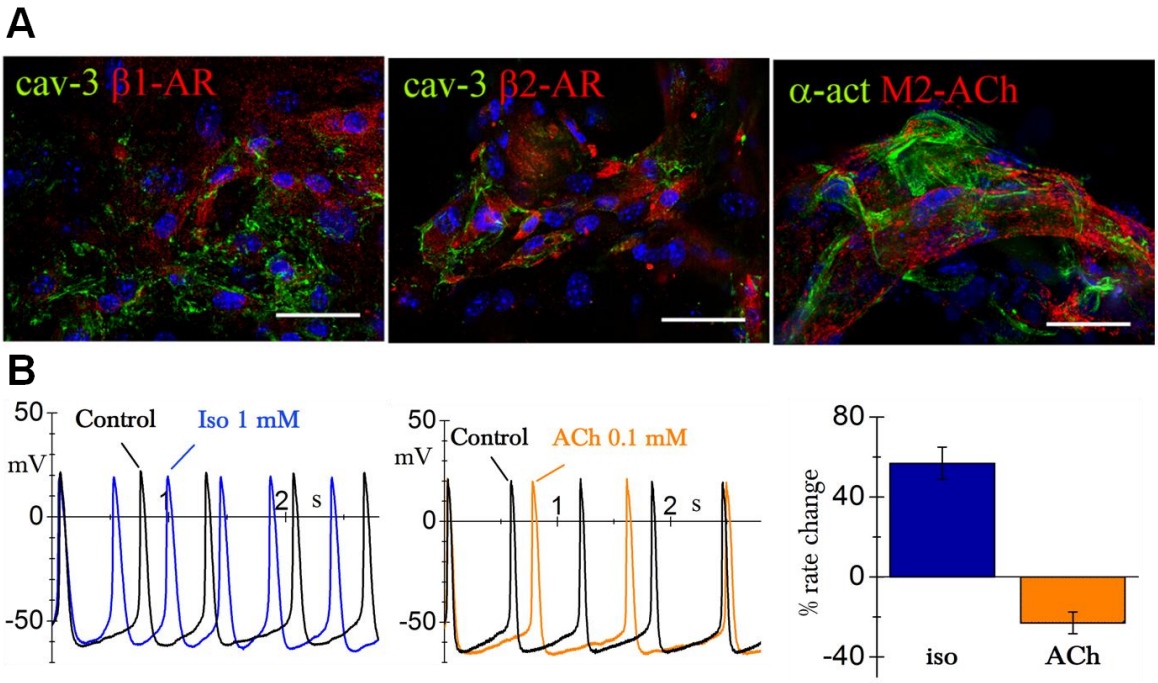

Figure 21: Autonomic modulation of the activity of CD166-selected cells.
(**A**) Confocal images showing coexpression of caveolin-3 with β1-adrenergic and β2-adrenergic receptors and of α-actinin with M2 muscarinic receptors. Nuclei were stained with DAPI. Calibration bars,50 μm. (**B**) Spontaneous action potentials recorded during control and during perfusion of 1 μmol/L isoproterenol (Iso) and 0.1 μM acetylcholine (Ach) from CD166-selected cells; the bar graph shows the mean rate changes caused by the autonomic agonists.

CD166-selected cells can connect to and pace co-cultured neonatal ventricular cardiomyocytes

To definitively identify CD166-selected cells as SAN-like cells, they need to really function as a pacemaker, that is they should be able to connect to and pace an excitable cardiac substrate. We evaluated the pacemaker ability of CD166-selected cells by co-culturing them with neonatal rat ventricular cardiomyocytes (NRVMs). We plated NRVMs either on top of aggregates derived from $CD166^+$ or $CD166^-$ cells. In the same dishes, part of the NRVM were plated alone, not in contact with CD166-selected cells (**Figure 22A**).

To test whether CD166-selected cells can connect to NRVMs, we evaluated connexin 43 (Cx43) expression in the co-cultures. We used ESC engineered clones expressing the GFP under HCN4 promoter, so that CD166-selected cells were recognizable from the co-cultured NRVMs. Cx43 (red) and GFP (green) staining shown in **figure 22B** demonstrates that Cx43 is expressed both in GFP^- NRVM and GFP^+ CD166-selected cells, in particular at the cell-to-cell contact points (white arrows). This suggests that these cells are able to connect to each other.

After 3-4 days of coculture, necessary to form proper cell-to-cell electrical connections, action potentials were recorded. **Figure 22C** shows representative traces recorded from NRVMs alone or from NRVMs in co-culture with $CD166^+$ cells. It is evident that NRVMs co-cultured with $CD166^+$ cells have a higher and more regular rate than NRVMs cultured alone. The firing rate remained instead slower and more irregular in NRVMs co-cultured with non-beating $CD166^-$ cells (data not shown). On average, NRVMs in co-culture with $CD166^+$-derived cells had a rate of 1.7±0.19 Hz (n=5), while NRVMs cultured alone or with $CD166^-$ derived cells presented a significantly lower rate, on average 0.84±0.09 Hz (n=7) and 0.82±0.17 Hz (n=6), respectively. This higher rate demonstrate the capacity of $CD166^+$ to drive the rate of the NRVMs.

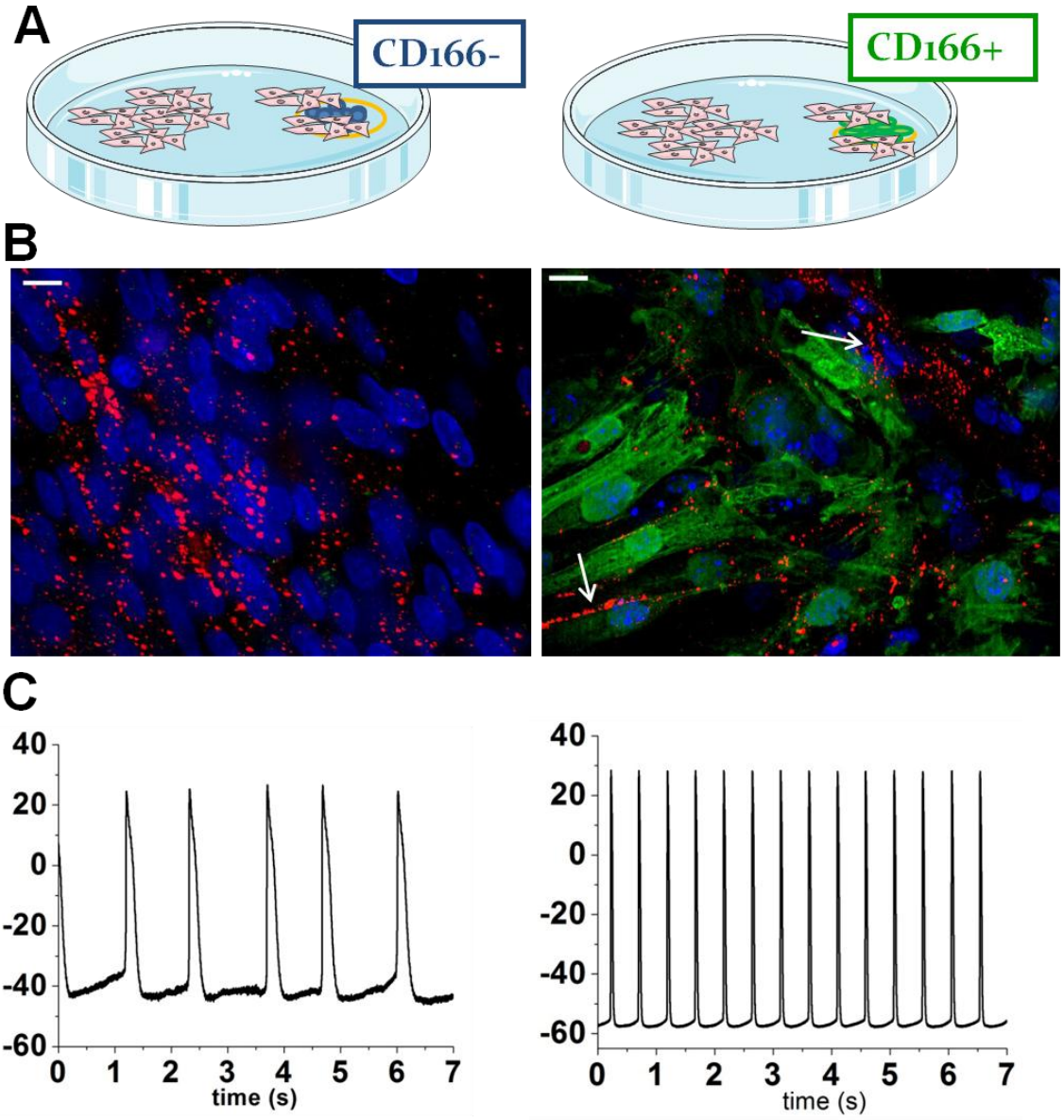

Figure 22: Co-culture of CD166-selected cells and NRVMs.
(**A**) Cartoon of the co-culture system, with NRVMs plated on either CD166$^-$ or CD166$^+$ cells or in a distal area of the dish. (**B**) Confocal images of NRVMs cultured alone (left) or in co-culture with CD166-selected cells (right) stained for Cx43 (red). CD166-selected cells are also stained for GFP. White arrows indicate the cell-to-cell contact point. Nuclei were stained with DAPI. Calibration bar 10 µm. (**C**) Spontaneous action potentials recorded from NRVMs cultured alone (left) or in co-culture with CD166-selected cells (right) in control solution.

CD166 is expressed in differentiating human iPSCs

Even though the data collected so far clearly demonstrate that it is possible to generate SAN-like cells from mouse ESC, the main challenge of our study is to

translate this selection strategy to a human substrate, determining whether CD166 is a good marker also for human SAN precursors.

First of all, we started a collaboration with the group of Prof. Dell'Era from University of Brescia, in order to obtain a pluripotent human substrate, the hiPSCs. We performed in vitro cardiac differentiation of hiPSCs, following the spontaneous differentiation protocol[23] (**Figure 23A**). We obtained auto-rhythmic beating clusters and were able to keep them in culture for long periods (from 30 to 60 days). The mature hiPSC-derived cardiomyocytes were characterized for the expression of cardiac markers, such as α-actinin and cardiac troponin (**Figure 23B**).

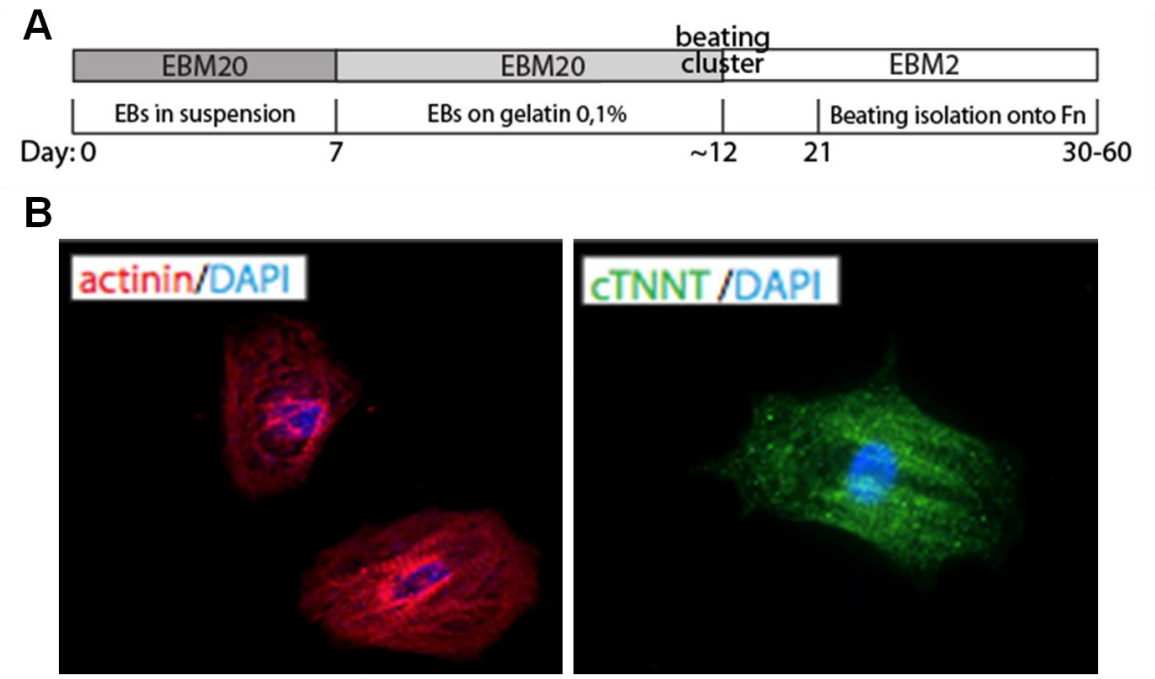

Figure 23: Cardiac differentiation of hiPSCs.
(**A**) Schematic time-course of the hiPSC differentiation protocol. Beating cluster are seen starting form day 12. (**B**) Confocal images of hiPSC-derived cardiomyocytes stained with α-actinin (red) or cardiac troponin T (green). Nuclei were stained with DAPI.

We then investigated the expression of human CD166 in our *in vitro* system. Although CD166 is expressed in human ESC- and iPSC-derived cardiomyocytes[61,105], in human fetal heart[61] and during endodermal differentiation of hiPSCs, its expression at different stages of spontaneous iPSC cardiac

differentiation has not been described. For this reason, we evaluated here by flow cytometry the percentage of CD166-positive cells during hiPSC *in vitro* differentiation.

We started analyzing the undifferentiated hiPSCs and found high percentage of $CD166^+$ cells (64,9%). **Figure 24A** shows an example of the cell sorting. We then evaluated the percentage of $CD166^+$ cells at different days of differentiation. From a first analysis it appears that a decrease of $CD166^+$ cells during the early days of differentiation occurs (day 11 = 12,7±4,7%), while afterwards a progressive increase can be observed (day 15= 21,7% day 20 = 25,4%; day 34 = 38,4±0,8%) (**Figure 24B**). This seems comparable to what occurs in mouse ESC differentiation, suggesting that the early days may be the more suitable for the selection of pacemaker precursors.

In any case, these are preliminary results and we need to evaluate in $CD166^+$ cells also the expression of a cardiac marker, such as α-actinin, to better identify the proper selection day.

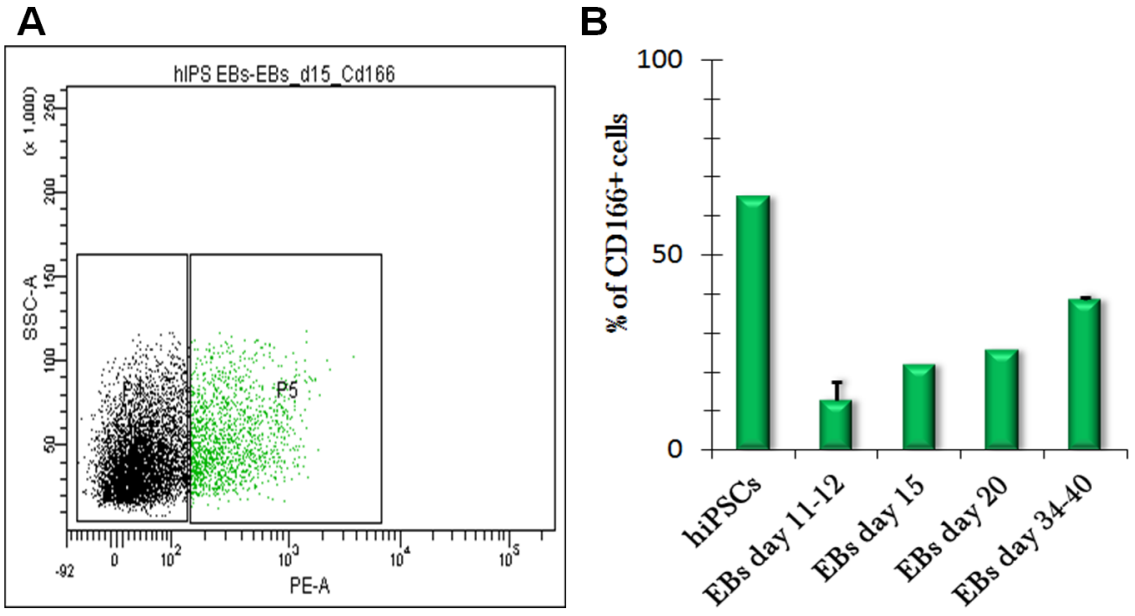

Figure 24: Flow cytometry analysis of $CD166^+$ cells during hiPSC differentiation.
(**A**) Representative dot plot from flow cytometry analysis of dissociated EBs, showing $CD166^-$ (black, P4) and $CD166^+$ populations (green, P5) at day 15 of hiPSC cardiac differentiation. (**B**) Bar graph displaying the mean percentage of $CD166^+$ cells in undifferentiated hiPSCs and at different days of differentiation.

DISCUSSION

The isolation of stem cell-derived cardiomyocytes sharing the characteristics of SAN cells appears of great relevance for different reasons. One important application is the generation of a cell substrate that can be implanted in patients, pace resident cells and restore the correct heart rhythm; that is the biological pacemaker. This results a particularly actual issue firstly because the electronic pacemaker currently in use present several still unresolved limitations[39,46]. Besides, the implantation rate of electronic pacemaker is growing in the recent years and is expected to further grow in the next years due to population ageing. Importantly, a biological pacemaker generated through this cell-based strategy not only can integrate in the tissue better than an electronic device, but also avoids modifications in the cell genome of the patient, thus it appears more controllable and suitable for clinical applications.

Another advantage arising from isolation of stem cell-derived pacemaker cells is the possibility of *in vitro* studies on autorhythmic mature cells that can be kept in culture for long periods, in order to test drugs acting on cardiac rhythm.

Because stem cell differentiation give rise to cells at various stages of differentiation and also at different cell types[7], one of the major challenges in obtaining a homogeneous population of stem cell-derived pacemaker cells is the selection method.

Previously, other researchers had attempted selecting SAN-like cells upon ESC differentiation, using HCN4 as a marker. This channel mediates the I_f current which is the main responsible for the slow diastolic depolarization phase of SAN cell spontaneous action potentials. Although HCN4 is expressed at high levels in SAN cells, extracellular antibody against this channel are not available. Thus, the selection of $HCN4^+$ living cells must involve a manipulation of cell genome, as performed in the study of Morikawa *et al.*. engineering ESCs for the expression of EGFP under HCN4 promoter[81]. Moreover, HCN4 is not only expressed in SAN

precursors but also in neuronal cells[36], and indeed in the same study the 65% of the HCN4-selected population expressed the neuronal marker Nestin and, not surprisingly, lacked spontaneous beating[81].

A more recent attempt of pacemaker cell selection used TBX3 overexpressing ESCs stably transfected with antibiotic resistance under Myh6 promoter[50]. Notably, Myh6 is the atrial-specific isoform and it was shown not to play a fundamental role in conduction system formation[33], thus this selection method appears controversial. Nonetheless, this antibiotic-based selection yielded 80% of pacemaker cardiomyocytes, stable in culture for several weeks[50]. However, also in this study they used engineered cells, which are less appropriate for clinical applications.

Although very useful for *in vitro* studies, these data underlie the need of alternative selection methods to build a biological pacemaker that can be really addressed to humans. A promising approach is based on endogenous cell surface markers expressed during stem cell differentiation. Until now, two markers have been shown to be expressed both in the developing heart and in ESC-derived cardiomyocytes: CD166 (or ALCAM)[61,105,109] and CD172a (or SIRPA)[29]. SIRPA is however expressed also in the adult heart, in both atria and ventricles, ruling against its possible use as a selection marker for pacemaker cells.

Here we selected pacemaker cells based on CD166 expression. This molecule has been previously used to select cardiovascular precursors from yolk sac, observing that cardiac cells originate from $CD166^{+}/Flk1^{-}$ precursors[84]. In agreement with this evidence, our $CD166^{+}$ cells did not express Flk1[109]. Recently, Rust *et al.* used CD166 to enrich in cardiomyocytes human ESC-derived cells[105]. They affirmed that the CD166-selected cells present an embryonic phenotype based on ion channel and structural protein expression, while our data on $CD166^{+}$ cells showed that they exhibit functional features of mature SAN cells (**Figure 1**).

We observed in CD166-selected cells maintained in culture for 3 weeks a morphology similar to SAN cells and the expression of the SAN-restricted HCN4

isoform not only at transcript but also at protein level, with a pattern similar to that found in the adult SAN (**Figure 17**).

The capability to generate SAN-like action potentials was then demonstrated by the functional presence of the main currents characterizing the heart conduction system. I_f current was recorded and its activation curve completely overlapped the one obtained in mouse SAN cells (**Figure 18**). This current can be also modulated by nervous system, thanks to the expression in our CD166-selected cells of β-adrenergic and muscarinic receptors, whose activation causes the stimulation or inhibition of cAMP synthesis respectively. The cAMP binding modifies HCN4 open probability influencing slow diastolic depolarization phase and thus firing rate[17]. Indeed we observed in CD166-selected cells an increase or a decrease in firing rate after adrenergic or muscarinic agonist administration, respectively (**Figure 21**). The effects observed are comparable to the effects reported in the literature on mouse SAN cells[3]. Furthermore, functional presence of I_{CaL} and I_{CaT} currents, involved in the slow and fast depolarization phases of pacemaker cell action potential, was observed following the administration of their respective blockers causing a decrease in firing rate, totally similar to that produced in the SAN cells (**Figure 19**).

Beside sharing characteristics of the SAN profile, the action potential firing of our CD166-selected cells also increased in the rate during time in culture, further attesting the maturation of $CD166^+$ cells (**Figure 20**). Importantly, we also demonstrated that our CD166-selected cells are able to electrically connect with other excitable cells and are also able pace other cells in co-culture imposing their faster beating rate, thus playing the pacemaker role similarly to the SAN (**Figure 22**).

These features are compatible only with a differentiated and mature phenotype. In agreement with this, our $CD166^+$ cells present negligible levels of proliferation and did not form teratomas *in vivo*. Instead, the CD166-selected cells of Rust *et al.* showed a high proliferation rate (20-30%)[105]. The clear differences between the

result of our selection and that of Rust *et al.* can derive from the different protocols used. In particular, their selection was operated at the peak of CD166 expression, while our selction was done at the differentiation day corresponding to the peak of α-actinin expression in $CD166^+$ cells. Notably, data from the literature showed that CD166 is specific for cardiomyocytes only in a determined time-window[43,84]. Here we have further strengthened this concept showing that in mouse embryos CD166 is co-expressed with HCN4 in the prospective SAN by embryonic day 10.5, but by day 12.5 CD166 expression broadens also to other regions and organs (**Figure 14**). Therefore, it appears important to compare CD166 expression with that of a cardiac marker, as we did using α-actinin, in order to avoid contamination of other lineage precursors. Nevertheless, the work of Rust *et al.* importantly showed that CD166 is expressed during hESC cardiac differentiation, thus opening the prospective of using this marker to select pacemaker cells also from human EBs.

More recently, also Lin *et al.* have used CD166 for cardiomyocytes selection during human stem cell differentiation[61]. They analyzed the expression of CD166 at mRNA level during hiPSC differentiation and showed that CD166 is expressed in undifferentiated hiPSCs, the expression decreases at the beginning of differentiation, increasing again by differentiation day 6 and remaining almost constant for the rest of the differentiation protocol. Lin *et al.* selected cardiomyocytes at differentiation day 20, when atrial and ventricular markers were already expressed, thus the differentiation was already advanced to the working myocardium fate.

Here we assessed whether through an early selection of $CD166^+$ cells it is possible to obtain pacemaker precursors, thus translating our isolation method accomplished in mouse cells to a human substrate. Clearly the possibility to isolate human SAN-like cells would be of great interest and would be a step forward in the project of generating a feasible biological pacemaker with clinical applications. We differentiated hiPSCs into cardiomyocytes following the spontaneous differentiation protocol (**Figure 23**). Analyzing $CD166^+$ cell percentage during

differentiation, we also found high fraction of CD166-expressing hiPSCs (64,9%). At day 11 of differentiation however the percentage of $CD166^+$ cells appears much lower (12,7%). This seems comparable to the trend of CD166 mRNA levels found in the initial phase by Lin *et al.*[61]. However, the differentiation protocol used by Lin *et al.* did not consist in a spontaneous differentiation through EB formation, but differentiation was induced adding specific factors to the culture medium and operating various subsequent selection steps by flow cytometry. These differences in protocol method and timing cannot permit a proper comparison. Notably, although Lin *et al.* protocol results much less time-consuming, forcing the differentiation toward cardiovascular cell types may produce disadvantages as well. Possibly, the differentiating cells could maintain for shorter time the primitive phenotype of pacemaker precursors, thus the proper time-window for CD166-based pacemaker cell isolation may result anticipated or reduced. For these reasons, we consider more suitable for our aims to use the spontaneous differentiation protocol.

From day 11 of our differentiation protocol, the percentage of $CD166^+$ cells increased steadily and at day 34-40 of differentiation it was approximately 40%. This increasing of $CD166^+$ fraction is consistent with the trend previously observed during mouse ESC differentiation (**Figure 1**). The percentage of $CD166^+$ cells at the day of selection in mouse cells was around 10-15%. Here during hiPSC differentiation, a similar percentage was observed at day 11-12. We can then speculate that day 11-12 may represent a suitable day for pacemaker precursors selection during hiPSC differentiation. Anyway, to better identify a suitable selection day based on CD166 expression we believe that it would be important to evaluate also a cardiac marker expression, as pointed out before. Unfortunately this was not possible in the experiments performed here, due to the less efficient differentiation of hiPSCs compared to that of mouse ESCs, producing not enough cells for subsequent gene expression analysis. Next experiments will focused on increasing the amount of cells available upon differentiation. In addition, it remains

to be elucidated whether the human CD166-selected cells are able to re-aggregate and spontaneously beat in culture after the cell sorting, as did mouse CD166^{+} cells. In conclusion, with this study we functionally characterized mouse CD166-selected cells, showing that they behave like SAN cells, are able to respond to autonomic stimulation and are able to act as a pacemaker *in vitro*. We also began using a human cell substrate, with the aim of adapting our selection protocol on human differentiating iPSCs. Showing that CD166 is expressed during differentiation not only of mouse ESCs but also of hiPSCs opens the possibility to isolate hiPSC-derived pacemaker cells, that can be really used for the generation of a patient-specific biological pacemaker.

PART II:

FUNCTIONAL ANALYSIS OF M54T MIRP1 MUTATION FOUND IN A PATIENT WITH IDIOPATHIC EPILEPSY

FOREWORD

Aim and relevance of the project

This project aims to find and functionally characterize genetic mutations in idiopathic epileptic patients, in order to provide mechanistic explanation of the disease and possibly test specific treatments for reverting the functional effects. Remarkably, the idiopathic epilepsy is the form associated with a genetic etiology[64], thus the phenotype of these patients is probably due to some mutations in their genome. Although some mutations have been related to epilepsy, none of them showed a co-segregation with the pathological phenotype, thus further investigations are needed to identify the causative dysfunction leading to the disorder.

In this project, we focused in particular on HCN channels as candidates to be altered in epileptic patients, since there are more and more evidence in the literature linking these channels to epilepsy[25,28,65,85,108,119]. Few years ago our group started a genetic screening on a population of 185 patients affected by idiopathic generalized epilepsy and 209 controls, analyzing both HCN channel and their accessory protein genes (caveolin3, MiRP1, TRIP8b, filamin A) . In this study only patients who had a familiar history of epilepsy were enrolled. After the screening, we selected mutations that caused a non-synonymous aminoacid variation in the protein. From this screening emerged for example the novel mutation E515K in the HCN2 gene. The electrophysiological characterization revealed that the E515K mutation had a loss of function phenotype caused by a large negative shift of the channel's activation, outside the physiological range of voltages. Expression of the wt or the E515K mutant in rat neonatal neurons demonstrated also that the mutation significantly increased membrane excitability[28].

During the last year of my PhD I have analyzed the functional effect of the M54T mutation of MiRP1 on HCN channel properties and more generally on neuronal excitability. This mutation was indeed found in heterozygosis in a patient with

idiopathic generalized epilepsy and in her daughter, who was affected by febrile seizures (**Figure 25**). The M54T mutation involves the transmembrane region of the peptide, causing a change from a nonpolar to a polar aminoacid. This mutation was previously found by Nathawe *et al.*, in a cardiopathic individual with Long-QT syndrome and sinus bradycardia. Because of the known interaction of MiRP1 with HCN channels and the bradycardia, they focused their attention on the effects of M54T MiRP1 on HCN channels, co-expressed in neonatal cardiomyocytes. Nathawe *et al.* showed that M54T mutation caused a 80% decrease in HCN4, but not HCN2, current density and caused also a slowing in the activation kinetics of both HCN4 and HCN2[86] only in a restricted range of voltages.

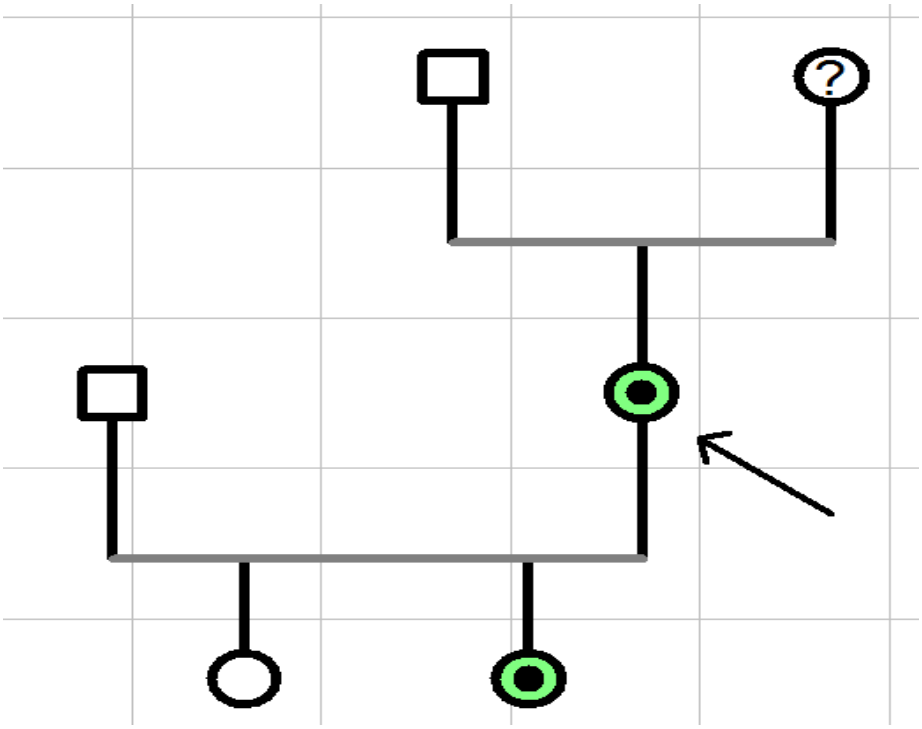

Figure 25: M54T mutation in a family genetic tree.
The scheme shows women as circles and men as squares. The arrows indicates the proband. In green the individuals affected by some form of epilepsy. The filled circle identifies individuals carrying M54T mutation.

Because it is known from the literature that MiRP1 deletion in the brain causes alteration of HCN channel properties and increases neuron excitability, we

hypothesized that the functional interaction of M54T MiRP1 with HCN channels could be possibly involved in the generation of the epileptic condition.

For these reasons, we decided to functionally analyze the effects of M54T MiRP1 mutation, and especially the possible effect on HCN2 and HCN4 channels properties. The strategy was to overexpress HCN channels and the WT or mutated MiRP1 in a heterologous cellular system previously used to assess the functional effect of MiRP1 on HCN channels, and then to analyze the electrophysiological properties of HCN2 and HCN4 currents. Among HCN channel isoforms, we considered HCN2 and HCN4, because an effect of the mutation was already observed on these channels[86]; besides, HCN2 is the most expressed in the brain, while HCN4 plays a pivotal role in the thalamic oscillations[10,110].

Since the effects of MiRP1 as accessory subunit have been shown to vary significantly depending on the cell type used, we subsequently assessed the effect of the mutation in a neuronal context. Here we also evaluated the effect of the mutation on neuronal excitability.

INTRODUCTION

The HCN channels in the central nervous system

HCN channels are cation channels activating upon membrane hyperpolarization, as already described in the first part of this thesis. They are expressed not only in the heart but also, importantly, in the central nervous system (CNS). In particular, in the brain HCN1 is found in the neocortex, in the cerebellar cortex, in the hippocampus and in the brain stem; HCN2 is expressed almost ubiquitously in the brain, but especially in the thalamus and in the brain stem nuclei. HCN4 expression is instead generally low in the CNS, except for the thalamic nuclei and the olfactory bulb, where high levels are found[80,89,107,110].

The I_f current mediated by HCN channels is also called I_h in the CNS, because of its activation in hyperpolarization. In the brain, it was first discovered in hyppocampal pyramidal neurons and named initially "queer" current[40] (I_q). Also in some regions of the CNS, such as in thalamocortical neurons, in the inferior olive neurons of the brainstem and in hippocampal striatum oriens interneurons, I_h can act as a pacemaker current, thus inducing spontaneous activity[99]. In the thalamocortical neurons, regularly spaced short firings are observed when they are hyperpolarized, in physiological condition during non-REM sleep or in pathological condition during absence seizures[8]. This action potential profile is named the "burst mode" and has been associated to a decrease transfer of information to the cortex[115]. In this mode, the activation of I_h by hyperpolarization sustains the phase of slow depolarization that activate T-type calcium channels, which in turn further depolarize the membrane reaching the threshold for action potential firing (**Figure 26**). The consequent inactivation of T-type calcium channels terminates the spike and since at those voltages HCN channels are closed, a subsequent hyperpolarization occurs, which in turn leads to the re-opening of HCN channels and therefore to the begin of another cycle. Interestingly, HCN2 KO mice have a higher susceptibility to fire in the burst mode upon an excitatory input, than wild-type animals[65], possibly because they have a more hyperpolarized resting

membrane potential (RMP); this implies that less T-type calcium channels are in the inactive state and thus they are more easily activated[10].

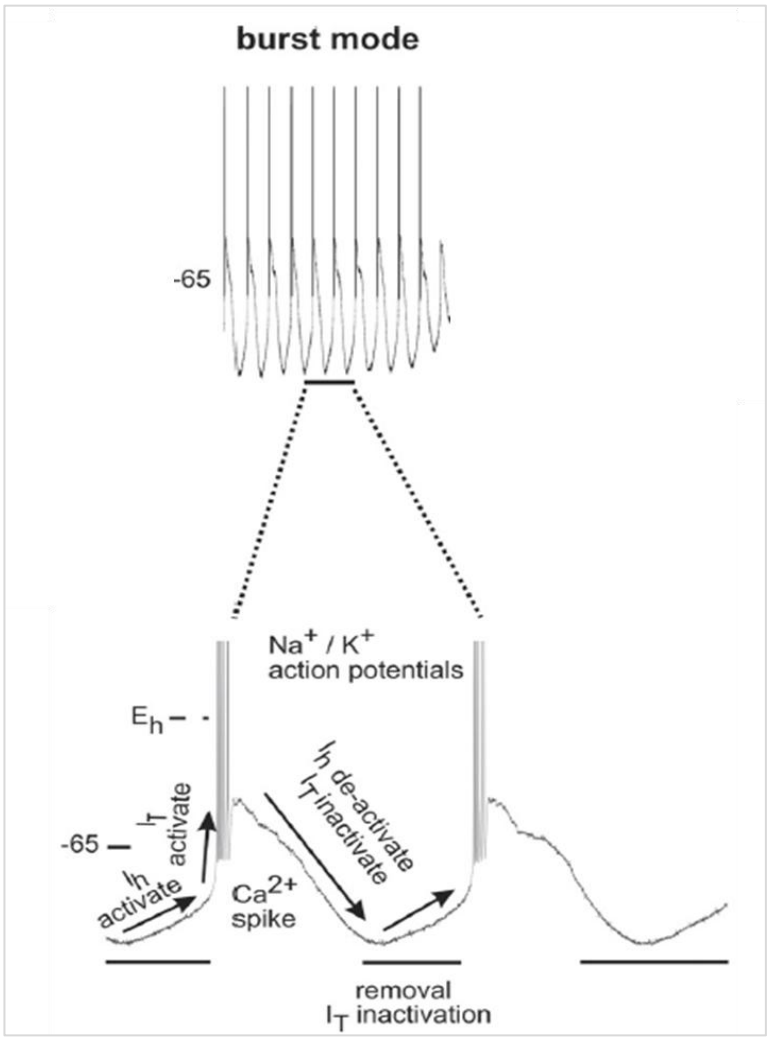

Figure 26: Firing mode of thalamocortical neurons.
The upper panel shows recording of thalamocortical action potentials. The panel below shows an higher temporal resolution of thalamocortical firing, indicating the currents involved. (f*rom Biel et al. 2009*)

In other cells of the CNS that are normally inactive, the I_h is not responsible for the generation of the action potentials but its properties make it fundamental in the control of membrane excitability, in stimuli responsiveness and in the control of neuronal networks[8,10] activity. Specifically, I_h plays two main roles in neurons: it contributes to set the RMP and it controls its oscillations. Indeed, HCN channels are partially open at voltages near the RMP, thus they mediate a tonic inward depolarizing current influencing the membrane potential[91] (**Figure 27**). Though an

inward depolarizing current is by definition an excitatory current, since it brings the RMP closer to the firing threshold, the constitutively activated I_h lowers at the same time the membrane resistance[91]; therefore, following the Ohm's law, for a given current input, the variation of membrane potential is smaller than it would be in the absence of I_h[10], resulting in an inhibitory effect. Thus, I_h plays a dual role in determining neuron excitability[30]. The effect on a single-neuron excitability depends on the balance between the depolarized RMP and the input resistance (or membrane resistance), which in turn is affected by other intrinsic properties, such as neuron type, developmental stage and neuromodulation[30].

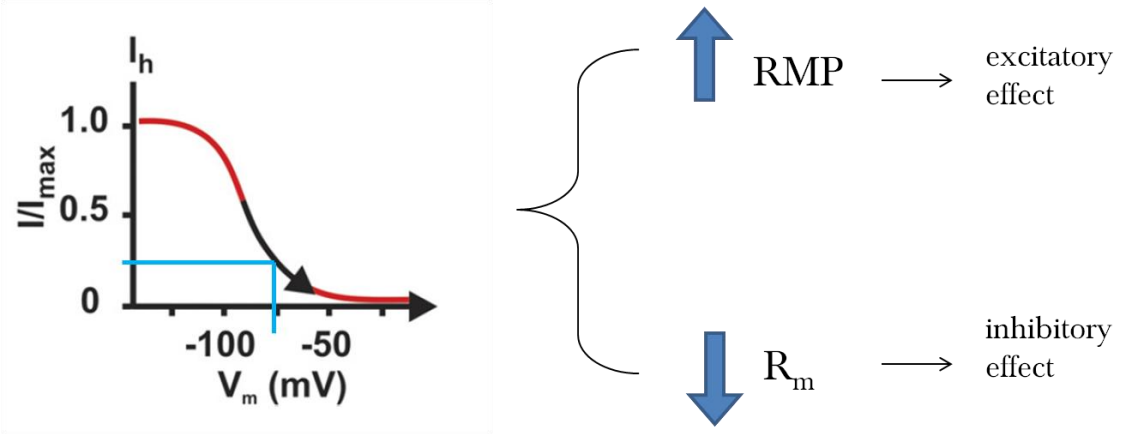

Figure 27: Main roles of the I_h in the neurons.
The graph illustrate the I_h activation curve, showing in particular that at voltages near RMP the open probability of HCN channel is >0. HCN channels mediating a depolarizing current have both an excitatory effect increasing RMP and an inhibitory effect decreasing membrane resistance. (*adapted from Biel et al 2009*)

Another function of HCN channels concerns the control of RMP oscillations, counteracting both excitatory and inhibitory subthreshold stimuli: this means that when an inhibitory hyperpolarizing input arrives, a greater fraction of HCN channels opens, causing a depolarization back toward the the original RMP. This is called the "depolarizing voltage sag" (**Figure 28A**). On the other hand, an excitatory depolarizing input produces a progressive increase in the fraction of closed HCN channels, thus determining the loss of the tonic depolarizing I_h, leading indirectly to a ripolarization of membrane potential toward its initial resting

value. Thus, I_h can also generate the "hyperpolarizing voltage sag" effect[10] (**Figure 28B**).

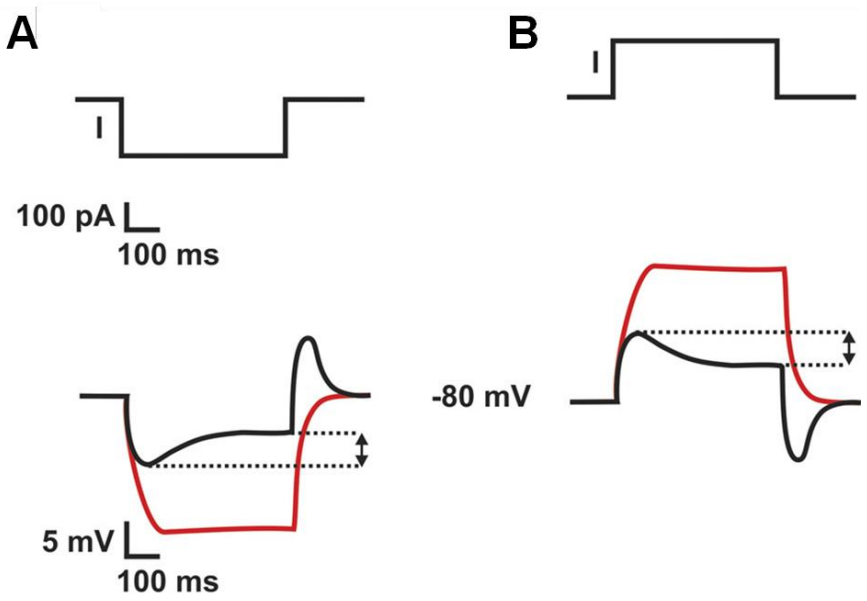

Figure 28: I_h actively opposes changes in membrane voltage.
Cartoon of a current-clamp experiment in a neuron. In the presence of I_h (black traces), a hyperpolarizing current step induces a depolarizing voltage sag (arrow, **A**) and a depolarizing current step induces a hyperpolarizing voltage sag (arrow, **B**). Blockade of I_h by cesium eliminates the sag (red traces).

The reduction of membrane resistance caused by I_h reflects in the dendrites an increase in the amplitude attenuation of EPSPs. EPSPs spreading from the dendrites to the soma normally degrade over distance along neuron membrane. Since the passive propagation of the electric stimulus from a dendrite to the soma depends not only on intracellular resistance and membrane capacitance, but also on membrane resistance, the presence of I_h that lowers membrane resistance causes further EPSP attenuation (**Figure 29**). This effect is very relevant for the control of the process of dendritic integration. Indeed, single EPSPs are too weak to reach the action potential threshold at the trigger cone, thus several EPSPs must be integrated in order to generate an action potential. Logically, one could expect the temporal summation of distal EPSPs to be greater than that of proximal EPSPs. Instead this is not the case thanks to I_h, because HCN channel expression follows a somato-dendritic gradient (**Figure 29**), thus I_h density is higher in the distal rather

than in the proximal dendrites, dampening with a larger extent the distal inputs[66]. As an important consequence, the effects of EPSP become independent to their location[127].

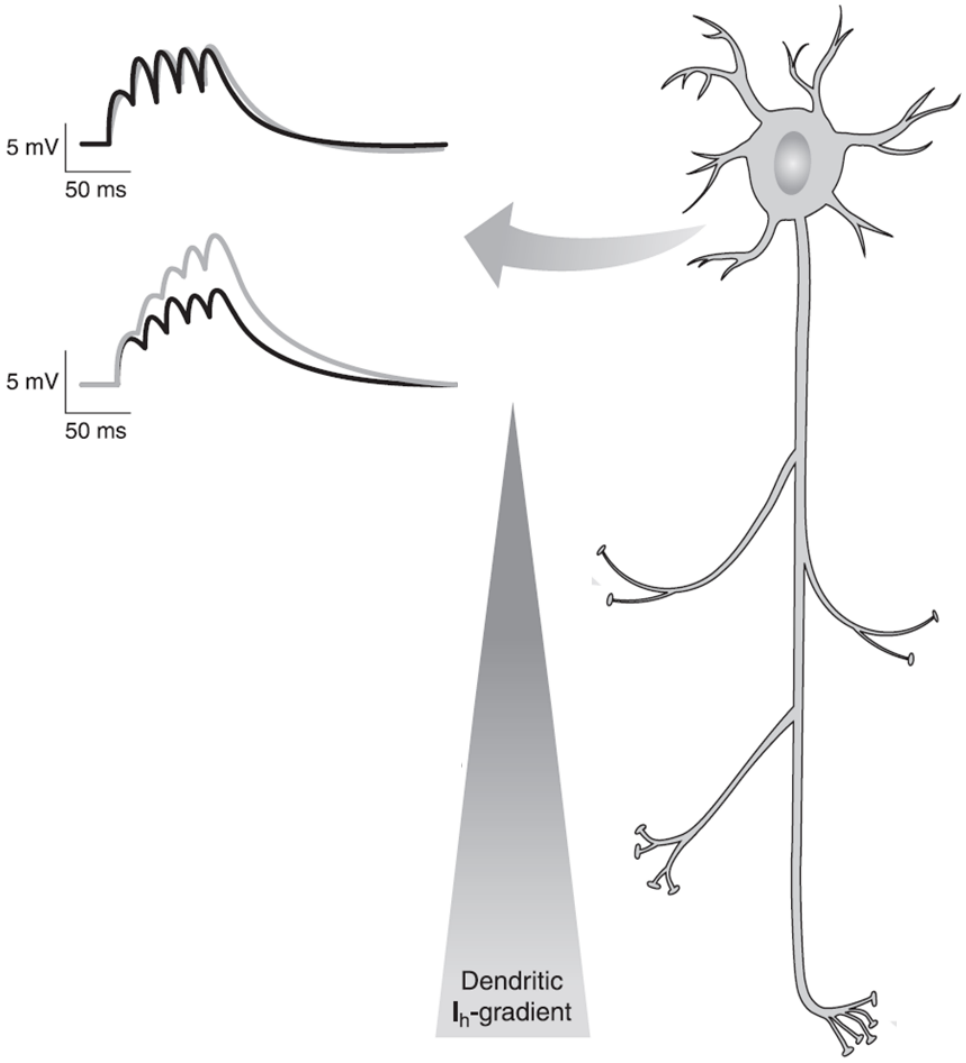

Figure 29: The somato-dendritic gradient of HCN channel expression.
The cartoons shows the somato-dendritic gradient of I_h normalizing localization dependence of temporal summation. Summation of EPSPs from proximal (black trace) and distal (gray trace) dendrites recorded at the soma after propagation. The voltage recordings are shown before (top panel) and after (bottom panel) inhibition of I_h by the selective blocker ZD 7288. (*adapted from Biel et al 2009*)

Epilepsy and HCN channels

HCN channels dysfunctions has been associated mostly with cardiac diseases, due to mutations in the HCN4 gene. In the CNS also, acquired alterations of HCN1 and HCN2 channels, have been associated with pathological conditions, such as subarachnoid hemorrhage[8,60], neuropathic pain[32] and notably epilepsy.

Epilepsy is a condition or a group of conditions involving transient disorders in cerebral function caused by the occurrence of abnormal firing burst of large population of neurons and characterized by recurrent seizures[64]. This effect is considered the result of an abnormal regulation of neuronal excitability that favors hypersynchrony[88]. It is the third most common brain disorder and approximately one third of the affected subjects do not respond satisfactorily to current treatments[98]. Epilepsy is divided into idiopathic, cryptogenic and symptomatic forms. Idiopathic epilepsy is the type in which the primary etiology is genetic, and can be generalized or focal (partial). The idiopathic generalized epilepsy includes the childhood and juvenile absence epilepsy, juvenile myoclonic epilepsy and epilepsy with grand mal seizures on awakening. The mutated genes that have been associated with these epilepsies largely involve voltage- or ligand-gated ion channels[64,90] (**Table 1**). These epilepsies present a complex pattern of inheritance, suggesting an interaction of several susceptibility genes[24,59].

Table 1: Genes associated with idiopathic epilepsies

Gene	Locus
Sodium channel	
Sodium channel, neuronal type I α subunit	2q24
Voltage-gated sodium channel β1 subunit	19q13.1
Sodium channel, neuronal type II α subunit	2q24
Calcium channel	
Calcium channel, voltage-dependent P/Q type α1 subunit	19p
Calcium channel, voltage-dependent, T-type α1H subunit	16p13
Calcium channel, voltage-dependent, β4 subunit	2q22-23
Potassium channel	
Potassium voltage-gated channel, KQT-like subfamily, member 2	20q13
Potassium voltage-gated channel, KQT-like subfamily, member 3	8q24
Potassium large conductance calcium-activated channel, subfamily M, α member 1	10q22.3
Chloride channel	
Chloride channel 2	3q26
Acetylcholine receptor	
Cholinergic receptor, neuronal nicotinic, α4 subunit	20q13
Cholinergic receptor, neuronal nicotinic, β2 subunit	1q21
Cholinergic receptor, neuronal nicotinic, α2 subunit	8p21
γ-Aminobutyric acid receptor	
γ-Aminobutyric acid receptor α1	5q34
γ-Aminobutyric acid receptor γ2	5q34
γ-Aminobutyric acid receptor δ	1p36
Others	
Leucine-rich, glioma-inactivated 1	10q24
EF-hand domain (C-terminal)-containing 1	6p12-11
Malic enzyme 2	18q21
Sushi repeat-containing protein X-linked 2	Xq21.22-q23
Corticotrophin releasing hormone	8q13

(*from Santoro et al. 2003*)

The link of HCN channel alterations and epilepsy in animal models

Initial evidences of HCN channel involvement in epilepsy came from rat models. Hyperthermic febrile seizure rat models presented regional changes in hippocampal HCN channel subunit expressions, with a down-regulation of HCN1 and an up-regulation of HCN2 in the hippocampal CA1 neurons[15]. Other rat models, the Wistar Albino Glaxo rats bred in Rijswijk (WAG/Rij), which spontaneously develop seizures, presented a significant reduction of the I_h in pyramidal neurons, with a decreased levels only of HCN1 and not of HCN2[116]. This was associated both with a hyperpolarized RMP and an increase in temporal summation, facilitating dendritic burst firing, which can contribute to network excitability[56,116]. Moreover, another study showed that also the sensibility to cAMP

may contribute to the pathogenesis, as an increase in the cAMP-insensible isoform HCN1 was observed in thalamo-cortical neurons of these rats[18].

Another concrete evidence linking HCN channel dysfunction with the disorder was provided by KO mice. HCN2-KO mice display significant reduction of I_h in the thalamocortical neurons and thus a more hyperpolarized RMP, compared to the WT mice. Notably, HCN2-KO mice display spontaneous absence epileptic seizures[65]. Also the deletion of HCN1 produces a similar effects in mice[108], although the seizures were not spontaneous.

HCN channels dysfunctions in epileptic patients

Among susceptibility genes for epilepsy in humans, HCN channels are found. Indeed, some mutations in HCN1 and HCN2 have been identified in patients affected by epilepsy. In particular, one study found a single HCN1 polymorphism in a patient and never in the healthy controls, and two non-synonymous mutations in HCN2[119]. One of these, a deletion of 3 proline in HCN2 gene, was observed also in another independent study, where they demonstrated through in vitro expression of the mutant channel that it causes an increase in the I_h[25]. However, the effect on neuronal excitability was not investigated.

Recently, a study of our group found the homozigous E515K loss-of-function mutation of the HCN2 gene in a patient with idiopathic generalized epilepsy, causing a large negative shift of HCN2 activation curve and slower activation kinetics in heterologous expression system; this was maintained also in rat neonatal cortical neurons, resulting in a strongly reduced contribution of I_h to activity which was associated with an increased neuron excitability compared to the WT[28] (**Figure 30**).

Finally, through the new technology of high-throughput all-exome sequencing, a recent study found some *de novo* point mutations in HCN1 gene in patients with infantile epileptic encephalopathy[85].

In any case, all the mutations found in patients have not been found to co-segregate with disease, thus they cannot be considered as causative of epileptic phenotype, but only a possible susceptibility trait[92].

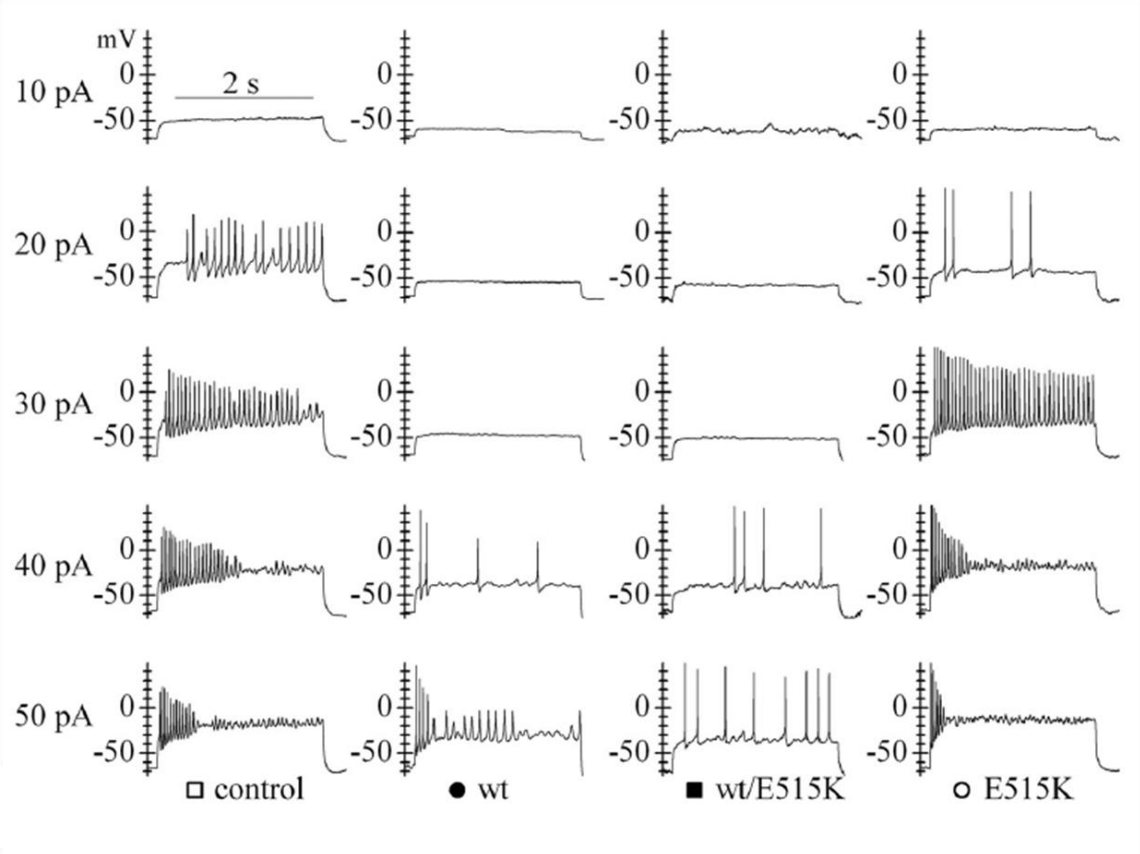

Figure 30: Increased neuron excitability in neurons transfected with E515K HCN2.
Sample voltage traces recorded during injection of 10 –50 pA depolarizing current steps into neonatal rat cortical neurons. (*from DiFrancesco et al 2011*)

Beside genetic screening, some studies focused on investigating the expression of HCN channel in human brain tissue, but they did not found differences in the transcript levels in epileptic patient compared to controls, except for the dentate gyrus, where high levels of HCN1 were found in patients. This was surprising since normally HCN1 is not expressed in that region of the brain[9]. Notably, in this case an upregulation was observed and not a loss of function.

Another study analyzed neocortical neurons obtained from epilepsy surgeries and found a lower expression of I_h in patients with more frequent seizures compared to those with more sporadic ones. This suggested that a loss of HCN function may be associated with more severe forms of epilepsy[125]. However, no control comparisons were possible for this experiment. It must be noticed that these changes in the expression may be not the cause, but rather a compensatory response to abnormal excitability during seizures[8].

Is HCN channel alteration causative of epilepsy?

From literature data it appears that epilepsy can be associated with both, up- and down-regulation of HCN channels and especially of HCN1, depending on the brain region[10]. This is consistent with the dual action of I_h on neuron excitability described before, which can result in an excitatory or inhibitory effect depending on the context[30].

Interestingly, in rat epilepsy model it was noticed that when seizures were chronically suppressed, the observed alterations in ion channels, including HCN1, were reversed[12]. This suggests that HCN channel deregulation in this model is not causative for epilepsy, but it can amplify the effect of spontaneous seizures[92]. On the other hand, it has been pointed out that HCN channel can have also a causative role[69], since in rat models with pilocarpine-induced epileptic state the changes in HCN channels occur before the spontaneous seizures[52]. Ultimately, the mechanism of HCN channel alteration can be either dependent or independent on previous recurrent seizure. Thus, the increased neuronal excitability due to downregulation of dendritic HCN channel may be associated with both the trigger of epileptogenesis and maintenance of the epileptic state[51].

MinK-related peptide 1 (MiRP1)

MiRP1, encoded by the gene KCNE2, is a member of the MinK(minimal K^+ channel protein)-related protein family comprising 4 members, which are characterized by a single transmembrane peptide, with the C-terminus in the cytoplasm and the N-terminus placed in the cytosol[70] (**Figure 31**). MiRP1 expression has been found in the heart, especially in the SAN and Purkinje fibers, and in rat and human brain[1,49,94], including the hippocampus, the thalamus and the hypothalamus[121].

MiRP1 is composed by 123 amino acids and was firstly discovered in the 1999 by Abbott and colleagues by homology-searching in the rat genome, showing that it can assemble with hERG potassium channel, acting as β-subunit and altering its properties, such as activation curve (shifted positively), kinetics of activation

(slower) and deactivation (more rapid). This assemble is necessary to generate the rapid delayed rectifier potassium current I_{Kr}[1].

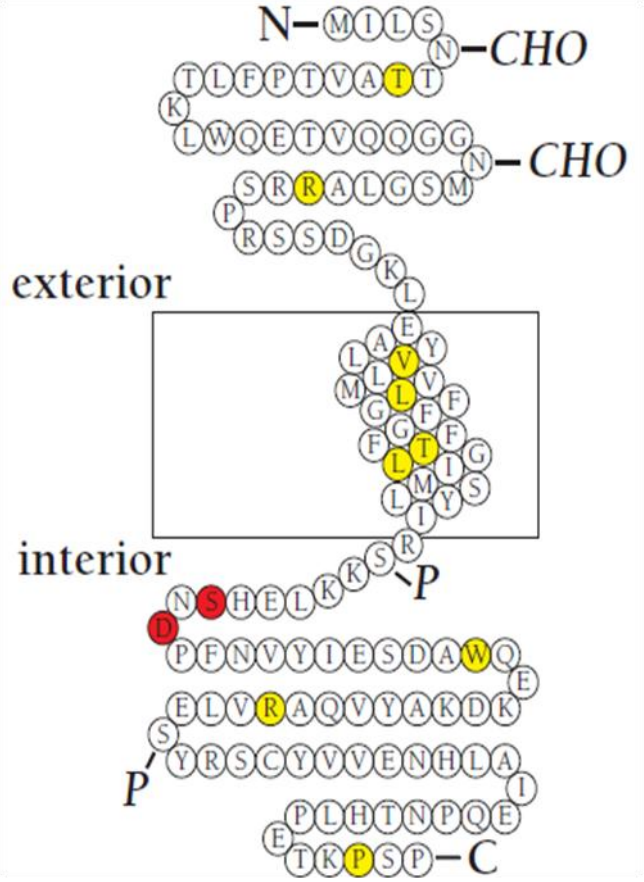

Figure 31: Schematic representation of the MiRP1 peptide.

Although in this work no association with other tested potassium channels was found (KCNQ1, KCNQ2, Shaker, Kv1.3, Kv1.5, Kv1.6, Kv2.1)[1], other works presented data showing the interaction of MiRP1 with Kv4.2[135] and KCNQ1[121]. More recently, it has been demonstrated that MiRP1 associates with the complex KCNQ1-MinK and in ventricular myocytes causes the reduction of the mediated I_{Ks} current[49]. The variety of the possible interaction of MiRP1 make it characterized by a promiscuity of functions. The molecular basis and specificity of MiRP1-ion channels interaction are largely unknown[62] and studies are still ongoing investigating new possible interacting channels. Very recently, it has been shown that MiRP1 can also interact with L-type calcium channels, decreasing calcium

current magnitude in cardiomyocytes, although no effect was found in heterologous expression system[62].

Interestingly, it has been shown also that MiRP1 can interact with HCN channels, changing their expression and gating properties both in heterologous expression systems and in cardiomyocytes[14,22,95,132]. These effects are however isoform and species dependent. Notably, some researchers have questioned the regulatory properties of MiRP1 for HCN channels[14,86], since lack of effects were observed upon co-trasfection of the peptide with the four isoforms of rabbit HCN channels in HEK cells[4] or with human HCN2 and HCN4 in cardiomyocytes[86].

Given the expression of MiRP1 and HCN channels in the heart and in the brain, further investigations on the impact of MiRP1 on HCN isoforms may provide useful insights for the understanding and for therapeutic manipulation of rhythmic activity[14].

MiRP1 mutations and KO mice

Inherited variants of MiRP1 gene have been found at the same time of its discovery and have been associated with cardiac diseases, in particular with congenital and drug-induced long-QT syndrome, via alteration of the rapid outward rectifying current I_{Kr} generated by its interaction with hERG[1]. This probably arises from prolonged ventricular action potentials arising from reduced K+ flux[2]. The MiRP1 mutations included M54T, I57T, V65M and A116V[1,47,112]. The channels assembled with HERG and the human M54T MiRP1 showed a three-fold more rapid deactivation kinetics of this complex; V65M MiRP1 caused a slower activation and a more rapid inactivation of the channel; instead, A116V MiRP1 had the effect of decreasing current density[1,47]. These mutations were found also in patients with acquired arrhythmia subsequent to drug administration and a study demonstrated that the combination of the drug and the mutation led to long-QT interval in these subjects[112]. Another mutation found by Abbott and collegues was then discovered to be a polymorphism present in 1,6% of the caucasian population of USA; it was however shown that ERG channels assembled with this

MiRP1 variant were more sensible to drugs acting as potassium channel blockers, thus this mutation can predispose to acquired cardiac arrhythmias[112].

Recently, Nathawe *et al.* found the M54T MiRP1 mutation in a patient with long-QT syndrome and sinus bradycardia. They have shown that HCN channel properties expressed in neonatal rat cardiomyocytes are altered by this mutation; in particular the M54T causes slower kinetics of activation of both HCN2 and HCN4 and a decrease in the current density of HCN4. This was the first evidence of an effect produced by MiRP1 mutation on HCN channels[86].

Thus far, the identified mutation in MiRP1 in humans have been associated only to cardiac diseases and then studied *in vitro* with functional analysis.

MiRP1 function *in vivo* has also been studied using KO mice. These mice were firstly generated by the group of Abbott and the first phenotype identified involved gastric acid secretion. These mice were affected by achlorhydria, hypergastrinemica, gastric glandular hyperplasia[100] and iron-deficient anemia[106]. The phenotype was caused an abnormal distribution of ERG in gastric glands. They showed also an impaired targeting of ERG and Kv1.3 to the choroid plexus epithelium (CPe) membrane, leading to an increase the anion secretion in the cerebrospinal fluid[101]. In subsequent study, they observed mice pubs and found that the thyroid hormone biosynthesis was disrupted, leading to hypothyroidism, alopecia and cardiac abnormalities such as hypertrophy, fibrosis and reduced fractional shortening[102]. Finally, they also showed that deletion of MiRP1 causes a delayed ventricular ripolarization in adult mice[103], and deepening the analysis, a multisystem syndrome was observed, involving both cardiac and extra-cardiac tissue and metabolic disorders[45].

In recent years, another work investigated the effects of MiRP1 deletion focusing on HCN channels. Using brain slices of KO mice they found that MiRP1 deletion causes a negative shift in the I_h activation curve, a slowdown of the gating kinetics and a decrease in I_h current density. In addition, the expression of HCN1 and HCN2 channels was reduced in whole-brain extracts. As a result, an increase in input resistance and temporal summation was observed. Importantly, they found an overall increased intrinsic excitability with enhanced burst duration in

corticothalamic neurons, implying the presence of augmented excitatory input to the thalamus[131].

These effects suggest a functional interaction of MiRP1 with HCN channels in physiological condition, notably in the brain, supporting *in vitro* analysis on heterologous and cardiac expression systems. It is however important to mention that in this paper the author reported also that MiRP1 and HCN1 or HCN2 did not co-immunoprecipitate[131], an evidence arguing against their interaction. Thus, further researches would be helpful to clarify HCN channel-MiRP1 interaction.

MATHERIALS AND METHODS

Generation of wild-type (WT) hMiRP pIRES II plasmid

The plasmid was built from pIRES II vector and cDNA encoding WT hMiRP. The latter was excised from a pCI-Neo vector, using the restriction enzyme EcoRI (FastDigest enzymes Fermentas™), and then moved to into pIRES II vector which was cut with the same enzyme. WT hMiRP was inserted into the vector using *T4 Ligase* (Thermo Scientific™). The correct insertion of the plasmid was verified by digestion with two enzymes (BamHI and NheI, FastDigest Fermentas) cutting one inside and one outside the inserted band, so that two bands of a determined length were visible in gel electrophoresis. The plasmid obtained was then amplified in DH5α competent bacterial cells (transformation protocol below).

Generation of M54T mutated hMiRP pIRES II plasmid

A QuikChange II XL Site-Directed Mutagenesis Kit (Agilent technologies™) was used with proper forward primer (5'-ccaatcatcaccgtgaggtacaggatgacatagtag-3') and reverse primer (5'-ctactatgtcatcctgtacctcacggtgatgattgg-3') to insert the T→C substitution into WT hMiRP pIRES II corresponding to M54T mutation.

Then DpnI was added, which digest only parental DNA because it recognises methylated region. Using specific competent bacterial cells (XL10 GOLD), the plasmidic DNA was amplified.

PCR condition

- H_2O MilliQ to 50 µL
- Reaction Buffer 10 X 10 ng
- Quick solution 3 µL
- Primers forward 125 ng
- Primers reverse 125 ng
- dNTPs 1 µL
- dsDNA template 10ng

- P*fuULTRA* HF DNA polymerase (2.5 U/µl) 1 µl

Cycle	Temperature	Time
1	95°C	1’
18	95°C	50”
	60°C	50”
	68°C	1’/Kb of plasmid
1	68°C	7’

Digestion of the Amplification Products

1 µL of the DpnI restriction enzyme (10U/µl) was added directly to each amplification reaction, then the reactions was immediately incubated at 37°C for 1 hour to digest the parental supercoiled DNA.

Transformation of DH5α competent cells and XL10-Gold Ultracompetent Cells

DH5α bacterial cells were transformed to amplify the WT hMiRP containing plasmid. They were kept at -80°C and thaw on ice upon use. Then, the 10 ng of plasmid were added and incubated on ice for 30 minutes. Finally the cells were put at 42°C for 45 seconds and then on ice for 1 minute. They were then let to grow in 900 µL of liquid LB medium at 37°C for 1 hour, before plating them on agar dishes containing the appropriate antibiotic for the plasmid vector. The dishes were incubated overnight at 37°C.

XL10-Gold ultracompetent cells were used to transform the mutated plasmid treating them first with βME, then adding up to 10 ng of plasmid and incubating the reactions on ice for 30 minutes for each transformation. After a heat-pulse in a 42°C water bath for 30 seconds, the tubes were incubated on ice for 2 minutes

adding next 500 µL of preheated NZY^+ broth and incubating the tubes at 37°C for 1 hour with shaking at 250 rpm. Finally, the proper volume of reaction was plated on antibiotic-containing agar dishes, incubating the transformation plates at 37°C for >16 hours.

The day after the colonies were picked and let growing in liquid LB medium for another night. Subsequently, the plasmid DNA was extracted using NucleoSpin Plasmid Kit (Macherey-Nagel).

The correct insertion of the desired mutation was then further confirmed by direct sequencing.

Isolation of cortical neurons

Cortical neurons were isolated from post-natal day 2 (P2) CD rat pups (Harlan Laboratories). Rats were anesthetized (isofluorane) and decapitated; then, brains were quickly removed and placed in ice-cold dissociation medium containing the following (in mM): 134 Na-isethionic acid, 23 glucose, 15 HEPES, 2 KCl, 4 $MgCl_2$, 0.1 $CaCl_2$, and 10 kynurenic acid, pH 7.2. The cerebral cortex was isolated using fine tweezers, chopped into small pieces, and digested in a dissociation medium containing 1.3 mg/ml protease (type XIV; Sigma) for 20 min at 37°C in agitation. The tissue pieces were then rinsed twice in dissociation medium and mechanically dissociated using a series of progressively thinner fire-polished Pasteur pipettes. The dissociated neurons were plated onto poly-D-lysine-coated 35 mm dishes at a density of $1.5x10^6$ cells in a solution of dissociation medium and culture medium. After 1 h at 37°C and 5% CO_2, this solution was replaced with Neurobasal complete culture medium (see below).

Transfection of heterologous system: CHO cells

These cell are used because they present negligible expression of ion channels. They were grown in Hamster Nutrient, 10% FBS, 1,5 g/L $NaHCO_3$, 2mM L-glutamine, 1X PenStrep (Life Technologies). Cells were maintained in incubator at

37°C with 5% of CO_2. One day before transfection cells were detached from the dish with trypsin and re-plated at a proper density in a 35mm plate. The experiment was carry out following standard protocol of *FuGENE® HD* Transfection Reagent (Promega®) using 3:1 ratio volume/weight. CHO cells were transfected with 1 µg of HCN2 or HCN4 alone or with 0,77 µg of hMiRP WT, M54T or both. For each transfection the transfection solution containing plasmidic DNA, Fugene HD in ratio 3:1 and medium without serum to 100 µl was prepared and after 15 minutes, the transfection solution was added drop by drop into 35 mm dish with 900 µl of culture medium. After 8h into the incubator at 37°C the medium was removed and 2 mL of clean culture medium was added.

Transfection of neonatal rat cortical neurons

Cells plated onto poly-D-lysine-coated 35 mm dishes were grown in a soil with Neurobasal A culture medium (Life Technologies) supplemented with B27 (Life Technologies), 1 mM Glutamax-I (Life Technologies), 10 ng/ml β-FGF(Life Technologies), 50 U/ml penicillinG (Sigma), and 50 µg/ml streptomycin (Sigma). Cells colture were maintained in incubator at 37°C with 5% of CO_2. After one day from isolation, cortical neurons were transfected following standard protocol of *Lipofectamine™ 2000.*

For each dish Mix A was prepared in a polystyrene tube and Mix B in 1.5 mL tube; Mix A was at rest for 5 minutes, meanwhile Mix B was prepared. After 5 minutes, Mix B was added in Mix A and after 20 minutes at room temperature in the dark, the transfection solution was added drop by drop in the 35 mm dish with 900 µL of culture medium. After 24 hours into the incubator at 37°C the medium was removed and 2 mL of clean culture medium was added.

Mix A: 7,5µL of Lipofectamine 2000 and OptiMEM (Life Technologies) to 250 µL

Mix B: DNA and OptiMEM (Life Technologies) to 250 µL.

Different combination of plasmids was used, particularly 1 μg of channel (HCN2 or HCN4) alone or with 0,77 μg of MiRP WT, M54T or both. We also transfected only 1 μg of empty vector (pIRES), hMiRP WT or M54T.

Electrophysiology

Functional analysis of M54T mutation both in CHO cells and neurons were carry out through patch clamp experiment. 48 hours after transfection, CHO cells were detached from dish using trypsin and re-plated in 35 mm dish at single cell dilution in order to evaluate the properties of the currents while the cortical neurons were not detached. Dishes were placed on the inversion microscope plane and cells were perfused with physiological solution. Particularly, CHO cells were perfused with an external solution to improve dissection of the I_h current containing the following (in mM): 110 NaCl, 0,5 $MgCl_2$, 1,8 $CaCl_2$, 5 Hepes NaOH, 30 KCl, 1 $BaCl_2$, 2 $MnCl_2$, 0,1 NiCl, 0,2 Nifedipine, pH 7,4. Pipettes contained the following (in mM): 10 NaCl, 130 KCl, 1 EGTA, 5 HEPES-KOH, 0.5 $MgCl_2$, 2 ATP (Na salt), 0.1 GTP (Na salt), and 5 phosphocreatine, pH 7.2. Cortical neurons were superfused with an external solution containing the following (in mM): 129 NaCl, 1.25 NaH_2PO_4, 1.8 $MgSO_4$, 1.6 $CaCl_2$, 3 KCl, 10 Na-HEPES, 35 glucose, pH 7.4. The pipette solution contained the following (in mM): 120 K-gluconate, 15 KCl, 2 $MgCl_2$, 0.2 EGTA, 20 phosphocreatine, 2 ATP-Na, 0.2 GTP-Na, 0.1 leupeptin, 10 K-HEPES, pH 7.2. The borosilicate glass pipettes, once filled with intracellular solution, had a resistance between 5 and 10 MΩ. GFP-expressing cells were selected for patch-clamp analysis. The study of the currents was carry out with patch clamp techniques in voltage clamp mode using whole-cell configuration. The study of the action potentials was carry out with patch clamp technique in current clamp mode using whole-cell configuration. In cortical neurons current-clamp recordings, the membrane potential was kept at -70 mV. All experiment were made at room temperature.

A specific software (Clampex 9.2, Axon Instruments®) generated the protocols (see protocol below) used for stimulating the cells.

Analysis of I_h Current in single cells

Activation curves of HCN channel-mediated current (I_h) were obtained from the analysis of current tails at -135 mV. The Boltzman equation was used to interpolate the activation curve. The holding potential is maintained to -35 mV; activation curves were recorded using potential steps from -35 mV to -135 mV followed by a step at -135 mV. Each steps of potential was applied as long as necessary to reach the steady state of the current at that specific potential.

The time constants of activation and deactivation were obtained using mono-exponential function:

$$I_t = I_\infty \, (1\text{-}e^{-t/\tau})$$

where τ is the time constant defined as the time necessary to raise 63% of the current at stationary state. Deactivation traces were recorded using potential steps between -75 mV and +25 mV preceded by a step at -135 mV in order to fully activate the I_h current.

Density current was evaluated at each steps by the ratio between the current and the capacity of the cell in which the current was recorded.

Comparison of all data was made with independent Student's t test or one-way ANOVA followed by Fisher test for means comparison and significance level was set to $p<0.05$.

RESULTS

Functional analysis of M54T MiRP1 mutation on HCN2 properties in heterolgous expression system

Previous literature data showed an effect of M54T mutation on HCN2 in cardiomyocytes[86]. Here, in order to better dissect the effect of M54T MiRP1 mutation on HCN channels, we co-transfected WT or mutated MiRP1 with HCN2 channel in an heterologous system, the CHO cells. We also co-trasnfected HCN2 with the same amount of WT and M54T MiRP1 to mimic the heterozygous condition. The plasmids encoding WT or mutated MiRP1 contained also the enhanced green fluorescent protein (EGFP) under an IRES region, so that cells expressing MiRP1 were recognizable. As a control, we also co-transfected HCN2 with the pIRES2-EGFP empty vector. 48 hours after transfection, we recorded the HCN2 current in the EGFP-positive cells; **Figure 32A** shows representative normalized current traces recorded during application of hypepolarizing steps from -35 to -135 mV (holding potential -35 mV) in cells co-transfected with HCN2 and WT MiRP1 (HCN2+WT), M54T MiRP1 (HCN2+M54T) and both WT and M54T MiRP1 (HCN2+WT/M54T) or the empty vector (control). Voltage dependence, current density and kinetics of HCN2 were compared.

Analyzing the tail currents at -135 mV, we derived the activation curve of HCN2 that was then fitted to the Bolzmann equation to obtain the values of half-activation ($V_{1/2}$) and of inverse slop factor (s). Single activation curves were used to calculate the mean activation curves displayed in **figure 32B** for control (white), HCN2+WT (black), HCN2+M54T (orange) or HCN2+WT/M54T (orange and black). All the activation curves resulted essentially overlapped (figure 1B) and indeed statistical analysis revealed no significant difference ($p>0,05$) in the values of the mean $V_{1/2}$ or s (control: $V_{1/2}$ = -76,1±2,4 mV, s = 9,1±0,8 mV, n = 10; HCN2+WT: $V_{1/2}$ = -79,2±2,6 mV, s = 8,7±0,5 mV, n = 16; HCN2+M54T: $V_{1/2}$ = -75,4±1,8 mV, s =

8,6±0,6 mV, n = 23; HCN2+WT/M54T: $V_{1/2}$ = -73,4±1,8 mV, s = 10,0±0,5 mV, n = 23), demonstrating that the voltage dependence of HCN2 was not modified.

We then evaluated whether M54T mutation could alter HCN2 current density. In **figure 32C** the mean current density against membrane voltages is plotted for control, HCN2+WT, HCN2+M54T or HCN2+WT/M54T transfected cells. Even in this case, no significant difference were observed among mean values according to one-way ANOVA and Fisher test ($p>0,05$). This demonstrates that the M54T mutation does not modify HCN2 expression at the plasma membrane.

Finally, we compared the time constants (τ) of activation and deactivation of HCN2. These constants indicate the time necessary to reach the 63% of steady state current. They were obtained fitting with a mono-exponential function current traces recorded at different membrane voltages during the activation and deactivation protocols. **Figure 32D** shows average time constants of activation and of deactivation as a function of voltage. We can observe a slower activation of HCN2 at -85 mV and at -95 mV in cells co-transfected with HCN2 and M54T MiRP1 compared to control, HCN2+WT or HCN2+WT/M54T. These differences were statistically significant (ANOVA, $p<0,05$). Mean τ value at -85 mV for HCN2+M54T was 1,67±0,25 s (n = 15), compared with 0,95±0,15 s for the control (n = 9), 1,11±0,20 s for HCN2+WT (n = 12) and 1,02±0,08 s for HCN2+WT/M54T (n = 14); τ at -95 mV were: 0,87±0,11 s for HCN2+M54T, 0,54±0,07 s for the control, 0,61±0,09 s for HCN2+WT and 0,57±0,04 s for HCN2+WT/M54T. A similar effect has been previously reported using cardiomyocytes[86]. We did not observe instead any significant difference in the activation time constants at other membrane voltages, nor in the time constants of deactivation (**Figure 32D**).

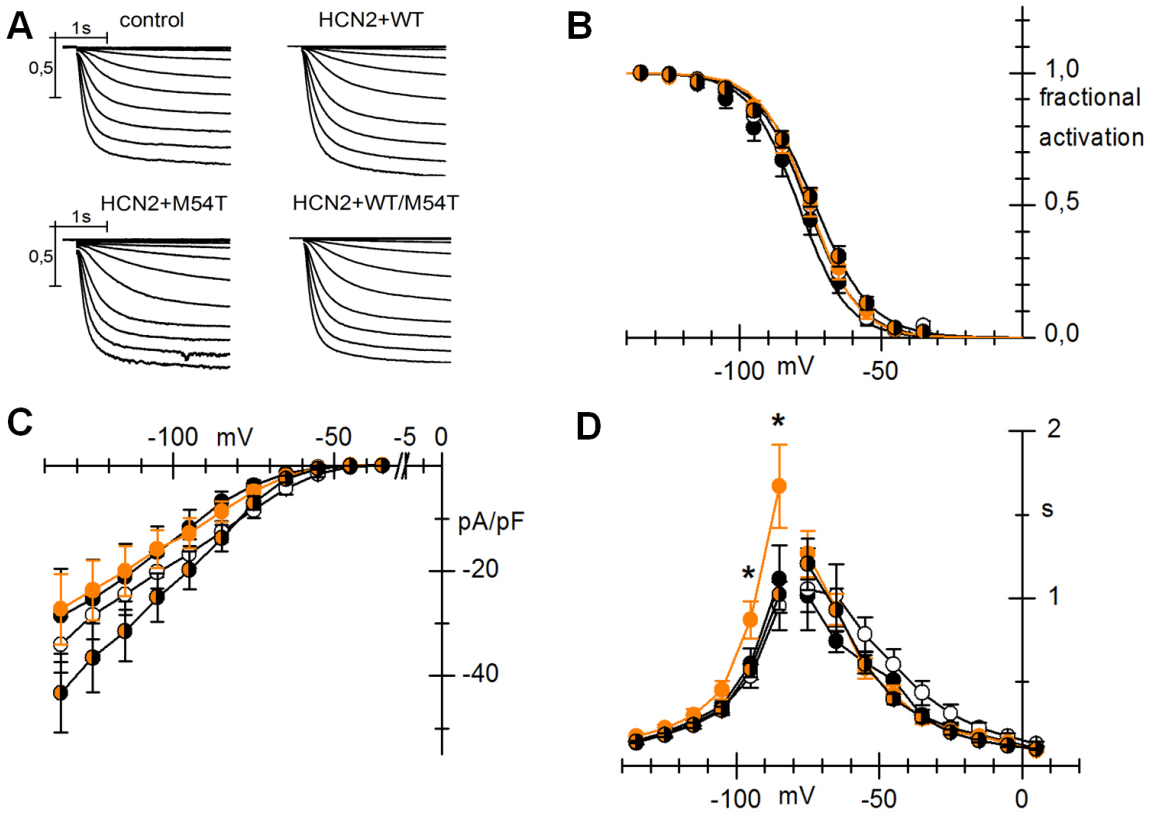

Figure 32: Effects of WT or M54T MiRP1 on the properties of HCN2 current expressed in CHO cells.

(**A**) Representative normalized current traces recorded with hyperpolarization steps to the range of -35/ -135 mV (interval -10 mV) from a holding potential of -35 mV. Tail currents at -135 mV not shown. (**B**) Plots of mean activation curves of control (white), HCN2+WT (black), HCN2+M54T (orange) and HCN2+WT/M54T (orange and black). Lines are the best fitting by the Bolzmann equation. (**C**) Current intensities normalized to cell capacitance plotted against membrane voltages (I-V curves) for control (white), HCN2+WT (black), HCN2+M54T (orange) and HCN2+WT/M54T (orange and black). Points represent the mean (±S.E.M.) of current density for each cell. (**D**) Mean activation and deactivation time constant curves of control (white), HCN2+WT (black), HCN2+M54T (orange) and HCN2+WT/M54T (orange and black). Points represent the mean (±S.E.M.) of the τ calculated for each cell. Activation time constants are significantly different in HCN2+M54T at -95 and -85 mV (*p<0,05).

Functional analysis of M54T MiRP1 mutation on HCN4 properties in heterolgous expression system

M54T MiRP1 mutation has been previously assessed in cardiomyocytes also on HCN4 isoform. Thus, we evaluated the effect of M54T MiRP1 mutation in CHO cells performing the same co-transfection conditions as before, but using instead HCN4. Representative recording of HCN4 current for control (white), HCN4+WT

(black), HCN4+M54T (orange) and HCN4+WT/M54T (orange and black) are shown in **Figure 33A**.

We compared the mean activation curve of HCN4 shown in **figure 33B** and found no differences in the mean $V_{1/2}$ or s values (control: $V_{1/2}$ = -69,6±2,0 mV, s = 9,9±0,7, n = 5; HCN4+WT: $V_{1/2}$ = -70,0±2,1 mV, s = 11,5±0,6, n = 7; HCN4+M54T: $V_{1/2}$ = -70,6±1,8 mV, s = 12,5±0,5, n = 8; HCN4+WT/M54T: $V_{1/2}$ = -73,6±2,2 mV, s = 12,4±0,4, n = 9). This demonstrates that M54T mutation does not influence HCN4 voltage dependence.

We then analyzed HCN4 current density, since literature data showed that it is decreased by 80% in the presence of the M54T mutation[86], in cardiomyocytes. Conversely, in our cells we did not observe any significant difference in current densities (**Figure 33C**).

Nathawe *et al.* have shown that also activation kinetics[86] were affected by the M54T MiRP1. Thus we analyzed both HCN4 activation and deactivation τ and found no difference in the activation kinetics (**Figure 33D**). A slower deactivation was however observed in cells expressing HCN4+M54T, but only from -45 to -25 mV.

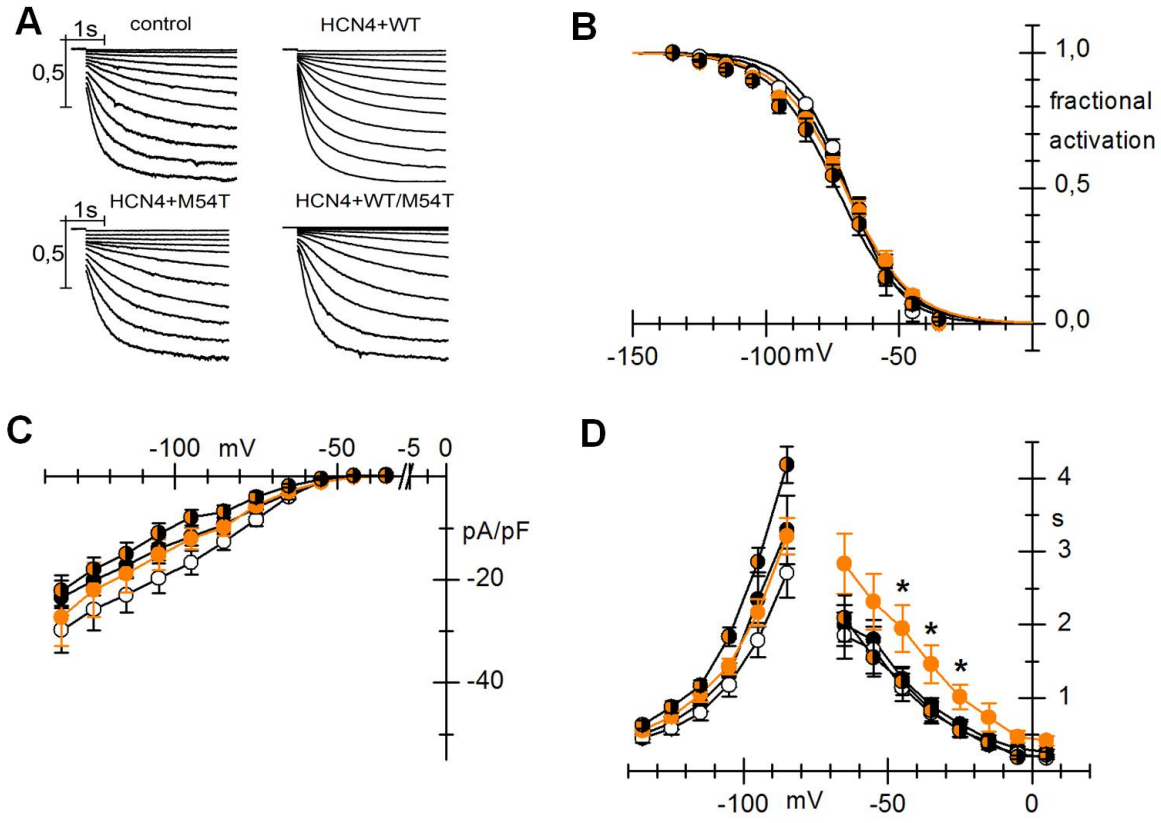

Figure 33: Effects of WT or M54T MiRP1 on the properties of HCN4 current expressed in CHO cells.

(**A**) Representative normalized current traces recorded with hyperpolarization steps to the range of -35/ -135 mV (interval -10 mV) from a holding potential of -35 mV. Tail currents at -135 mV not shown. (**B**) Plots of mean activation curves of control (white), HCN4+WT (black), HCN4+M54T (orange) and HCN4+WT/M54T (orange and black). Lines are the best fitting by the Bolzmann equation. (**C**) Current intensities normalized to cell capacitance plotted against membrane voltages (I-V curves) for control (white), HCN4+WT (black), HCN4+M54T (orange) and HCN4+WT/M54T (orange and black). Points represent the mean (±S.E.M.) of current density for each cell. (**D**) Mean activation and deactivation time constant curves of control (white), HCN4+WT (black), HCN4+M54T (orange) and HCN4+WT/M54T (orange and black). Points represent the mean (±S.E.M.) of the τ calculated for each cell. Deactivation time constants are significantly different in HCN4+M54T at -25, -35 and -45 mV (*p<0,05).

Functional analysis of M54T MiRP1 mutation on HCN2 and HCN4 expressed in neonatal rat cortical neurons

Since it has been shown that the effect of MiRP1[86], as well as the biophysical properties of HCN channels[95], can vary depending on the cell type in which they are expressed, we decided to test a possible effect of the mutation on HCN channels in a neuronal context. We co-transfected neonatal rat cortical neurons

with WT or mutated MiRP1 and HCN2 or HCN4. We still transfected HCN channels because neonatal neurons express only very low levels of endogenous I_h, as shown in **figure 34A** (left, non transfected cell). Instead, for simplicity we did not include the co-transfections of HCN channel and WT/M54T MiRP1.

From HCN2 current traces recorded (**Figure 34A**, right), we derived the activation curves. Since these neurons are particularly sensitive to strong membrane hyperpolarization we used a protocol of only 5 steps with hyperpolarizing step in the range -35 to -115 mV to avoid cell death. The mean activation curves displayed in **figure 34B** confirm the results found in the heterologous system, showing no difference in the voltage dependence of HCN2 (control: $V_{1/2}$ = -75,1±2,1 mV, s = 6,4±1,6; WT: $V_{1/2}$ = -73,6±2,6 mV, s = 8,1±0,90, n = 6; M54T: $V_{1/2}$ = -76,0±2,2 mV, s = 8,5±0,4, n = 12).

We then analyzed the activation time constants, since this HCN2 property was the only affected by the presence of the mutation in the heterologous system. Again, the results in neurons confirmed those previously obtained in CHO cells: as displayed in the plot of **figure 34D**, showing time constants against voltage, the time constants of activation were significantly slowed ($p<0,05$) in presence of the M54T MiRP1 at -85 mV (WT = 0,58±0,04 s, n = 4; M54T = 1,00±0,08 s, n = 7), but not at other voltages.

Finally, we also analyzed HCN2 current density in the different conditions, but again we did not find any difference (**Figure 34C**), demonstrating that M54T MiRP1 mutation does not affect HCN2 expression also in this neuronal system.

We also evaluated possible effects of M54T mutation on HCN4 channel properties in this neuronal context. Due to the slower activation of HCN4, the activation curve protocol required longer hyperpolarization, causing cell death in most of the cases. We then used only a single hyperpolarizing step to record the current density at -115 mV, since this feature was the one strongly reduced in the presence of M54T mutation in cardiomyocytes[86]. Again, we observed that neurons co-transfected with HCN4 and WT MiRP1 had a current density of -16,7±3,4 pA/pF,

which was not significantly different from that of -13,9±3,2 pA/pF found in presence of M54T mutation.

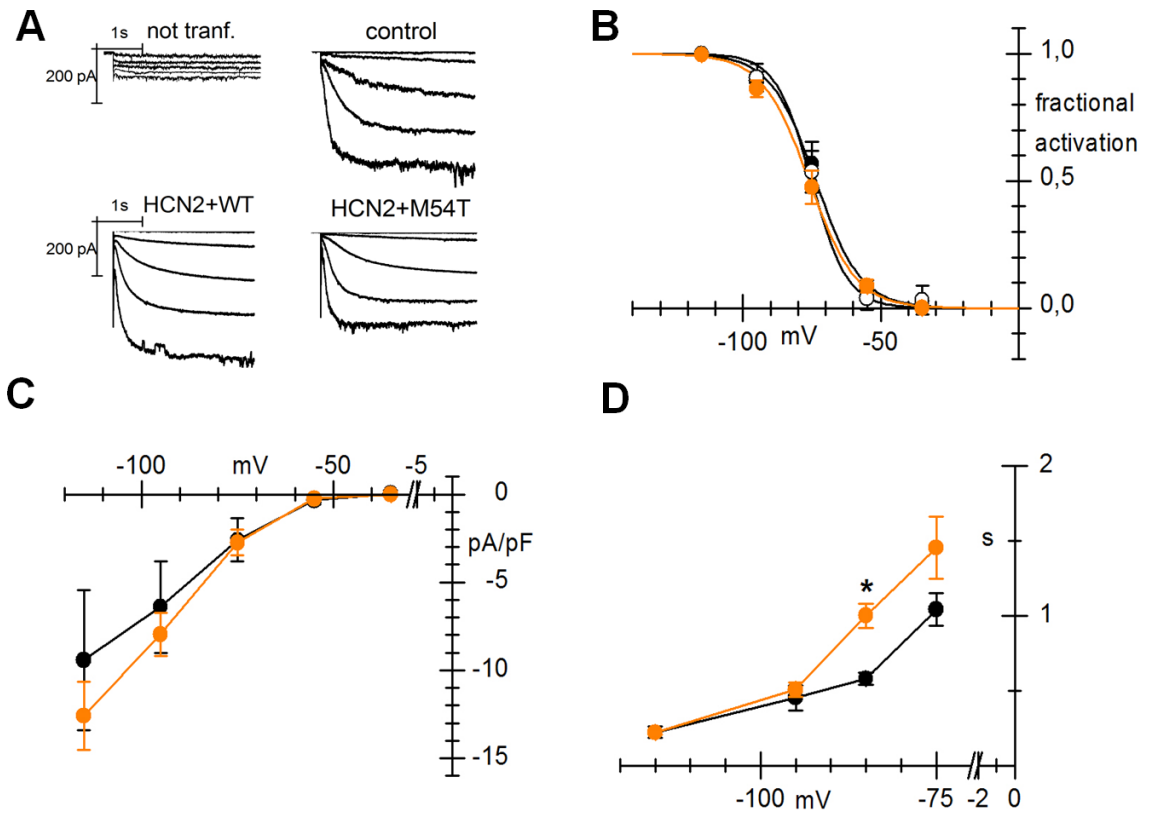

Figure 34: Effects of WT or M54T MiRP1 on the properties of HCN2 current expressed in neonatal rat cortical neurons.

(**A**) Representative current traces recorded with hyperpolarization steps to the range of -35/-115 mV (interval -20 mV) from a holding potential of -35 mV. Tail currents at -115 mV not shown. (**B**) Plots of mean activation curves of control (white), HCN2+WT (black) and HCN2+M54T (orange) neurons. Lines are the best fitting by the Bolzmann equation. (**C**) Current intensities normalized to cell capacitance plotted against membrane voltages (I-V curves) for HCN2+WT (black) and HCN2+M54T (orange) neurons. Points represent the mean (±S.E.M.) of current density for each cell. (**D**) Mean activation time constant curves of HCN2+WT (black) and HCN2+M54T (orange). Points represent the mean (±S.E.M.) of the τ calculated for each cell. Activation time constants are significantly different in HCN2+M54T at -85 mV (*p<0,05).

Effects of WT or M54T MiRP1 on neuronal excitability

M54T MiRP1 mutation did not produce relevant effects on HCN channel current in the neurons. However, we questioned whether it can cause some effects on neuronal excitability acting on other ion channels, since MiRP1 is a β-subunit also

of many potassium channels[1,47,63,121]. Previously in our laboratory, we observed that high density of HCN channel current (>5 pA/pF) caused a strong decrease in neuronal excitability. Since in the co-transfection experiments described before HCN channel current density was always higher than 5 pA/pF, the effect of MiRP1 on excitability could not be clearly evaluated.

We decided then to perform another set of experiments, transfecting only WT or mutated MiRP1 in rat neonatal cortical neurons. Also in this case we transfected the empty vector as a control. After 48 hours from transfection, we recorded the action potentials generated upon stimulation with depolarizing current steps of progressively higher amplitude (10-60 pA). **Figure 35A** shows representative examples of action potentials recorded upon current injection (10-50 pA) in neurons transfected with empty vector (control), WT MiRP1 (WT) or M54T MiRP1 (M54T). As evident in the sample traces, neurons transfected with the WT MiRP1 display an overall increased excitability compared to the neurons transfected with the empty vector. The subsequent analysis revealed that they present a two-fold decrease relative to the control of the threshold current necessary to trigger action potentials, as shown in the bar graph of **figure 35B** displaying the mean threshold currents. In addition, the generated action potentials have a higher firing rate in WT MiRP1 transfected neurons than in control neurons. **Figure 35C** shows the mean firing rate relative to the injected current for control (white), WT (black) and M54T (orange) neurons. Surprisingly, neurons transfected with the M54T MiRP1 exhibit instead an excitability similar to the control neurons and significantly lower than the WT MiRP1 transfected neurons, as demonstrated by both the higher threshold current (**Figure 35B**) and the reduced firing rate (**Figure 35C**).

These results show that MiRP1 increases neuronal excitability and that M54T mutation reverts this function. The molecular partner of MiRP1 causing this effect remain to be investigated. Notably, the decreased neuronal excitability due to M54T MiRP1 mutation does not directly correlate with the epileptic phenotype,

which is caused by neuron hyperexcitability; however, due to the interplay between excitatory and inhibitory neurons in signal integration, it is difficult to predict an *in vivo* effect.

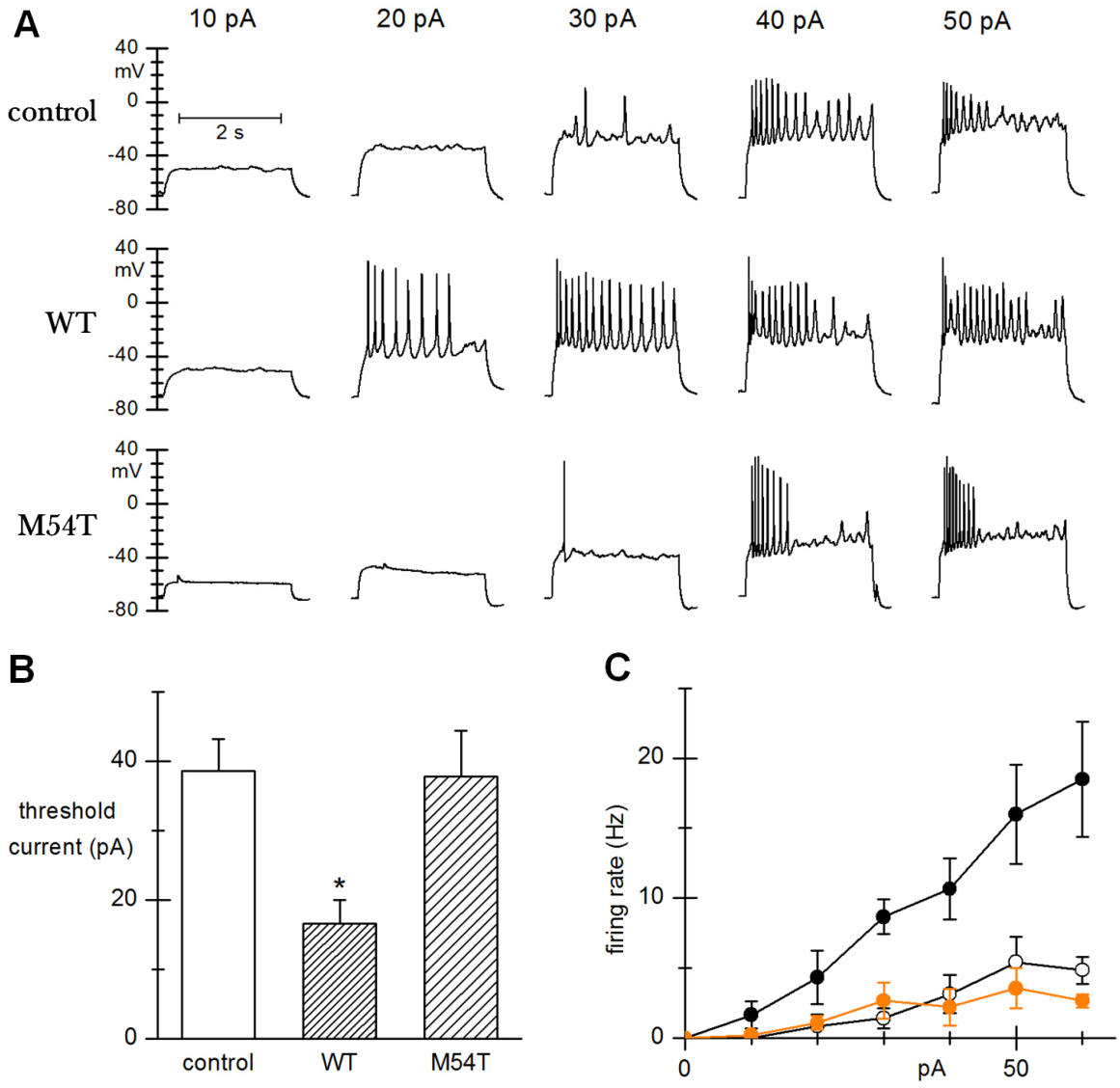

Figure 35: Effect of WT or M54T MiRP1 on neuron excitability.
(**A**) Sample voltage traces recorded during injection of 2.5 s,10 –50 pA depolarizing current steps into neonatal rat cortical neurons. All measurements were performed with resting voltage held at -70 mV. (**B**) Bar graph of mean threshold current required to trigger action potential firing; values were 38,6±4,6 pA (n=7), 16,6±3,3 pA (n=6), 37,8±6,6 pA (n=9) for control, wt and m54t neurons, respectively. According to one-way ANOVA, wt threshold current was significantly slower than that of control or m54t. (**C**) Mean rate of firing recorded upon current injection. WT (black circles, n=6) are clearly less excitable than control (white circles, n=7) and M54T-expressing cells (orange circles, n=9).

DISCUSSION

Epilepsy is a very common brain disorder in the human population and many affected patients (33%) do not respond to pharmacological treatments[98]. In idiopathic epilepsies protein dysfunctions causing the pathological phenotype are mostly due to genetic mutations[64]. Identifying and characterizing new mutations in this type of epileptic patients would be helpful both to better understand the cause of the disorder and to provide new targets for the pharmacological research.

Many of the mutated proteins found in epileptic patients are ion channels, including HCN channels[64]. Despite the evidence in animal models clearly linking HCN channel dysfunctions to epilepsy[15,65,108,116], few mutations of HCN channels have been identified in epileptic patients and have been functionally characterized for their epileptogenic effect[25,28,85]. Investigations concerning the screening for new mutations are ongoing during the recent years and can be helpful to clarify HCN channel contribution to the disorder.

Our group has begun to screen 185 idiopathic epileptic patients, evaluating both HCN channels and accessory proteins that normally interact and modulate these channels. For example, it has been shown in a rat model of epilepsy a reduction in the interaction between TRIP8b (tetratricopeptide-repeat containing Rab8b) and HCN1, normally stabilizing its somato-dendritic expression[114].

MiRP1 is one of these HCN-interacting proteins. It has been initially defined as HCN channel β-subunit from *in vitro* studies in Xenopus oocytes[132], then further studies analyzed its role on HCN channel modulation in other heterologous expression systems[4,14,22] and in cardiomyocytes[86,95]. In these studies, MiRP1 is shown to modify HCN current density and kinetics. Besides, another study demonstrated that MiRP1 deletion in an animal model produces alteration of HCN channels in the brain, leading to an increased neuronal excitability[131].

Upon the genetic screening we performed here, we found the M54T MiRP1 mutation in an epileptic patient and in her daughter, who presented febrile seizures

(**Figure 25**). This mutation involves the transmembrane region of the peptide, causing a change in aminoacid polarity. Because of the already mentioned evidence of functional interaction between MiRP1 and HCN channels (especially in the brain), the involvement of HCN channel alterations in the etiology of epilepsy and because of a previous work showing a reduction of HCN4 current caused by the M54T MiRP1[86], we considered this mutation a good candidate to be involved in the epileptogenesis.

We firstly assessed the effect of the mutation on HCN channels in a heterologous system. We did not find any significant effect neither on HCN2 nor on HCN4 currents exept for a mild slowing of activation time constants of HCN2 only at -85 and -95 mV (**Figure 32**). Notably, a similar effect on HCN2 activation was seen also by Nathawe *et al.* in cardiomyocytes, at -65 and -75 mV[86]. We also found a slower deactivation of HCN4 (**Figure 33**). This was not observed before in cardiomyocytes, where they instead observed again a slower activation at -65 and -75 mV and importantly a strong decrease (80%) in the current density at -110 mV[86], which we did not found in our system. The effect we observed on HCN channel time constants, since are relative to only limited membrane voltages, appears unlikely to cause the epileptic phenotype.

Our *in vitro* data on heterologous system showing that the M54T MiRP1 mutation has no effect on HCN channels are then in contrast with previous data on cardiomyocytes. Nonetheless, the effect of MiRP1 on HCN channels is very controversial and appears strongly species and context dependent.

Notably, no effect of human WT MiRP1 on human HCN channels was observed in Nathawe *et al.* work on transfected cardiomyocytes[86], as well as in a previous work from our laboratory on transfected HEK cells[4]. Also in the study here presented, human HCN channel properties did not differ in cells co-transfected with HCN2 or HCN4 and the human WT MiRP1 compared to cells transfected with only HCN2 or HCN4 channel (Figure n. and n.). Thus, our data play against a possible role of MiRP1 as HCN channel β-subunit. Another possibility is that the

effect cannot be identifiable in our heterologous context and consequently neither can the effect of M54T mutation.

Indeed, evidences from the literature show that the effects of MiRP1 on HCN channels can significantly vary depending on the cellular context in which it is expressed. For example, the work of Yu *et al.* showed that rat WT MiRP1 increases current density and accelerates kinetics of activation of mouse HCN1 and HCN2, when expressed in Xenopus oocytes[132]. However, Decher *et al.* showed that human MiRP1 not only increases current density, but also shift negatively HCN4 activation curve; and conversely to what was shown in Xenopus oocytes, MiRP1 decelerates activation kinetics of the channel in CHO cells stably expressing HCN4[22]. Subsequently, Qu *et al.* demonstrated instead that rat MiRP1 co-transfected with mouse HCN2 in neonatal rat cardiomyocytes causes a 4-fold increase of current density and accelerates both activation and deactivation kinetics of HCN2[95]. More recently, Brandt *et al.* analyzed the effect of MiRP1 on HCN channel in CHO cells, showing that current densities of all HCN isoforms were increased and their activation kinetics were accelerated[14].

To address the question of whether MiRP1 and its M54T mutation can affect HCN channel properties in a neuronal context, we co-transfected WT or mutated MiRP1 with HCN2 or HCN4 in neonatal rat cortical neurons. These cells express minor levels of HCN channels and MiRP1, thus the endogenous rat protein cannot saturate the human proteins expressed via transfection.

Even in this cell system, our data did not show any effect of the M54T mutation on HCN2 or HCN4 channel properties. We only found a deceleration in the activation kinetics of HCN2 at -85 mV (**Figure 34**), that again appears insufficient to trigger the epileptic phenotype. Moreover, although we tested a different and more context-specific cell system, again no differences were observed in presence of the WT MiRP1 compared to the condition transfected with only HCN2 (**Figure 34**).

Taken together these results show that also in neuronal context neither WT nor M54T MiRP1 affect HCN channel properties. Notably, MiRP1 deletion was

demonstrated to alter I_h current properties in brain slices of adult mice, suggesting that MiRP1 is instead necessary for the correct HCN channel function[131]. Thus, the functional interaction of MiRP1 and HCN channels in neurons remains unclear. It is possible that the interaction is more complex than it seemed; for example it could be mediated by other proteins *in vivo*, or could be specific for a certain neuronal context, as the corticothalamic neurons.

Given the lack of WT MiRP1 effect on HCN channels in all the used cell systems, it is not surprising that M54T mutation in turn does not produce any alteration. Nonetheless, Nathawe *et al.* previously found this same mutation to affect HCN channel properties in cardiomyocytes even in the absence of an effect of the WT MiRP1[86]. They explained this discrepancy as a different interaction of MiRP1 with HCN channels depending on the cellular context, as already mentioned, but still without giving clear explanations on the possible underlying mechanism.

We then reasoned that M54T MiRP1 mutation may be involved in the epileptic disorder by acting on other ion channels, such as HERG, which has been largely characterized to assemble with MiRP1[1,47,63,121], or other potassium or calcium channels[48,62,103]. To verify this hypothesis, we analyzed neuronal excitability in presence of WT or mutated MiRP1. Since the high expression of HCN channel itself was demonstrated to decrease neuron excitability[28], for these experiments we transfected in neonatal rat cortical neurons only WT or mutated MiRP1. In this way the effect on excitability of HCN current was abolished, since endogenous I_h is small in these neurons.

Unexpectedly, we found that neurons transfected with the mutated MiRP1 appear less excitable than neurons transfected with the WT MiRP1. More stimulation was necessary to induce the generation of action potentials in M54T-transfected neurons compared to the WT; in addition, upon current injection beyond threshold, M54T-transfected neurons had a slower firing rate compared to the WT (**Figure 35**). The excitability of M54T-transfected neurons was instead comparable to that of control neurons, transfected with the empty vector. Indeed the presence

of WT MiRP1 induced higher excitability, while this effect was reverted by the presence of M54T mutation.

The effect observed goes in the opposite direction of MiRP1 loss-of-function shown on brain slices of MiRP1 KO mice, where an overall increase excitability was observed[131]. Nevertheless, the effect of a point mutation is not really comparable with a deletion, particularly because the mutation can produce also a gain-of-function. Moreover, in our case the effect is not strictly mediated by HCN channels as in the study on KO mice[131]. The possible mediators of this reduced neuron excitability caused by M54T MiRP1 remain still to be investigated.

In conclusion, this study functionally characterized the M54T MiRP1 mutation, showing that it produces no effect on HCN2 and HCN4 channel properties in both heterologous and neuronal *in vitro* systems. This mutation appears however to cause a reduction of neuron excitability, possibly acting on other ion channels, which remain to be determined. The reduced excitability is anyway not compatible with the epileptic phenotype, which has been associated instead with increased neuron excitability[64]. In addition, very recently the screening on the mother of the epileptic patient revealed that she carries M54T mutation even if she is not affected by epilepsy and has never experienced epileptic seizures in her life. Thus, M54T MiRP1 mutation found in an epileptic patient resulted to be not involved in the generation of the disorder.

REFERENCES

1. Abbott GW, Sesti F, Splawski I, Buck ME, Lehmann MH, Timothy KW, Keating MT, Goldstein SA. MiRP1 forms *I*Kr potassium channels with HERG and is associated with cardiac arrhythmia. *Cell*. 1999; 97: 175–187.
2. Abbott GW. KCNE2 and the K (+) channel: the tail wagging the dog. *Channels (Austin)*. 2012 ; 6(1):1-10. Review.
3. Alig J, Marger L, Mesirca P, Ehmke H, Mangoni ME, Isbrandt D. Control of heart rate by cAMP sensitivity of HCN channels. *Proc Natl Acad Sci U S A*. 2009; 106(29):12189-94.
4. Altomare C, Terragni B, Brioschi C, Milanesi R, Pagliuca C, Viscomi C, Moroni A, Baruscotti M, DiFrancesco D. Heteromeric HCN1-HCN4 channels: a comparison with native pacemaker channels from the rabbit sinoatrial node. *J Physiol*. 2003; 549:347–359.
5. Anokye-Danso F, Trivedi CM, Juhr D, Gupta M, Cui Z, Tian Y, Zhang Y, Yang W, Gruber PJ, Epstein JA, Morrisey EE. Highly efficient miRNA-mediated reprogramming of mouse and human somatic cells to pluripotency. *Cell Stem Cell*. 2011; 8(4):376-88.
6. Arnold SJ, Huang GJ, Cheung AF, Era T, Nishikawa S, Bikoff EK, Molnár Z, Robertson EJ, Groszer M. The T-box transcription factor Eomes/Tbr2 regulates neurogenesis in the cortical subventricular zone. *Genes Dev*. 2008; 22(18):2479-84.
7. Barbuti A, Crespi A, Capilupo D, Mazzocchi N, Baruscotti M, DiFrancesco D. Molecular composition and functional properties of f-channels in murine embryonic stem cell-derived pacemaker cells. *J Mol Cell Cardiol*. 2009; 46(3):343-51.
8. Benarroch EE. HCN channels: function and clinical implications. *Neurology*. 2013; 80(3):304-10.
9. Bender RA, Soleymani SV, Brewster AL, Nguyen ST, Beck H, Mathern GW, Baram TZ. Enhanced expression of a specific hyperpolarization-activated cyclic nucleotide-gated cation channel (HCN) in surviving dentate gyrus granule cells of human and experimental epileptic hippocampus. *J Neurosci*. 2003; ;23(17):6826-36.
10. Biel M, Wahl-Schott C, Michalakis S, Zong X. Hyperpolarization-activated cation channels: from genes to function. *Physiol Rev*. 2009; 89:847–885.
11. Birnie D, Williams K, Guo A, Mielniczuk L, Davis D, Lemery R, Green M, Gollob M, Tang A. Reasons for escalating pacemaker implants. *Am J Cardiol*. 2006; 98(1):93-7.
12. Blumenfeld H, Klein JP, Schridde U, Vestal M, Rice T, Khera DS, Bashyal C, Giblin K, Paul-Laughinghouse C, Wang F, Phadke A, Mission J, Agarwal RK, Englot DJ, Motelow J, NersesyanH, Waxman SG, Levin AR. Early treatment suppresses the development of spike-wave epilepsy in a rat model. *Epilepsia*. 2007; 49:400–409.
13. Bowen MA, Patel DD, Li X, Modrell B, Malacko AR, Wang WC, Marquardt H, Neubauer M, Pesando JM, Francke U, et al. Cloning, mapping, and characterization of activated leukocyte-cell adhesion molecule (ALCAM), a CD6 ligand. *J Exp Med*. 1995; 181(6):2213-20.
14. Brandt MC, Endres-Becker J, Zagidullin N, Motloch LJ, Er F, Rottlaender D, Michels G, Herzig S, Hoppe UC: Effects of KCNE2 on HCN isoforms: Distinct modulation of membrane expression and single channel properties. *Am J Physiol Heart Circ Physiol*. 2009; 297:H355-363.
15. Brewster A, Bender RA, Chen Y, Dube C, Eghbal-Ahmadi M, Baram TZ. Developmental febrile seizures modulate hippocampal gene expression of hyperpolarization-activated channels in an isoform-and cell-specific manner. *J Neurosci*. 2002; 22:4591–4599.

16. Brown HF, DiFrancesco D, Noble SJ. How does adrenaline accelerate the heart? *Nature* 1979; 280(5719):235-6.

17. Bucchi A, Baruscotti M, Robinson RB, DiFrancesco D. Modulation of rate by autonomic agonists in SAN cells involves changes in diastolic depolarization and the pacemaker current. *J Mol Cell Cardiol.* 2007; 43(1):39-48.

18. Budde T, Caputi L, Kanyshkova T, Staak R, Abrahamczik C, Munsch T, Pape HC: Impaired regulation of thalamic pacemaker channels through an imbalance of subunit expression in absence epilepsy. *J Neurosci.* 2005; 25:9871-9882.

19. Burdon T, Smith A, Savatier P. Signalling, cell cycle and pluripotency in embryonic stem cells. *Trends Cell Biol.* 2002; 12(9):432-8. Review.

20. Burns FR, von Kannen S, Guy L, Raper JA, Kamholz J, Chang S. DM-GRASP, a novel immunoglobulin superfamily axonal surface protein that supports neurite extension. *Neuron.* 1991; 7(2):209-20.

21. Cho HC, Kashiwakura Y, Marban E. Creation of a biological pacemaker by cell fusion. *Circ Res.* 2007; 100(8):1112-5.

22. Decher N, Bundis F, Vajna R, Steinmeyer K. KCNE2 modulates current amplitudes and activation kinetics of HCN4: influence of KCNE family members on HCN4 currents. *Pflu¨gers Arch.* 2003; 446: 633–640.

23. Di Pasquale E, Song B, Condorelli G. Generation of human cardiomyocytes: a differentiation protocol from feeder-free human induced pluripotent stem cells. *J Vis Exp.* 2013; (76)

24. Dibbens LM, Heron SE, Mulley JC. A polygenic heterogeneity model for common epilepsies with complex genetics. *Genes Brain Behav.* 2007; 6(7):593-7. Review

25. Dibbens LM, Reid CA, Hodgson B, Thomas EA, Phillips AM, Gazina E, Cromer BA, Clarke AL, Baram TZ, Scheffer IE, Berkovic SF, Petrou S.Augmented currents of an HCN2 variant in patients with febrile seizure syndromes. *Ann Neurol.* 2010; 67(4):542-6.

26. DiFrancesco D, Tortora P. Direct activation of cardiac pacemaker channels by intracellular cyclic AMP. *Nature* 1991; 351:145–147.

27. DiFrancesco D, Tromba C. Inhibition of the hyperpolarizationactivated current (if) induced by acetylcholine in rabbit sino-atrial node myocytes. *J Physiol* 1988; 405:477–491.

28. DiFrancesco JC, Barbuti A, Milanesi R, Coco S, Bucchi A, Bottelli G, Ferrarese C, Franceschetti S, Terragni B, Baruscotti M, DiFrancesco D. Recessive loss-of-function mutation in the pacemaker HCN2 channel causing increased neuronal excitability in a patient with idiopathic generalized epilepsy. *J Neurosci.* 2011; 31(48):17327-37.

29. Dubois NC, Craft AM, Sharma P, Elliott DA, Stanley EG, Elefanty AG, Gramolini A, Keller G. SIRPA is a specific cell-surface marker for isolating cardiomyocytes derived from human pluripotent stem cells. *Nat Biotechnol.* 2011; 29:1011-8.

30. Dyhrfjeld-Johnsen J, Morgan RJ, Soltesz I. Double Trouble? Potential for Hyperexcitability Following Both Channelopathic up- and Downregulation of I(h) in Epilepsy. *Front Neurosci.* 2009; 3(1):25-33.

31. Edelberg JM, Huang DT, Josephson ME, Rosenberg RD. Molecular enhancement of porcine cardiac chronotropy. *Heart* . 2001; 86:559-62.

32. Emery EC, Young GT, McNaughton PA. HCN2 ion channels: an emerging role as the pacemakers of pain. *Trends Pharmacol Sci.* 2012; 33:456–463.

33. England J, Loughna S. Heavy and light roles: myosin in the morphogenesis of the heart. *Cell Mol Life Sci.* 2013; 70(7):1221-39.

34. Fujiwara H, Tatsumi K, Kosaka K, Sato Y, Higuchi T, Yoshioka S, Maeda M, Ueda M, Fujii S. Human blastocysts and endometrial epithelial cells express activated leukocyte cell adhesion molecule (ALCAM/CD166). *J Clin Endocrinol Metab*. 2003; 88(7):3437-43.

35. Fusaki N, Ban H, Nishiyama A, Saeki K, Hasegawa M. Efficient induction of transgene-free human pluripotent stem cells using a vector based on Sendai virus, an RNA virus that does not integrate into the host genome. *Proc Jpn Acad Ser B Phys Biol Sci*. 2009; 85(8):348-62.

36. Garcia-Frigola C, Shi Y, Evans SM. Expression of the hyperpolarization-activated cyclic nucleotidegated cation channel HCN4 during mouse heart development. *Gene Expr Patterns*. 2003; 3:777-83.

37. George MS, Abbott LF, Siegelbaum SA. HCN hyperpolarization-activated cation channels inhibit EPSPs by interactions with M-type K(1) channels. *Nat Neurosci*. 2009; 12:577–584.

38. Gessert S, Maurus D, Brade T, Walther P, Pandur P, Kühl M. DM-GRASP/ALCAM/CD166 is required for cardiac morphogenesis and maintenance of cardiac identity in first heart field derived cells. *Dev Biol*. 2008; 321(1):150-61.

39. Haeberlin A, Zurbuchen A, Schaerer J, Wagner J, Walpen S, Huber C, Haeberlin H, Fuhrer J, Vogel R. Successful pacing using a batteryless sunlight-powered pacemaker. *Europace*. 2014; 16(10):1534-9.

40. Hailiwell JV, Adams PR. Voltage-clamp analysis of muscarine excitation in hippocampal neurons. *Brain Res*. 1982; 250:71-92.

41. Heffron DS, Golden JA. DM-GRASP is necessary for nonradial cell migration during chick diencephalic development. *J Neurosci*. 2000; 20(6):2287-94.

42. Hescheler J, Fleischmann BK, Lentini S, Maltsev VA, Rohwedel J, Wobus AM, Addicks K. Embryonic stem cells: a model to study structural and functional properties in cardiomyogenesis. *Cardiovasc Res*. 1997 Nov;36(2):149-62. Review.

43. Hirata H, Murakami Y, Miyamoto Y, Tosaka M, Inoue K, Nagahashi A, Jakt LM, Asahara T, Iwata H, Sawa Y, Kawamata S. ALCAM (CD166) is a surface marker for early murine cardiomyocytes. *Cells Tissues Organs*. 2006; 184(3-4):172-80.

44. Hu YF, Dawkins JF, Cho HC, Marbán E, Cingolani E. Biological pacemaker created by minimally invasive somatic reprogramming in pigs with complete heart block. *Nat Biotechnol*. 2013; 31(1):54-62.

45. Hu Z, Kant R, Anand M, King EC, Krogh-Madsen T, Christini DJ, Abbott GW. Kcne2 deletion creates a multisystem syndrome predisposing to sudden cardiac death. *Circ Cardiovasc Genet*. 2014; 7(1):33-42.

46. Hwang GT, Park H, Lee JH, Oh S, Park KI, Byun M, Park H, Ahn G, Jeong CK, No K, Kwon H, Lee SG, Joung B, Lee KJ. Self-powered cardiac pacemaker enabled by flexible single crystalline PMN-PT piezoelectric energy harvester. *Adv Mater*. 2014; 26(28):4880-7

47. Isbrandt D, Friederich P, Solth A, Haverkamp W, Ebneth A, Borggrefe M, Funke H, Sauter K, Breithardt G, Pongs O, Schulze-Bahr E. Identification and functional characterization of a novel KCNE2 (MiRP1) mutation that alters HERG channel kinetics. *J Mol Med*. 2002; 80, 524–532.

48. Jiang M, Xu X, Wang Y, Toyoda F, Liu XS, Zhang M, Robinson RB, Tseng GN: Dynamic partnership between KCNQ1 and KCNE1 and influence on cardiac IKs current amplitude by KCNE2. *J Biol Chem*. 2009; 284:16452-16462.

49. Jiang M, Zhang M, Tang DG, Clemo HF, Liu J, Holwitt D, Kasirajan V, Pond AL, Wettwer E, Tseng GN. KCNE2 protein is expressed in ventricles of different species, and changes in its

expression contribute to electrical remodeling in diseased hearts. *Circulation.* 2004; 109: 1783–1788.

50. Jung JJ, Husse B, Rimmbach C, Krebs S, Stieber J, Steinhoff G, Dendorfer A, Franz WM, David R. Programming and isolation of highly pure physiologically and pharmacologically functional sinus-nodal bodiesfrom pluripotent stem cells. *Stem Cell Reports*. 2014; 2(5):592-605.

51. Jung S, Jones TD, Lugo JN Jr, Sheerin AH, Miller JW, D'Ambrosio R, Anderson AE, Poolos NP. Progressive dendritic HCN channelopathy during epileptogenesis in the rat pilocarpine model of epilepsy. *J Neurosci*. 2007; 27:13012-13021.

52. Jung S, Warner LN, Pitsch J, Becker AJ, Poolos NP. Rapid loss of dendritic HCN channel expression in hippocampal pyramidal neurons following status epilepticus. *J Neurosci*. 2011; 31(40):14291-5.

53. Kapoor N, Liang W, Marbán E, Cho HC. Direct conversion of quiescent cardiomyocytes to pacemaker cells by expression of Tbx18. *Sci Transl Med*. 2014; 6(245):245-94.

54. Kehat I, Khimovich L, Caspi O, Gepstein A, Shofti R, Arbel G, Huber I, Satin J, Itskovitz-Eldor J, Gepstein L. Electromechanical integration of cardiomyocytes derived from human embryonic stem cells. *Nat Biotechnol*. 2004; 22(10):1282-9.

55. Kim JB, Sebastiano V, Wu G, Araúzo-Bravo MJ, Sasse P, Gentile L, Ko K, Ruau D, Ehrich M, van den Boom D, Meyer J, Hübner K, Bernemann C, Ortmeier C,Zenke M, Fleischmann BK, Zaehres H, Schöler HR. Oct4-induced pluripotency in adult neural stem cells. *Cell*. 2009; 136(3):411-9.

56. Kole MH, Brauer AU, Stuart GJ. Inherited cortical HCN1 channel loss amplifies dendritic calcium electrogenesis and burst firing in a rat absence epilepsy model. *J Physiol*. 2007; 578: 507–525.

57. Lacinová L. Voltage-dependent calcium channels. *Gen Physiol Biophys*. 2005; 24 Suppl 1:1-78. Review.

58. Laflamme MA, Chen KY, Naumova AV, Muskheli V, Fugate JA, Dupras SK, Reinecke H, Xu C, Hassanipour M, Police S, O'Sullivan C, Collins L, Chen Y, Minami E, Gill EA, Ueno S, Yuan C, Gold J, Murry CE. Cardiomyocytes derived from human embryonic stem cells in pro-survival factors enhance function of infarcted rat hearts. *Nat Biotechnol*.2007; 25(9):1015-24.

59. Lenzen KP, Heils A, Lorenz S, Hempelmann A, Sander T. Association analysis of malic enzyme 2 gene polymorphisms with idiopathic generalized epilepsy. *Epilepsia*. 2005 ; 46(10):1637-41.

60. Li B, Luo C, Tang W, et al. Role of HCN channels in neuronal hyperexcitability after subarachnoid hemorrhage in rats. *J Neurosci*. 2012; 32:3164–3175.

61. Lin B, Kim J, Li Y, Pan H, Carvajal-Vergara X, Salama G, Cheng T, Li Y, Lo CW, Yang L. High-purity enrichment of functional cardiovascular cells from human iPS cells. *Cardiovascular Research*. 2012; 95(3):327-35.

62. Liu W, Deng J, Wang G, Zhang C, Luo X, Yan D, Su Q, Liu J. KCNE2 modulates cardiac L-type Ca(2+) channel. *J Mol Cell Cardiol*. 2014; 72:208-18.

63. Lu Y, Mahaut-Smith MP, Huang CL, Vandenberg JI. Mutant MiRP1 subunits modulate HERG K+ channel gating: a mechanism for pro-arrhythmia in long QT syndrome type 6. *J Physiol*. 2003; 551(Pt 1):253-62.

64. Lu Y, Wang X. Genes associated with idiopathic epilepsies: a current overview. *Neurol Res*. 2009 ; 31(2):135-43.

65. Ludwig A, Budde T, Stieber J, Moosmang S, Wahl C, Holthoff K et al. Absence epilepsy and sinus dysrhythmia in mice lacking the pacemaker channel HCN2. *Embo J*. 2003; 22: 216–224.

66. Magee JC. Dendritic Ih normalizes temporal summation in hippocampal CA1 neurons. *Nat Neurosci*. 1999; 2: 848.

67. Marionneau C, Couette B, Liu J, Li H, Mangoni ME, Nargeot J, Lei M, Escande D, Demolombe S. Specific pattern of ionic channel gene expression associated with pacemaker activity in the mouse heart. *J Physiol* 2005; 562:223–234.

68. Matsui Y, Zsebo K, Hogan BL. Derivation of pluripotential embryonic stem cells from murine primordial germ cells in culture. *Cell*. 1992; 70(4):841-847.

69. McClelland S, Flynn C, Dube´ C, Richichi C, Zha Q, Ghestem A, Esclapez M, Bernard C, Baram TZ: Neuron-restrictive silencer factor-mediated hyperpolarization-activated cyclic nucleotide gated channelopathy in experimental temporal lobe epilepsy. *Ann Neurol*. 2011; 70(3):454-64

70. McCrossan ZA, Abbott GW. The minK-releted peptides. *Neuropharmacology.* 2004; 47:787–821.

71. McPherson CA, Rosenfeld LE. Heart Book Chapter 16 Heart Rhythm Disorders *Lancet*. 1993; 341(8854):1189-93.

72. Miake J, Marbán E, Nuss HB. Biological pacemaker created by gene transfer. *Nature*. 2002; 419(6903):132-3.

73. Migliore M, Migliore R. Know your current I(h): interaction with a shunting current explains the puzzling effects of its pharmacological or pathological modulations. *PLoS One*. 2012; 7(5):e36867.

74. Mistrik P, Mader R, Michalakis S, Weidinger M, Pfeifer A, Biel M. The murine HCN3 gene encodes a hyperpolarization-activated cation channel with slow kinetics and unique response to cyclic nucleotides. *J Biol Chem*. 2005; 280:27056–27061.

75. Mommersteeg MT, Domi´nguez JN, Wiese C, Norden J, de Gier-de Vries C, Burch JBE, Kispert A, Brown NA, Moorman AFM, Christoffels VM. The sinus venosus progenitors separate and diversify from the first and second heart fields early in development. *Cardiovascular Research.* 2010; 87:92–101

76. Mommersteeg MT, Hoogaars WM, Prall OW, de Gier-de Vries C, Wiese C, Clout DE, Papaioannou VE, Brown NA, Harvey RP, Moorman AF, Christoffels VM. Molecular pathway for the localized formation of the sinoatrial node. *Circ Res*. 2007; 100(3):354-62.

77. Mond HG, Proclemer A. The 11th world survey of cardiac pacing and implantable cardioverter defibrillators: calendar year 2009–a WorldSociety of Arrhythmia's project. *Pacing Clin Electrophysiol*. 2011; 34(8):1013-27.

78. Moorman AF, Christoffels VM, Anderson RH, van den Hoff MJ. The heart-forming fields: one or multiple? *Philos Trans R Soc Lond B Biol Sci*. 2007; 362(1484):1257-65. Review.

79. Moorman AF, Christoffels VM. Cardiac chamber formation: development, genes, and evolution. *Physiol Rev*. 2003; 83(4):1223-67. Review.

80. Moosmang S, Biel M, Hofmann F, Ludwig A. Differential distribution of four hyperpolarization-activated cation channels in mouse brain. Biol Chem. 1999 ; 380(7-8):975-80.

81. Morikawa K, Bahrudin U, Miake J, Igawa O, Kurata Y, Nakayama Y, Shirayoshi Y, Hisatome I. Identification, isolation and characterization of HCN4-positive pacemaking cells derived from murine embryonic stem cells during cardiac differentiation. *Pacing Clin Electrophysiol*. 2010;33(3):290-303.

82. Moroni A, Barbuti A, Altomare C, Viscomi C, Morgan J, Baruscotti M, DiFrancesco D. Kinetic and ionic properties of the human HCN2 pacemaker channel. *Pflu¨ gers Arch* 2000; 439:618–626.

83. Mummery C, Ward-van Oostwaard D, Doevendans P, Spijker R, van den Brink S, Hassink R, van der Heyden M, Opthof T, Pera M, de la Riviere AB, Passier R, Tertoolen L. Differentiation of human embryonic stem cells to cardiomyocytes: role of coculture with visceral endoderm-like cells. *Circulation*. 2003; 107(21):2733-40.

84. Murakami Y, Hirata H, Miyamoto Y, Nagahashi A, Sawa Y, Jakt M, Asahara T, Kawamata S. Isolation of cardiac cells from E8.5 yolk sac by ALCAM (CD166) expression. *Mech Dev*. 2007; 124(11-12):830-9.

85. Nava C, Dalle C, Rastetter A, Striano P, de Kovel CG, Nabbout R, Cancès C, Ville D, Brilstra EH, Gobbi G, Raffo E, Bouteiller D, Marie Y,Trouillard O, Robbiano A, Keren B, Agher D, Roze E, Lesage S, Nicolas A, Brice A, Baulac M, Vogt C, El Hajj N, Schneider E, Suls A, Weckhuysen S, Gormley P, Lehesjoki AE, De Jonghe P, Helbig I, Baulac S, Zara F, Koeleman BP, Haaf T, LeGuern E, Depienne C. De novo mutations in HCN1 cause early infantile epileptic encephalopathy. *Nat Genet*. 2014; 46(6):640-5.

86. Nawathe PA, Kryukova Y, Oren RV, Milanesi R, Clancy CE, Lu JT, Moss AJ, Difrancesco D, Robinson RB. An LQTS6 MiRP1 mutation suppresses pacemaker current and is associated with sinus bradycardia. *J Cardiovasc Electrophysiol*. 2013; 24(9):1021-7.

87. Nishimura K, Sano M, Ohtaka M, Furuta B, Umemura Y, Nakajima Y, Ikehara Y, Kobayashi T, Segawa H, Takayasu S, Sato H, Motomura K, Uchida E, Kanayasu-Toyoda T, Asashima M, Nakauchi H, Yamaguchi T, Nakanishi M. Development of defective and persistent Sendai virus vector: a unique gene delivery/expression system ideal for cell reprogramming. *J Biol Chem*. 2011; 286(6):4760-71.

88. Noam Y, Bernard C, Baram TZ. Towards an integrated view of HCN channel role in epilepsy. Curr Opin Neurobiol. 2011 Dec;21(6):873-9.

89. Notomi T, Shigemoto R. Immunohistochemical localization of Ih channel subunits, HCN1-4, in the rat brain. *J Comp Neurol*. 2004 ; 471(3):241-76.

90. Ottman R, Hirose S, Jain S, Lerche H, Lopes-Cendes I, Noebels JL, Serratosa J, Zara F, Scheffer IE. Genetic testing in the epilepsies–report of the ILAE Genetics Commission. *Epilepsia*. 2010 ; 51(4):655-70.

91. Pape HC. Queer current and pacemaker: the hyperpolarization-activated cation current in neurons. *Annu Rev Physiol*. 1996; 58:299-327. Review

92. Pools NP. Hyperpolarization activated cyclic nucleotide gated (HCN) ion channelopathy in epilepsy. *In: Noebels JL, Avoli M, Rogawski MA, Olsen RW, Delgado-Escueta AV, editors. Jasper's Basic Mechanisms of the Epilepsies [Internet]. 4th edition. Bethesda (MD): National Center for Biotechnology Information (US)*. 2012.

93. Potapova I, Plotnikov A, Lu Z, Danilo P Jr, Valiunas V, Qu J, Doronin S, Zuckerman J, Shlapakova IN, Gao J, Pan Z, Herron AJ, Robinson RB, Brink PR, Rosen MR, Cohen IS. Human mesenchymal stem cells as a gene delivery system to create cardiac pacemakers. *Circ Res*. 2004; 94(7):952-9.

94. Pourrier M, Zicha S, Ehrlich J, Han W, Nattel S. Canine ventricular KCNE2 expression resides predominantly in Purkinje fibers. *Circ Res*. 2003; 93: 189–191.

95. Qu J, Kryukova Y, Potapova IA, Doronin SV, Larsen M, Krishnamurthy G, Cohen IS, Robinson RB. MiRP1 modulates HCN2 channel expression and gating in cardiac myocytes. *J Biol Chem*. 2004; 279:43497–43502.

96. Qu J, Plotnikov AN, Danilo P Jr, Shlapakova I, Cohen IS, Robinson RB, Rosen MR. Expression and function of a biological pacemaker in canine heart. *Circulation*. 2003; 107(8):1106-9.

97. Rana MS, Christoffels VM, Moorman AF. A molecular and genetic outline of cardiac morphogenesis. *Acta Physiol* . 2013; 207(4):588-615. Review.

98. Reid CA1, Phillips AM, Petrou S. HCN channelopathies: pathophysiology in genetic epilepsy and therapeutic implications. *Br J Pharmacol*. 2012; 165(1):49-56.

99. Robinson RB, Siegelbaum SA: Hyperpolarization-activated cation currents: from molecules to physiological function. *Annu Rev Physiol*. 2003; 65:453-480.

100. Roepke TK, Anantharam A, Kirchhoff P, Busque SM, Young JB, Geibel JP, et al. The KCNE2 potassium channel ancillary subunit is essential for gastric acid secretion. *J Biol Chem*. 2006; 281:23740-7.

101. Roepke TK, Kanda VA, Purtell K, King EC, Lerner DJ, Abbott GW. KCNE2 forms potassium channels with KCNA3 and KCNQ1 in the choroid plexus epithelium. *FASEB J*. 2011; 25:4264-73.

102. Roepke TK, King EC, Reyna-Neyra A, Paroder M, Purtell K, Koba W, et al. Kcne2 deletion uncovers its crucial role in thyroid hormone biosynthesis. *Nat Med.* 2009; 15:1186-94.

103. Roepke TK, Kontogeorgis A, Ovanez C, Xu X, Young JB, Purtell K, et al. Targeted deletion of kcne2 impairs ventricular repolarization via disruption of I(K,slow1) andI(to,f). *FASEB J.* 2008; 22:3648-60.

104. Rosen MR. Gene therapy and biological pacing. *N Engl J Med*. 2014; 371(12):1158-9.

105. Rust W, Balakrishnan T, Zweigerdt R. Cardiomyocyte enrichment from human embryonic stem cell cultures by selection of ALCAM surface expression. *Regen Med*. 2009; 4(2):225-37.

106. Salsbury G, Cambridge EL, McIntyre Z, Arends MJ, Karp NA, Isherwood C, Shannon C, Hooks Y; The Sanger Mouse Genetics Project, Ramirez-Solis R, Adams DJ, White JK, Speak AO. Disruption of the potassium channel regulatory subunit Kcne2 causes iron-deficient anemia. *Exp Hematol*. 2014; pii:S0301-472X(14)00623-7.

107. Santoro B, Chen S, Luthi A, Pavlidis P, Shumyatsky GP, Tibbs GR, Siegelbaum SA. Molecular and functional heterogeneity of hyperpolarization-activated pacemaker channels in the mouse CNS. *J Neurosci*. 2000; 20:5264–5275.

108. Santoro B, Lee JY, Englot DJ, Gildersleeve S, Piskorowski RA, Siegelbaum SA, Winawer MR, Blumenfeld H. Increased seizure severity and seizure-related death in mice lacking HCN1 channels. *Epilepsia*. 2010; 51(8):1624-7.

109. Scavone A, Capilupo D, Mazzocchi N, Crespi A, Zoia S,Campostrini G, Bucchi A, Milanesi R, Baruscotti M, Benedetti S, Antonini S, Messina G, DiFrancesco D, Barbuti A. Embryonic stem cell-derived CD166+ precursors develop into fully functional sinoatrial-like cells. *Circ Res*. 2013; 113(4):389-98.

110. Seifert R, Scholten A, Gauss R, Mincheva A, Lichter P, Kaupp UB. Molecular characterization of a slowly gating human hyperpolarization-activated channel predominantly expressed in thalamus, heart, and testis. *Proc Natl Acad Sci USA* 1999; 96:9391–9396.

111. Seki T, Yuasa S, Oda M, Egashira T, Yae K, Kusumoto D, Nakata H, Tohyama S, Hashimoto H, Kodaira M, Okada Y, Seimiya H, Fusaki N, Hasegawa M, Fukuda K. Generation of induced pluripotent stem cells from human terminally differentiated circulating T cells. *Cell Stem Cell*. 2010; 7(1):11-4.

112. Sesti F, Abbott GW, Wei J, Murray KT, Saksena S, Schwartz PJ, Priori SG, Roden DM, George Jr AL, Goldstein, S.A., 2000b. A common polymorphism associated with antibiotic-induced cardiac arrhythmia. *Proc Natl Acad Sci*. USA 97, 10613–10618.

113. Shi W, Wymore R, Yu H, Wu J, Wymore RT, Pan Z, Robinson RB, Dixon JE, McKinnon D, Cohen IS. Distribution and prevalence of hyperpolarization-activated cation channel (HCN) mRNA expression in cardiac tissues. *Circ Res* 1999; 85:1–6.

114. Shin M, Brager D, Jaramillo TC, Johnston D, Chetkovich DM. Mislocalization of h channel subunits underlies h channelopathy in temporal lobe epilepsy. *Neurobiol Dis*. 2008; 32:26–36.

115. Steriade M, Timofeev I. Neuronal plasticity in thalamocortical networks during sleep and waking oscillations. *Neuron*. 2003; 37(4):563-76. Review.

116. Strauss U, Kole MH, Brauer AU, Pahnke J, Bajorat R, Rolfs A et al. An impaired neocortical Ih is associated with enhanced excitability and absence epilepsy. *Eur J Neurosci*. 2004; 19:3048–3058.

117. Takahashi K, Okita K, Nakagawa M, Yamanaka S. Induction of pluripotent stem cells from fibroblast cultures. *Nat Protoc*. 2007; 2(12):3081-9.

118. Takahashi K, Yamanaka S. Induction of pluripotent stem cells from mouse embryonic and adult fibroblast cultures by defined factors. *Cell*. 2006; 126(4):663-76.

119. Tang B, Sander T, Craven KB, Hempelmann A, Escayg A. Mutation analysis of the hyperpolarizationactivated cyclic nucleotide-gated channels HCN1 and HCN2 in idiopathic generalized epilepsy. *Neurobiol Dis*. 2008; 29:59–70.

120. Thollon C, Bedut S, Villeneuve N, Coge F, Piffard L, Guillaumin JP, Brunel-Jacquemin C, Chomarat P, Boutin JA, Peglion JL, Vilaine JP. Use-dependent inhibition of hHCN4 by ivabradine and relationship with reduction in pacemaker activity. *Br J Pharmacol.* 2007; 150:37–46.

121. Tinel N, Diochot S, Borsotto M, Lazdunski M, Barhanin J. KCNE2 confers background current characteristics to the cardiac KCNQ1 potassium channel. *EMBO J.* 2000 19: 6326–6330.

122. Viscomi C, Altomare C, Bucchi A, Camatini E, Baruscotti M, Moroni A, DiFrancesco D. C terminus-mediated control of voltage and cAMP gating of hyperpolarization-activated cyclic nucleotide-gated channels. *J Biol Chem*. 2001; 276:29930–29934.

123. Waldo AL, Wit AL. Mechanisms of cardiac arrhythmias. *Lancet*. 1993; 341(8854):1189-93. Review.

124. Weichert W, Knösel T, Bellach J, Dietel M, Kristiansen G. ALCAM/CD166 is overexpressed in colorectal carcinoma and correlates with shortened patient survival. *J Clin Pathol*. 2004; 57(11):1160-4.

125. Wierschke S, Lehmann TN, Dehnicke C, Horn P, Nitsch R, Deisz RA. Hyperpolarization-activated cation currents in human epileptogenic neocortex. *Epilepsia*. 2010; 51(3):404-14.

126. Willems E, Bushway PJ, Mercola M. Natural and synthetic regulators of embryonic stem cell cardiogenesis. *Pediatr Cardiol*.2009; 30(5):635-42.

127. Williams SR, Stuart GJ. Site independence of EPSP time course is mediated by dendritic I(h) in neocortical pyramidal neurons. *J Neurophysiol*. 2000; 83: 3177–3182.

128. Wobus AM, Boheler KR. Embryonic stem cells: prospects for developmental biology and cell therapy. *Physiol Rev*. 2005; 85(2):635-78. Review.

129. Xue T, Cho HC, Akar FG, Tsang SY, Jones SP, Marbán E, Tomaselli GF, Li RA. Functional integration of electrically active cardiac derivatives from genetically engineered human embryonic stem cells with quiescent recipient ventricular cardiomyocytes: insights into the development of cell-based pacemakers. *Circulation*. 2005; 111(1):11-20.

130. Yamanaka S. Pluripotency and nuclear reprogramming. *Philos Trans R Soc Lond B Biol Sci*. 2008; 363(1500):2079-87. Review

131. Ying SW, Kanda VA, Hu Z, Purtell K, King EC, Abbott GW, Goldstein PA. Targeted deletion of Kcne2 impairs HCN channel function in mouse thalamocortical circuits. *PLoS One*. 2012; 7(8):e42756.

132. Yu H, Wu J, Potapova I, Wymore RT, Holmes B, Zuckerman J, et al. MinK-related peptide 1: A betasubunit for the HCN ion channel subunit family enhances expression and speeds activation. *Circ Res.* 2001; 88:E84-7.

133. Yu J, Hu K, Smuga-Otto K, Tian S, Stewart R, Slukvin II, Thomson JA. Human induced pluripotent stem cells free of vector and transgene sequences. *Science*. 2009; 324(5928):797-801.

134. Yu J, Vodyanik MA, Smuga-Otto K, Antosiewicz-Bourget J, Frane JL, Tian S, Nie J, Jonsdottir GA, Ruotti V, Stewart R, Slukvin II, Thomson JA. Induced pluripotent stem cell lines derived from human somatic cells. *Science*. 2007; 318(5858):1917-20.

135. Zhang M, Jiang M, Tseng GN. MinK-related peptide 1 associates with Kv4.2 and modulates its gating function: potential role as beta subunit of cardiac transient outward channel? *Circ Res.* 2001. 88: 1012–1019.

136. Zhou YQ, Foster FS, Parkes R, Adamson SL. Developmental changes in left and right ventricular diastolic filling patterns in mice. *Am J Physiol Heart Circ Physiol*. 2003;285:H1563–H1575.